EXPERIMENTAL STUDY OF COOLING OF ELECTRONIC EQUIPMENT

BY

AJAY KUMAR SHRIVASTAVA

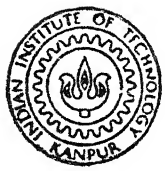

DEPARTMENT OF MECHANICAL ENGINEERING

INDIAN INSTITUTE OF TECHNOLOGY KANPUR

APRIL, 1992

EXPERIMENTAL STUDY OF COOLING OF ELECTRONIC EQUIPMENT

A Thesis Submitted
In Partial Fulfilment of the Requirements
for the Degree of

MASTER OF TECHNOLOGY

BY

AJAY KUMAR SHRIVASTAVA

to the

DEPARTMENT OF MECHANICAL ENGINEERING
INDIAN INSTITUTE OF TECHNOLOGY KANPUR

APRIL, 1992

CERTIFICATE

It is certified that the work contained in this thesis entitled, "EXPERIMENTAL STUDY OF COOLING OF ELECTRONIC EQUIPMENT" by Ajay Kumar Shrivastava has been carried out under my supervision and that this work has not been submitted elsewhere for a degree.

K Muralidhar

(Dr.K.Muralidhar)
Assistant Professor
Department of Mechanical Engg.

Dated:

April 30, 1992

ME-1992-M-SHR-EXP

ACKNOWLEDGEMENTS

I take this opportunity to thank Dr. K. Muralidhar for giving me a chance to work with him. It was mainly due to his guidance, interest, help and encouragement that I could perform this work. At the moments he acted tough which I now realize, helped me in finisning the thesis before it was delayed too much. He gave me a free hand to think and act and provided all the facilities in the lab. including some of the most modern and sophisticated instruments which made the task a lot easier and results very accurate.

Fabrication has been an important and difficult part of my thesis. The fabrication of the flow apparatus is dedicated to Mr. S.N. Sharma of Solar Energy Lab. It was due to his skills and efforts that some really complicated jobs were done in solar energy lab. itself avoiding innumerable visits to the central workshop.

I thank my friend K.N. Kiran Kumar for providing me help in my mid term project which is also a part of my thesis. I express my gratitude towards Ashish Singhai and Tarun Agarwal who always took a keen interest and trouble in solving my problems regarding computer matters. Ashish did not mind overlooking even his own problems and spent hours with me in computer centre.

Towards the end of my thesis the pressure was overwhelming. I am really indebted to Atul Verma, who despite his ill health, took all pains and shared my load to a large extent. Thanks are due to Ravindra Telang and V.S. Rao also who offered their help

in the last moments when I needed it the most. I am thankful to the Technical staff of F.M. Lab. and friend Rajnish Kashyap who gave me a good company in my lab. I am also grateful to P.M.V. Subba Rao for giving me useful advises at times.

Wingmates Rajeev Kumar Jain, Amit Shrivastava and P.S. Galagali always provided a cheerful company. I am thankful to the members of our cricket team with whom I played a number of matches and enjoyed the life. All in all it was nice and fruitful stay at IIT Kanpur except for a few sour moments shared with some members of cricket team.

Lastly I wish to express my sincerest gratitude toward my family members, especially my father, for allowing me to do whatever I liked. His words and letters have been a constant source of encouragement and inspiration through the program mainly in the end when I was getting little nervous because of the work load.

Ajay Kumar Shrivastava

CONTENTS

NOMENCLATURE

A	=	Surface area of heater
AR	=	Aspect ratio, L/H
D	=	Spacing between two parallel plates
g	=	Acceleration due to gravity
Gr	=	Grashoff number, $\frac{g\beta\Delta TL^3}{\nu^2}$
H	=	Protrusion of heater
h	=	Heat transfer coefficients
k	=	Thermal conductivity of fluid
L	=	Characteristic length of heater (vertical length parallel to flow)
l	=	Length of test cell parallel to the test beam
Nu	=	Nusselt number, hL/k
Pr	=	Prandtl number, $\mu C_p/k$
Q	=	Total heat rate
q	=	Heat flux
R	=	Resistance of heater
Ra	=	Rayleigh number, $\frac{g\beta\Delta TL^3}{\nu\alpha}$
Re	=	Reynolds number, $\frac{UL}{\nu}$
S	=	Spacing between the two heaters
T_c	=	Temperature of heated chip surface
T_∞	=	Ambient temperature
T_m	=	Mean temperature
ΔT	=	$(T_c - T_\infty)$
U	=	Centre line velocity
u	=	Velocity in axial direction
V	=	Voltage
v	=	Velocity in transverse direction

x	=	Axial coordinate
y	=	Transverse coordinate
ν	=	Kinematic viscosity
α	=	Thermal diffusivity
C_p	=	Specific heat
ρ	=	Density
μ	=	Viscosity
β	=	Thermal expansion coefficient $\frac{1}{T_c}$ / K
$\varepsilon(x)$	=	Fringe width at x location
ε	=	Emissivity

Subscript

1	=	heater 1, upper heater
2	=	heater 2, central heater
3	=	heater 3, lower heater

Configurations (Multichip heater)

Configuration	refers to	heater 1	heater 2	heater 3
C-H-C		cold	hot	cold
C-H-H		cold	hot	hot
H-H-H		hot	hot	hot
H-H-C		hot	hot	cold
H-C-H		hot	cold	hot

All the figures have dimensions in mm.

e of the Student	:	AJAY KUMAR SHRIVASTAVA
l No.	:	9010502
gramme	:	M.Tech.
artment	:	Mechanical Engineering
sis Title	:	Experimental Study of Cooling of Electronic Equipment
sis Supervisor	:	Dr.K. Muralidhar

ABSTRACT

The present work aims at determining the flow patterns and mperature field in arrays of heat generating circuit boards. The rcuit boards are modelled experimentally and the relationship etween maximum temperature and regime of flow (such as free, xed or forced convection) are sought to be determined. The fect of wall protrusion on flow and heat transfer are studied. the present work interferometry is used to get qualitative iformation about the flow field and to a cross check the results obtained by conventional techniques. In particular visualization f isotherms in the space between vertical flat surfaces with a distri- ition of discrete wall heaters using a Mach-Zhender interferometer s one of the objectives of the present study.

Chapter 1

INTRODUCTION

The cooling of electronic equipment continues to be an active field of investigations in heat transfer. Effective cooling of electronic equipment has become increasingly important as power dissipation and component density continue to increase substantially with the fast growth of electronics technology. This importance arises from reliability considerations, the desire to decrease the transit time of electronic signals and the advent of new computer configurations and measurement devices. Reliability revolves about control of the temperature levels of the critical components, while the transit time is diminished by shorter transmission distances, giving rise to closely positioned components and high densities of dissipated electrical power.

As solid state circuits are miniaturized large amount of thermal energy is generated due to flow of current-through gates and connections of smaller areas within a silicon chip. As computing and gate switching speed increases in a chip, heat generation also increases. Circuit miniaturization has advanced to such an extent that heat dissipation capability of system design has become one of the primary limiting factors. The main consideration in thermal design is to minimize the maximum temperature at the chip for a given set of design criteria. Recent advances in computing speed and improved

packaging density in modern digital computers, can be attributed to convection heat transfer research resulting in novel thermal design for handling high heat dissipation coefficients. The life of an integrated circuit device and that of other electronic components can be prolonged if the operating temperature is maintained at a value lower than the maximum specified by the manufacturer. As an estimate long-term reliability can be increased up to 50% for each 18°f (10°C) that a device is maintained below its maximum operating temperature.

To give an example of how large the heat flux can be consider the following numbers quoted by Oktay et al (1986). A power dissipation of 10W on a 5x5 mm^2 chip yields a heat flux of 5.E05 W/m^2 which is only 20 times less than that on the surface of sun. The sun's surface temperature is 6000°C while the design temperature of today's chips is 100°C.

Theoretically, if a chip working at this heat flux could somehow be tethered in still air at room temperature, its temperature would exceed 6000°C, assuming only natural convection and no radiation. With forced convection, the chip can be cooled to 1000°C with common gases and to about 50°C with common liquids. If on the other hand, the heat is conducted away by means of a copper stud pressed against the chip, the chip's temperature can be lowered to about 30°C, assuming that the copper stud is held at 25°C and that the contact between stud and chip is perfect. If a small air gap of say, 1 mm is introduced between the same chip and stud, the

chip will reach a temperature of 600°C. Immersion cooling with phase change can lower the chips temperature to approximately 30°C if water is the coolant, or to 45°C if fluorocarbons are used.

Thermal engineers face the challange of removing high heat fluxes by means of any of the heat transfer modes- natural or forced convection, conduction, or phase change - while maintaining relatively low component temperatures. The working temperatures of electronic components are dictated not only by their inherent performance requirements but also by stringent reliability demands.

Conventional Methods of Cooling

Four main considerations while designing any cooling system for electronic components are:

1. To maintain device temperature at low enough level to allow the system to operate.
2. To meet reliability goals for a wide range of environment conditions.
3. To hold the temperature variations within a fixed limit.
4. To meet requisite cooling requirements while fulfilling stringent acoustic noise restrictions.

On this basis we can have following methods for the cooling of an electronic equipment.

1. Natural Convection Cooling: This method is both silent and very reliable. It is cheap and does not introduce any kind of electromagnetic interference with the operating signals. Natural convection is the least effective way of removing heat. Moreover design considerations often mitigate against effective natural convection. Equipment for home and office is often laid out in compact horizontal packages. Open construction with vertically oriented heat generating components is best suited for natural convection. Prediction of natural convection air flow and cooling rates with less than ideal geometries and restricted flow paths poses a major challenge. In practice, circuit boards are separated by supporting shelves. Energy released from electronic chips is dissipated directly to the fluid by convection and to the wall by conduction. Heat conducted to the wall is eventually dissipated by convection to the adjacent channel.

2. Forced Cooling: At places with space restriction and high heat flux levels, forced convection is used to achieve acceptable cooling performance. A fan or a blower is used to blow the air or cooling fluid past the heated chips

mounted on the circuit boards. It results in a high value of the heat transfer coefficient and better cooling. Because of different geometries and flow paths in different systems the values of various flow parameters and pressure drop can not be calculated readily from first principles. Forced cooling is used in many personal computers and nearly all small computers. In a system box of a typical personal computer, space is at a premium and the airflow path is circuitous. Components that are sensitive to heat are located in several areas of the box, all of which must be reached by adequate air flow.

Besides giving better cooling and sufficient reliability this method of cooling has got some limitations too. The fan installed for cooling occupies sufficient space. It increases the cost of the system as the initial cost and running cost of the fan has to be taken into consideration. The fan also produces its own electromagnetic field which may in some cases, lead to the corruption of signal being received or tramsferred by the electronic equipment. A large capacity fan also produces objectionable noise.

Even with these limitation forced cooling is being adopted rapidly as the size of the IC chip is reducing day by day raising the heat flux level in electronic equipment.

III. Cooling with Fin Arrays: Fin arrays are widely used as heat sinks for cooling electronic equipment in natural

forced convection cooling. The most common configurations involve vertical surfaces having fins attached to them. The

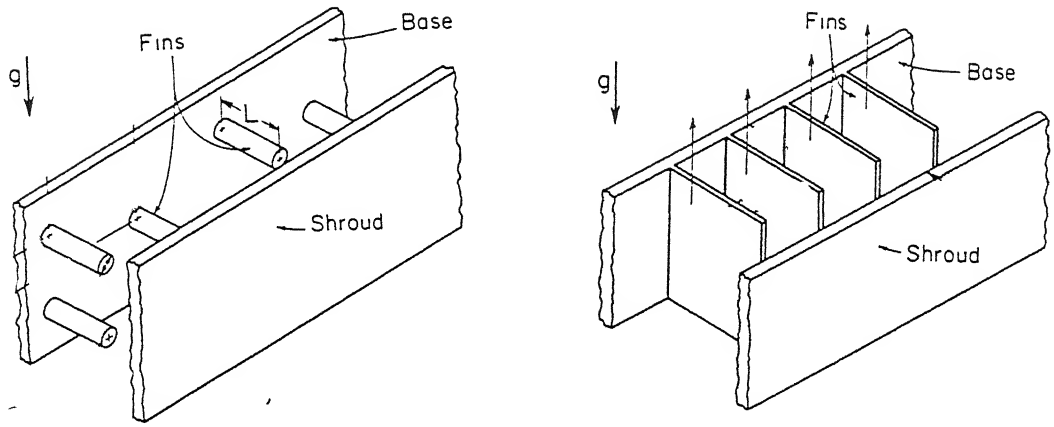

Fig. 1.1 : Cooling with fin arrays

heat is transferred to these fins first and from there is transferred to the air passing over it. Because of the increase in surface area better heat transfer is achieved. The heat transfer enhancement is also due to the disruption of thermal boundary layer development. Heat transfer from electronic devices may be enhanced by inserting ribs in the flow increasing convection heat transfer from downstream modules.

IV. Liquid Cooling:

(a) Indirect Liquid Cooling: This may also be termed as conduction coupled liquid cooling. The cooling of high

performance electronics has been complicated further by increasingly close placement of components having high heat fluxes as in latest multichip modules. For the effective cooling these thermal resistances must be

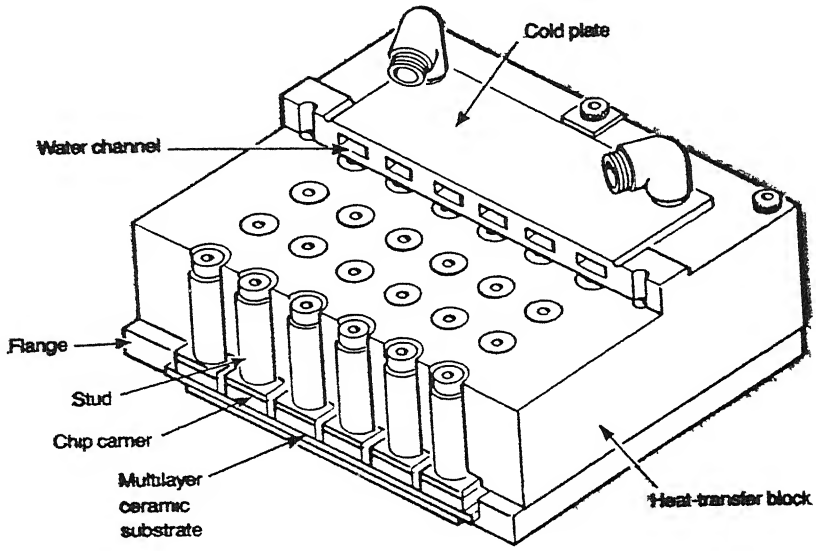

Fig.1.2 : Liquid cooling module

reduced from the internal heat source to external final heat sink. One of the methods of indirect liquid cooling is that in which the cold plate and the chip are fabricated as an integral unit. The structure resembles a miniature, longtidunally finned heat sink. Closure of the channel is achieved with a cover plate, and liquid is continuously pumped through the channel.

(b) Jet Impingement Cooling: The specific consideration of impinging liquid jets at hot spots to electronics cooling is relatively recent. An extensive study of single phase jet impingement cooling for microelectronic applications has been done by Jij and Dagan (1987). It reduces the thermal

resistance appreciably resulting in high values of heat transfer coefficients.

(V) Heat Transfer with Phase Change: Liquid immersion cooling in a pool or forced convection boiling is another method of cooling of very large systems having relatively high heat dissipation. In this method a chemically inert coolant of high dielectric strength and low boiling point is required which limits its applications. Boiling in dielectric fluids is also characterised by small values of critical heat flux and additional problem could include cyclic thermal stresses and electrical noise related to temperature fluctuations, device contamination due to impurities and increased complexity associated with the need of sealed chambers. In a two phase system a thermal stock can arise due to a sudden drop in surface temperature that occurs upon the incipient boiling. This phenomenon, called hysteresis, was encountered by Samant and Simon (1968) in experiments with flow boiling.

Forced convection boiling may occur when cooling is effected by an impinging jet, a channel flow, or a falling film. Impinging jets may be directed normal to the surface or at any angle off the normal. Forced convection boiling may also occur in free falling liquid films used to cool vertically mounted electronic chips.

Two Phase Thermosyphons: Another kind of two phase liquid immersion cooling is complete encapsulation of the electronic assembly. This method was first used for high power components and air borne electronic packages and was subsequently advocated for densely populated PCBs and chip arrays. Saturated or subcooled boiling occurs at the surface of the electronic component and condensation takes place within the liquid or at an encapsulated cold plate.

Chips are mounted to a substrate forming one wall of a module filled with a fluorocarbon. Heat is transferred from the chips to the coolant and from the coolant to the internal fins of a water cooled cold plate or an air cooled heat sink. Use of submerged condenser facilitates maintenance of subcooled conditions in the coolant.

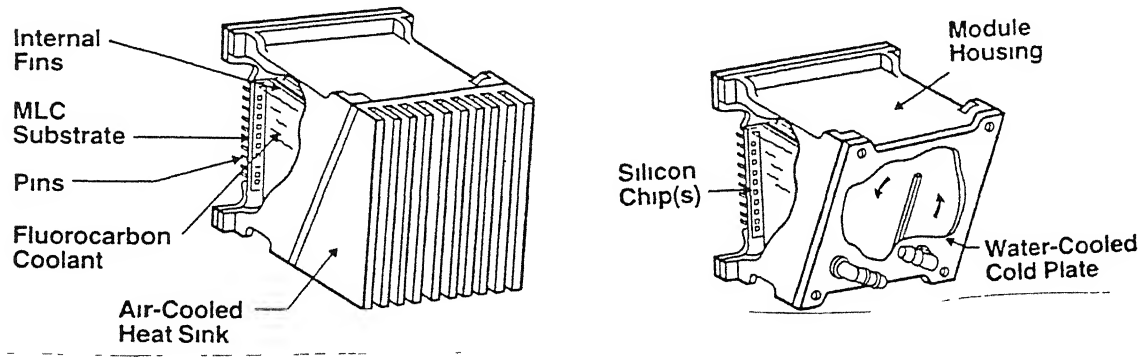

Fig.1.3 : Encapsulated two phase thermosyphons

The future electronic systems will have higher heat fluxes at the chip and packages level and cooling will be a

challenge. Although no new theories are required but basic work on some of the heat transfer mechanisms is needed. Boiling phenomenon on highly polished surfaces such as silicon chips ought to be better understood. More work is needed on condensation and cryogenic heat transfer as they apply to electronics cooling. The importance of thermal interfaces and contact resistances calls for an understanding of non elastic contact regimes as a function of pressure. Better methods of analysis and simulation are also required. As power dissipation grows, use of extended surfaces such as heat sinks will become more wide spread. A significant progress has been made in establishing a convection heat transfer knowledge base pertinent to problems of electronic cooling. It covers a wide range of geometries. With such results it is possible for a packaging engineer to assess, at least in an approximate sense, the relative merits of various options for a particular cooling problem. However the knowledge in this field is far from complete. Research needs are extensive in the field of air cooling systems through the development of advanced heat sink and/or flow distribution schemes. Significant improvements may also be made in the current, state of art indirect cooling systems. In direct cooling systems, literature is sparse and research needs to encompass a broad spectrum. Single and two phase thermosyphons offer excellent opportunities for achieving moderate to large heat fluxes under passive operating conditions. Research is needed to understand related flow and heat transfer effects better and to identify optimal design and operating conditions. Moderate to

large heat fluxes may be achieved under low flow mixed convection conditions, while very large fluxes (200 W/cm^2) require single pha forced convection or forced convection boiling. In each case an improved understanding of related flow phenomena is needed for many possible geometries. Extended surface arrangements that offer significant heat transfer enhancement should be identified. Emphasis should be given on the schemes that minimize adverse effect associated with increased pressure losses and diminished reliability. There is also a need for an improvement in understanding of effects related to the placement of discrete heat source on a substrate. In many cases the flows are three dimensional and conjugate effects are significant. There clearly is a need for experimental as well as numerical work to be done in this field applied to various problems. The general analysis programs that are available are complex and cumbersome. Relatively easy, interactive programs are needed not only for conduction but also for convection and boiling. Accurate airflow analysis codes for both free and forced convection must be able to handle the complex conditions encountered in electronics. Greatly expanded data bases and correlations would help in predicting flow velocities, pressure drops and heat transfer coefficients.

New experimental techniques are also called for especially in the measurement of low-velocity non-isothermal flow, the direct measurement of heat transfer coefficients, mixed convection flows, measurement of semiconductor device temperatures and flow measurements by infrared and optical techniques.

Literature Survey

One of the earliest books on cooling of electronic equipment is by Steinberg (1980). The book deals with empirical rules that must be observed in designing instruments. However it does not have thermal analysis that would predict regions of temperature peaks called as hot spots. Much of the experience in this area has been developed in the industry and this is available in the literature in the form of books (Kakac et al (1985), Kakac et al (1987); Krans and Bar-Cohen (1983); Aung (1983)).

Work has been done on the problem of discrete heat source mounted on a wall. Numerical and experimental results are available on this topic. For symmetrically heated, isoflux surfaces, local heat transfer coefficient have been measured by Siegel and Nom's and both fully developed and entry region solutions have been obtained (Aung, 1972; Aung et al 1972). Experiments performed by Wiotz and Stutzman (1982) yielded a correlation for the maximum plate

temperature which is in good agreement with the predictions of Aung et al (1972).

Conditions corresponding to heating at one plate, with the other plate insulated, have received special consideration. Numerical simulations (Miyatake and Fujii, 1972; Miyatake et al; 1973) as well as experiments (Sparrow et al 1984b; Miyamoto et al, 1986) have been performed for both isothermal and isoflux conditions at heated plate. For modified Rayleigh numbers upto $3x10^{14}$. Miyamoto et al (1986) observed transition to turbulence in upper portion of the channel, with an accompanying enhancement of the local Nusselt No. at the heated isoflux surface.

Afrid and Zebib (1989) have discussed natural convection air cooling of a heated component mounted on a vertical wall. They have carried out a numerical study natural convection air cooling of single and multiple uniformly heated devices. They have used a two dimensional, conjugate, laminar flow model. Effects of component thickness, the spacing between the components, nonpowered components and highly powered components have been studied.

A qualitative flow visualization and quantitative experimental study has been done by Tsang-Yuan Lin and Shon-Shing Hsich (1989) on natural convection heat transfer in vertical channels with asymmetrically placed discrete heated ribs. Both opposing and assisting flows configurations have

been considered. Based on the analyses of photographs and interferograms, it is suggested that turbulent flow should be expected when the local modified Rayleigh number is in the range of 1.29×10^7 to 9.43×10^9. The heat transfer data and flow visualization photographs indicate that the present rib geometry and stratification are two major reasons influencing the temperature of the heated ribs.

Ravine and Richards (1988) have studied natural convection from a discrete thermal source on a channel wall. This paper presents the results of an experimental study of natural convection heat transfer from a discrete thermal source located on the wall of a vertical channel.

Recent studies in natural convection in rectangular enclosures with protruding heaters on one vertical wall are by Kelleher et al (1987). Lee et al (1987) and Liu et al (1987). The first two papers report experimental(Part I) and numerical (Part II) studies of geometric effects of single two dimensional heaters mounted on one adiabatic vertical wall of an enclosure.

Work has been done on the problems involving forced convection. Aung (1983) presented heat transfer measurements for laminar flow past a backward facing step where the step walls are maintained at a constant temperature. Results are given for the local heat transfer distributions as well as the average value for all the step surfaces.

Shou-Shing Hsieh, Huei-Janshih and Ying-Jong Hong (1988) have studied laminar forced convection from surface mounted ribs. The study includes numerical and experimental aspects on low speed forced convection heat transfer near two dimensional transverse ribs in which the walls are held at a uniform temperature.

Early experimental studies of forced convection heat transfer from flush mounted sources are those of Baker (1972, 73), who considered silicon oil and R-113 in parallel flow over small chiplike heaters. Single-phase forced convection coefficients are seen to increase significantly with decreasing surface area and substantially exceed results associated with nucleate boiling as well as predictions based on two-dimensional boundary layer theory. Studies related to heat transfer from an array of discrete isothermal source flush mounted on one wall of a rectangular channel have been performed by Incropera et al (1986).

A common electronic package is one that involves forced air cooling of protruding components on a printed circuit board. Many such boards are stacked in a direction normal to the flow, forming parallel plate channels with the component covered board facing the smooth side of an adjoining board. Despite enormous variability of geometric conditions, systematic attempts have been made

to determine component coefficients and to develop methodologies for determining the effect of a component location in an array. In an early study Buller and Kilburn (1981) obtained heat transfer data for a single rectangular component and successfully correlated the data using a hybrid characteristic length based on features of both the flow and component geometries. In subsequent experiments, Sparrow and co-workers considered an array of component and systematically examined the effect of row number, missing and irregular components and barriers on the average convection coefficient for a single component in the array (Sparrow et al; 1982b, 1984a; Sparrow and Ots, 1985). Lehmann and Wirtz (1985) also considered the effect of rib spacing and channel height by placing ten unheated, repeating ribs upstream of a heated, two dimensional rectangular component. The effect of protruding ribs on flow and heat transfer in channels has been studied by Han et al (1984), Tanasawa et al (1984), Webb and Ramadhyani (1985). Ichimiya (1987) and Kelkar and Patankar (1987).

Under mixed convection conditions the flow is driven by an externally imposed pressure gradient as well as by buoyancy forces. If the channel is vertical, buoyancy acts, to augment or retard the flow, the channel is horizontal and heating occurs at the bottom of surface and buoyancy may induce a secondary flow. Heat transfer enhancement is most pronounced when the channel is horizontal and heat is

transferred from the bottom surface. In experiments performed for laminar flow between asymmetrically heated parallel plates (Osbome and Incropera, 1985) convection coefficients at the bottom plates were found to exceed those corresponding to pure forced convection. Enhancement was due to buoyancy-driven flow which replaced warmer parcels of fluid ascending from the plate with cooler fluid descending from the main flow.

Studies of mixed convection heat transfer from discrete sources are limited to the work of Kennedy and Zebib (1983) and Tomimura and Fujii (1987). For small heater strips flush mounted to the walls of a horizontal channel, Kennedy and Zebib observed the formation of logitudinal and spanwise vortices in air due to heating at the bottom and top surfaces respectively.

It is clear from the above survey that the electronics industry has evolved rules for thermal design based on experience but not analysis. On the other hand, analysis by research groups has been restricted to study of forced, mixed and free convective flow past a single or distributed heaters on a flat horizontal or vertical surface. A few experiments exist to describe flow in the vicinity of the wall heaters. For arrays only experiments exist, though these deal with only the overall thermo-hydraulic behaviour.

The problem of several vertical surfaces adjacent to each other having a distribution of heaters on them has not been studied at the level of details needed to evolve design rules for electronics applications. Certain other features such as the effect of protrusion on the formation of hot spots have not been systematically investigated. There does not appear to be any simple model for the prediction of thermal behaviour of an array of circuit boards.

Scope of Present Work

Work has been done on the problem of natural convection cooling of discrete heat source mounted on a wall. Little work exists on the problem of protruded heaters. The standard solutions available for the problem of flush mounted heater have been found to be inapplicable.

The present work aims at determining the flow patterns and temperature field in arrays of heat generating circuit boards. The circuit boards are modelled experimentally and the relationship between maximum temperature and regime of flow (such as free, mixed or forced convection) are sought to be determined. The effect of wall protrusion on flow and heat transfer are studied. Optical methods are useful in visualizing flow and thermal field and obtaining some of the relevant parameters. They are non-intrusive in nature and have the advantage of calculating local values at a particular point. In the present work interferometry is used to get qualitative information about the flow field

and to a cross check the results obtained by conventional techniques. In particular visualization of isotherms in the space between vertical flat surfaces with a distribution of discrete wall heaters using a Mach-Zhender interferometer is one of the objectives of the present study.

The work reported here is experimental in nature in an area which is vital to the electronic industry. The heat transfer problem is expected to become a serious limiting factor, once the industry starts using large scale integrated circuits and transputers. The work will be helpful in increasing the knowledge-base existing to address the problem of efficient heat removal from electronic systems.

Chapter 2

EXPERIMENTAL SETUP AND INSTRUMENTATION

The problem of interest here is the determination of heat transfer rates in circuit boards geometries since the maximum temperature reached any where in the system depends on them. Heat transfer is strongly controlled by buoyancy-driven motion of air in the space enclosed by circuit boards, by a superimposed draft of air or a combination of the two. In the absence of external flow, air movement arises from a density differential between the light air in the heated area and heavier air of the ambient. The chip is mounted on a circuit board like a protruded heat source mounted on a wall and the circuit boards are stacked parallel to each other in a cabinet. This can be experimentally modelled by a heat source in the form of heated metallic strip mounted on an insulating sheet plates. A second passive plate is kept parallel to the active board to simulate the circuit board array.

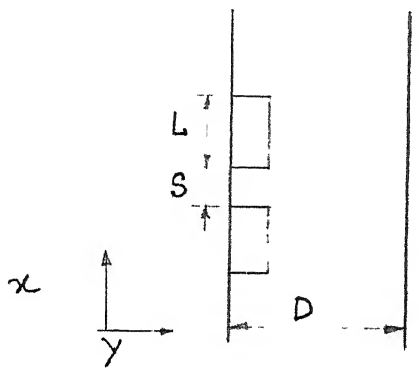

Fig.2.1 : Natural Convection Single Chip 2-D Configurations

The parameters governing the problem are the ratios L/H and H/D, the heating rate of each of the strips mounted on the vertical plates, the relative positions of heaters on adjacent boards and the extent to which they block the flow. In the present study measurement and analysis are carried out for a two & three dimensional heater at steady state.

Design of Experiments

The experiments conducted can be divided into two parts.

(a) Natural Convection Experiments

(b) Forced Convection Experiments

(a) Natural Convection Experiments: Experiments have been carried out for both single chip and multichip heaters. In the experiments with a single chip the heater consists of an aluminium strip. High quality nichrome wire is used to heat the aluminium strip. The resistance of nichrome wire is almost a constant for any change in temperature. The aluminium strip is mounted on a bakelite sheet having a groove cut on it. The strip is attached to the sheet with the help of brass screws. The nichrome wire is wound on a thin mica strip and is kept between the aluminium strip and bakelite sheet in the groove. To avoid direct contact of high temperature nichrome wire with aluminium strip or bakelite sheet, additional mica strips are placed between

nichrome heater and aluminium strips and nichrome heater and bakelite sheet. To prevent the heat transfer to the rear side of the bakelite sheet it is properly insulated on the back side with a thick thermocoal sheet.

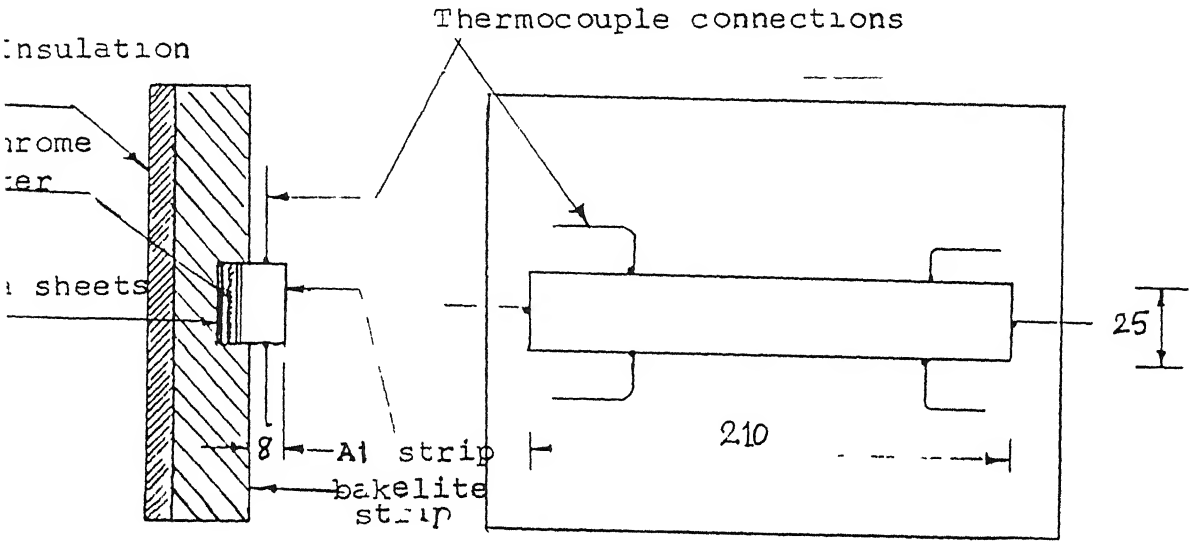

Fig.2.2 : Single chip two dimensional heater

To measure the temperature of heated strips Chromel-Alumel thermo-couples are used. The thermo-couple holes of size 2 mm diameter and 3 mm deep were drilled on the different portions of aluminium strip and the thermo-couple bead is fitted into them. The bead is kept in close contact with the strip.

The passive wall consists of smooth perspex sheet. The bakelite sheet with the heater is mounted on a stand and the passive perspex sheet is kept parallel to it. The distance between the two can be varied by moving the perspex sheet. The whole structure makes an enclosure. The

top and bottom sides of the enclosure are closed with some insulating plate. This setup generate a problem of

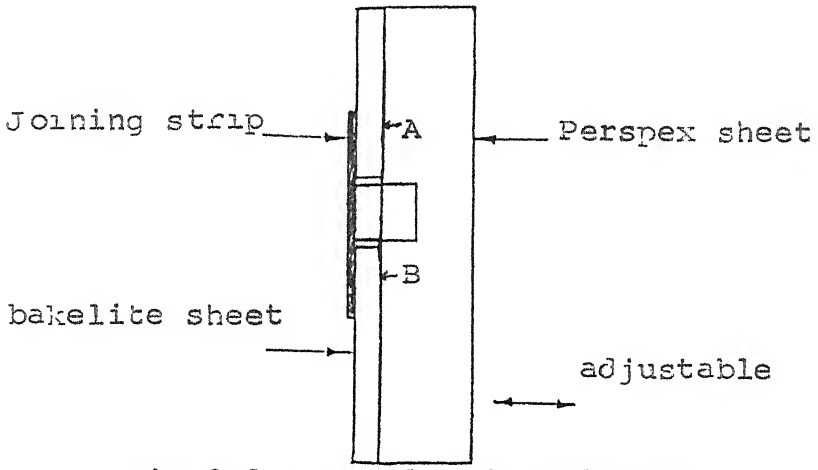

Fig.2.3 : A closed enclosure

conduction of heat from the heater to the bakelite sheet on the sides A and B of the heater. This phenomenon gives a distortion to the assumption of discrete heater mounted on a vertical wall. Moreover the problem of heat convected from the ends C and D of the heater violates two dimensionality of the problem. To avoid the heating of bakelite sheet and three dimensional heat transfer effects the test cell is modified. This is shown in Figure 2.4 . The aluminium strip with nichrome heater is mounted on the central bakelite strip and two more bakelite strips are joined to the central strip with a gap of 3 mm kept between the strips. This air gap between the strips reduces heat conduction of upper and lower sides (A and B) of the heater.

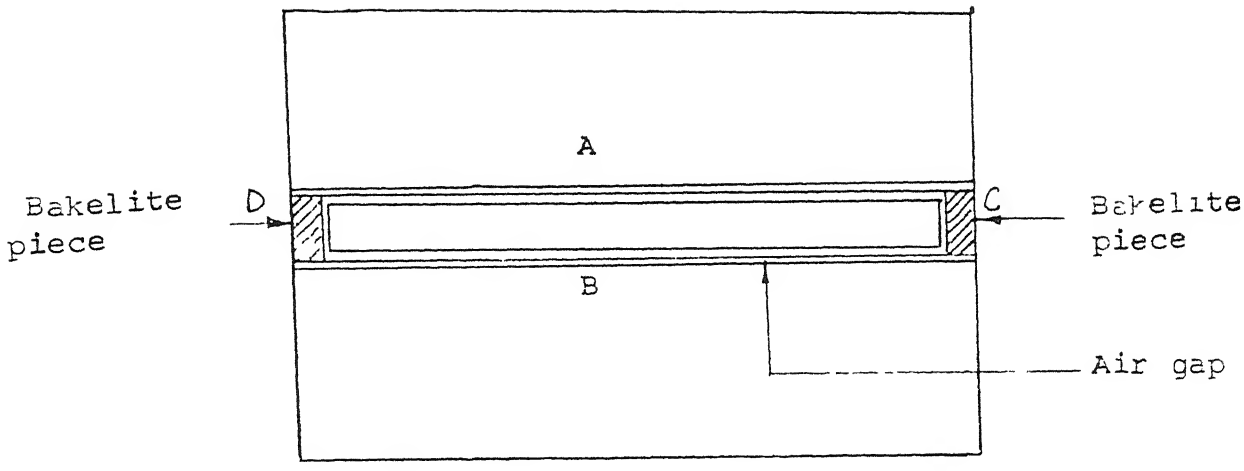

Fig.2.4 : Prevention of conductive heat transfer to supporting sheet

To avoid the three dimensional effect, two bakelite pieces were fixed on the both the ends (C and D) of the aluminium strip. This prevents the air from coming in contact with the heated strip and hence minimizes heat transfer from the ends. The multichip heater test cell consists of three copper strips mounted on the bakelite strips. Nichrome wire is used as a heater as in the single chip test cell. In this setup air gap is used between the two consecutive bakelite strips and bakelite pieces are used to avoid three dimensional effects. Chromel-Alumel thermocouple is used to measure the chip temperature.

To study the effect of a neighbouring wall, a perspex plate is kept parallel to active bakelite plate. The current through the three heaters is controlled by means of a variac. Each heater has independent connections to control the supply voltage.

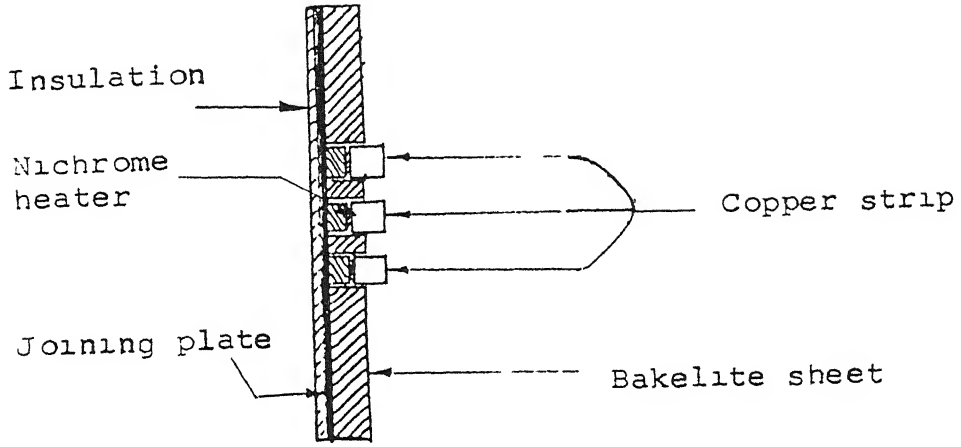

Fig. 2.5

To study the effect baffling the flow inside the enclosure a thin metallic strip is used. The metallic strip can be mounted anywhere inside the test cell by pasting it on the wall. The length of metallic strip is chosen to be

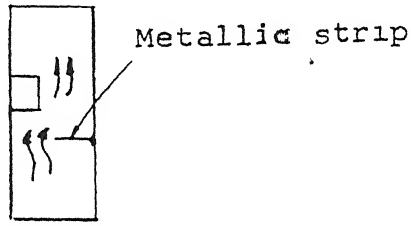

Fig. 2.6

equal to the length of heater. Larger lengths could block the mean flow and smaller lengths could be ineffective.

Forced Convection Cooling

A test cell has been fabricated to study the problem of forced convection cooling of electronic circuit boards. The test cell fabricated was vertical in orientation so as to have combined forced and mixed convection effects. It can be classified as an open circuit, and low speed wind tunnel. Figure 2.7 shows the overall view of the test

cell. The material used to construct the wind tunnel is perspex. The main parts of test cell are:

a. Entrance Cone
b. Honey comb and filter
c. Test section
d. Contracting adapter
e. Centrifugal blower
f. Rotameter.

a. Entrance Cone: Entrance cone has two parts, settling chamber and contraction cone (Fig. 2.8). Flow from the filter enters the settling chamber and becomes stable before entering the contraction cone. Small eddies formed by the screen and honey comb gradually decay.

Contraction Cone: Flow from the settling chamber enters the contraction cone. The contraction cone is a gradually converging cone. The decrease in cross-section takes place very smoothly. It decreases the free stream turbulence, increases the velocity and keeps boundary-layers thin. The contraction ratio in this test cell is 4.

b. Honey Comb: Honey combs are used to suppress the level of free stream turbulence that comes as input flow. The transverse component of velocity is suppressed when the flow passes through honey comb. Due to growth of shear instability and subsequent randomization of eddies, turbulence is

generated at the tips of honey comb cells. But this high frequency turbulence decays rapidly with the distance resulting in a net suppression of free stream turbulence by honey combs. The flow observes a small pressure drop while passing through the honey comb. The honey comb used in this test cell has a dimension of 500 mm x 250 mm x 75 mm.

Filter: A fine mesh screen is placed at the downstream of honey comb. It helps in the suppression of turbulence level.

c. Test Section: After the contraction cone the flow enters the test section. Some length is provided for the turbulence to decay. The area of the test section is 250mmx125mm. It has openings for locating static taps and inserting other probes. The test object that is single chip or multichip heater can be placed inside the tunnel. On one wall of test cell a recess is made to accommodate the heater which is mounted on the bakelite sheet. On the back side of the heater an air gap is used to prevent energy loss to the ambient. The heater assembly can be mounted on the wall of the wind tunnel with the help of screws. The connecting wires for heater and thermocouple are taken out from the back side of heater through a hole mode in the perspex sheet.

Inside the test section a perspex plate is placed parallel to the heater assembly to study the effect of the neighbouring wall. The distance between the heater assembly

and this perspex plate is kept adjustable. The end of this perspex plate facing the incoming flow is wedge-shaped so that the mean flow is disturbed to a minimum.

On the sides of the test section slots are made to have a provision for optical windows. To do the interferometric studies optical windows are required. Ordinary glass can not be used as windows for interferometric studies because it produces its own effects on light beam. A high quality polished glass is used as an optical window. The size of the glass is 50 mm x 50 mm. It is fixed in a perspex frame and can be slided over the slot. When interferometry is not done, the slots can be covered with an ordinary perspex sheet. Figure (2.9) shows the test section of wind tunnel.

d. Contracting Adapter:

It joins the test section with the blower opening. Since the dimensions of test section are quite large a contracting adapter is made. The area contraction ratio for adapter is 15 and height is 40cm.At the top end of the adapte piece of metallic pipe (diameter 2.5 cm) is fixed. This pipe is connected to the blower by a PVC flexible pipe.

e.Centrifugal Blower: The blower sustains the velocity up to 0.65 m/s in the wind tunnel. The specifications are given

below.

Specifications

Outlet - Radial

Voltage rating - 240 V

Current - 3.5 A

Discharge - 20 m^3/min

Power rating - 750 W

f. Rotameter: Both pitot tube and rotameter are used to measure the velocity in the wind tunnel. Since the cross-sectional area of wind tunnel is large the maximum velocity reached with above mentioned blower was 0.65 m/s. In electronic equipment the air velocities encountered are of similar order. Measurement of velocity as low as 0.15 m/s with a pitot tube is difficult. To make the measurements possible at such low velocities a low discharge rotameter is used. The rotameter capacity is 10 litres/sec. which corresponds to approximately 0.5 m/s velocity. Hence it was possible to measure the velocities on the lower side with the help of the rotameter. When measuring higher velocities the rotameter is kept out of circuit.

Instrumentation

The experiments involved instruments for the measurement of current, resistance, voltage, temperature, pressure, velocity, turbulence. For interferometry a Mach-Zhender

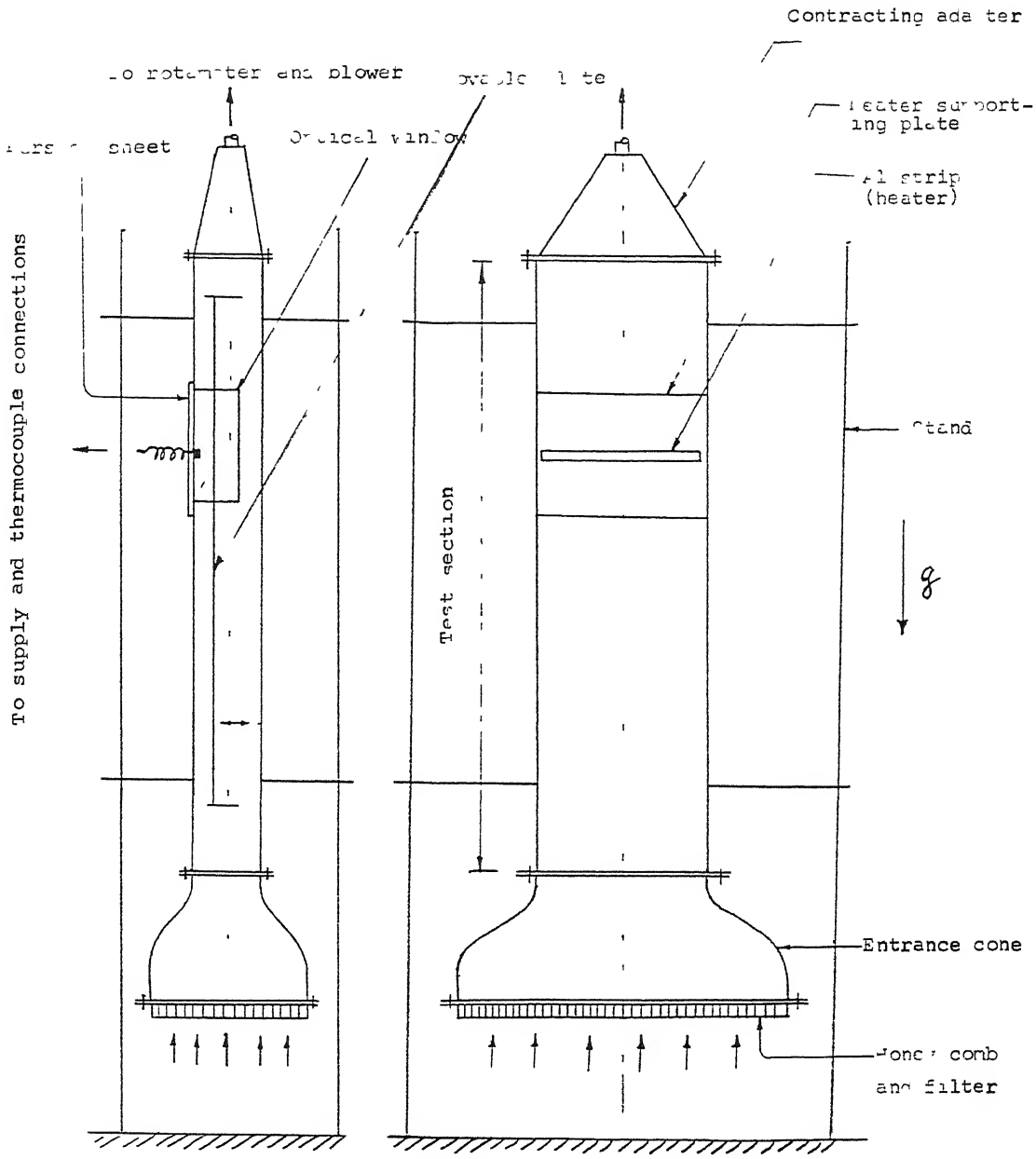

Fig.2.7 . Line diagram of flow apparatus

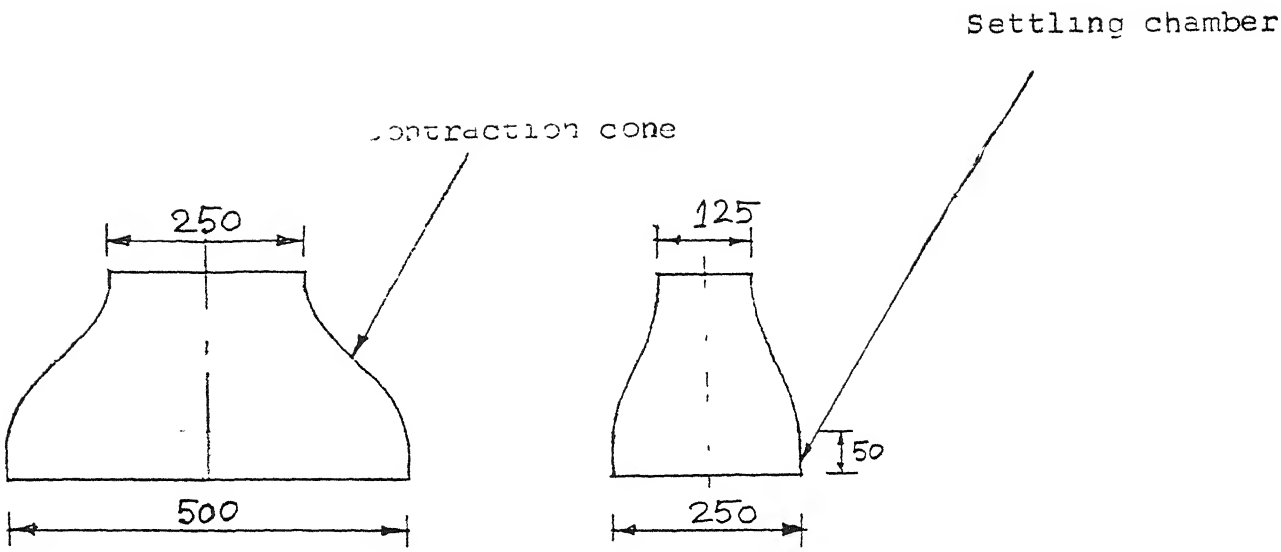

Fig.2.8 : Entrance cone

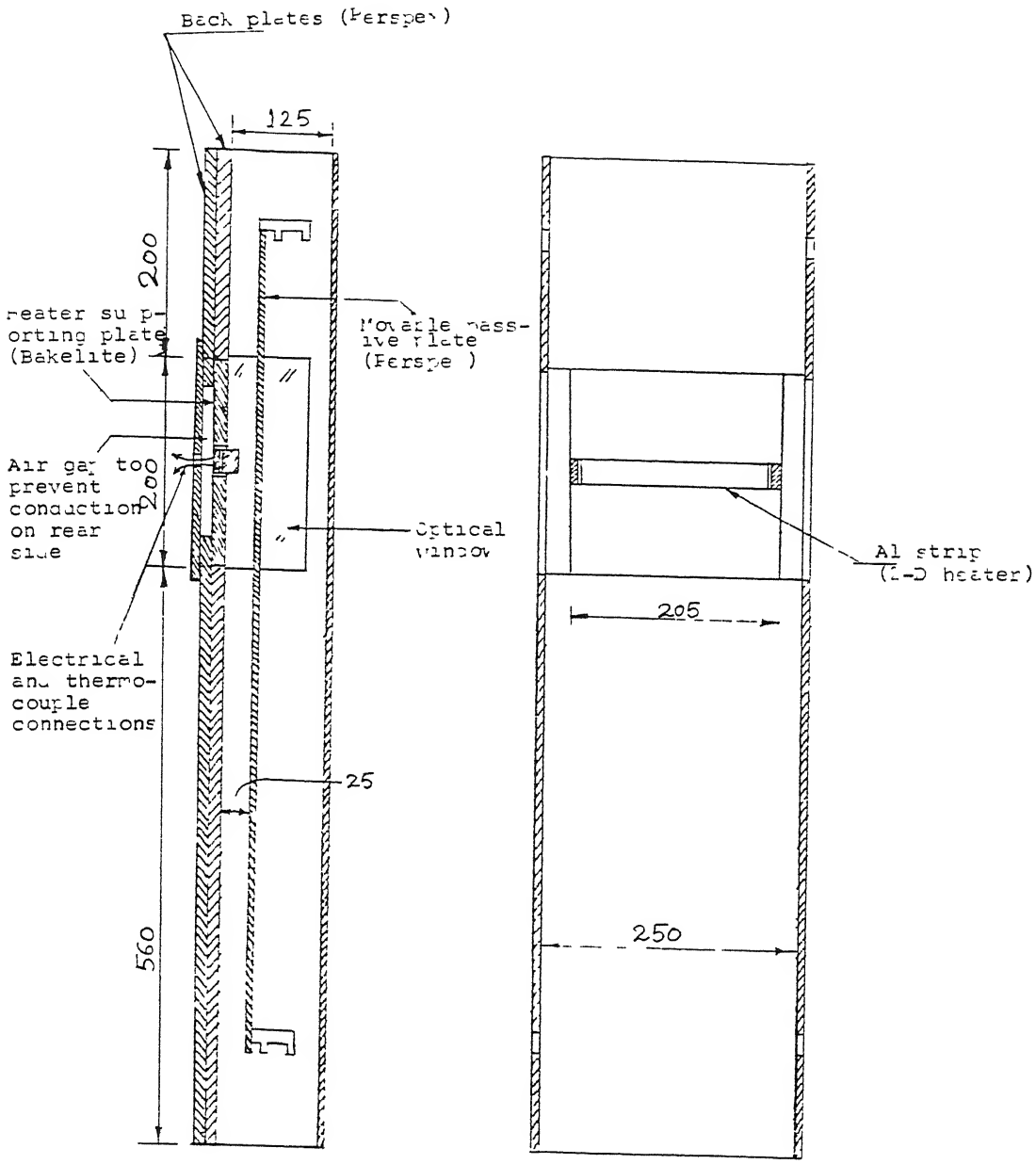

Fig. 2.9 : Test section of flow apparatus

interferometer having laser beam as a source of light is used.

Measurement of Electrical Quantities

Measurement of current, resistance and voltage was carried out with digital multimeter. The multimeter used were:

(a) Meco model 9A digital multimeter

Specifications:

Operating Principle	:	Dual Slope integration
Range	:	100 V DC, 750 V AC and 10A AC/DC
Power Supply	:	Two polarity
Display	:	LCD
Accuracy	:	AC Voltage: ± 1.5% of input + 8 counts
		DC Voltage: ± 1% of input + 4 counts
		Resistance: ± 0.7% input + 4 counts
		Current : ± 2% of input + 4 counts

A more sensitive and versatile multimeter was used to measure the millivolts generated by thermocouples in some experiments.

Make : Hewlett Packard

Model : 3457 A.

It has seven functions with $3\frac{1}{2}$ to $6\frac{1}{2}$ digits of resolution extendable to $7\frac{1}{2}$ digits at reading rates from 1 reading every 2 sec. to 1350 readings/sec. It has seven functions - dc acV, acI, dcI, Ohms, frequency and period.

Operating Temperature:	0 to 55°C	
Accuracy	: DC voltage - 0.0050%	+ 7 count
	AC voltage - 0.2%	+ 280 counts
	DC current - 0.07%	+ 604 counts
	AC current - 0.35%	+ 280 counts
	Resistance - 0.0045	+ 34 counts
	Frequency - 0.01%	

Variacs are used to step down the voltage. To stabilize the supply, two variacs in series are used. Voltage stabilizers of the servo-type are used to prevent under and over the voltages in the input. To protect the sensitive instruments from overloading a ferromagnetic type voltage stabilizer is used.

Measurement of Temperature

Thermocouples are used for the measurement of temperature. The thermocouples used are 18 gage K type thermocouple made of Chromel and Alumel. The thermocouples are formed by gas welding. Each thermocouple is individually tested against an standard thermocouple having ice point as a reference junction. Variation upto $\pm$0.1% are possible among the thermocouples over the range of temperature covered in this study. The thermocouples were connected to the 30 channel hybrid recorder. The description of which is

given below.

Hybrid Recorder

It has a capacity of taking input data from 30 channels simultaneously. It can be used for various types of thermocouples over a wide range of temperature. The reading can be displayed directly in the terms of emf generated or can be displayed in terms of temperature. It uses internal compensation instead of the ice point as a reference junction. There is no need to have ice point as a reference junction or adding the mV corresponding to room temperature every time. It can display the variation in temperature with time in the form of a graph. The data can be stored in the form of a graph. The data can be stored in the memory and can be printed. The instrument can be connected to a computer over a GPIB interface.

Specifications

Thermocouple type - K

Measurement range = - 200 to 1370°C

Resolution = 0.1°C

Accuracy = ± 0.07% reading ± 0.8°C

Thermocouple type - J

Measurement range = -200 to 1200°C

Resolution = -0.1°C

Accuracy = ± 0.07% ± 1.0°C

Ambient temperature 23±5°C, Humidity 80% or less

Measurement temperature unit - $^{o}C/^{o}F$ selectable

Reference contact correction - Internal/External selection possible.

The other temperature measuring device used was digital thermometer.

Make and Model - Therm 2280-3

Temperature range-

Ni(Cr) - Ni(K)	:	-200 to 1370^{o}C
Fe-Cu-Ni (U)	:	-200 to 600^{o}C
PtRh 10-Pt(S)	:	0 to 1760^{o}C
NTC	:	-30 to 80^{o}C
Resolution	:	0.1 K (thermocouples)

It is easily portable and gives the readings very accurately.

Pressure and Velocity Measurement

For pressure and velocity measurement a pitot tube connected to a sensitive manometer was used. This manometer can measure very low velocities and hence flow measurements could be performed in the mixed convection region.

Make - Furness Controls Limited

Maximum ΔP - 19.99 pascals

Velocities below 0.2 m/s are difficult to measure with a pitot tube. To measure the velocity in this range a rotameter is used. The discharge of rotameter varies from 0 to 10 lit/sec. The maximum discharge corresponds to a velocity of 0.5 m/s in

the tunnel.

Turbulence Measurement

While testing the wind tunnel the turbulence level was measured with the help of an rms voltmeter. The rms voltmeter gives the voltage corresponding to fluctuating component of velocity. The dc voltage corresponding to mean velocity can be taken out from manometer. The ratio of rms voltage to the mean voltage gives the turbulence level.

Specifications of rms voltmeter used are -

Make	- Hewlett Packard
Frequency response	- 10 Hz to 10 MHz
Range	- 1 mV to 300 volt (12 ranges) and -72 to +52 dBm.

Interferometry

The interferometric study was carried out using a Mach-Zhender interferometer. The Mach-Zhender interferometer is a popular instrument used in experimental studies of heat transfer in fluids.

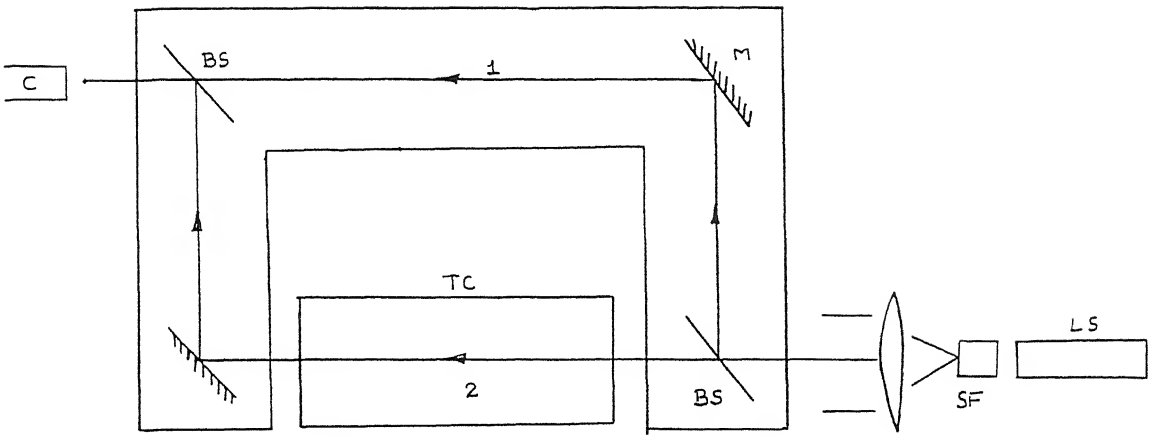

LS - Laser C - Camera

SF - Spatial filter 1 - reference beam

L - Lens 2 - test beam

M - Mirror TC - test cell.

Fig. 2.10

Laser is used as a coherent monochromatic light source. The laser beam passes through a spatial filter. Spatial filter expands the beam which is then passed through a convex lens which makes it parallel. The beam goes through the beam splitter. The beam splitter is semipolished mirror which allows 50% of tight to go through it and reflects remaining to a mirror. Unreflected part of beam passes through the heated test section and then falls on mirror which reflects it at 90°C. The other half of the beam reflected from beam splitter also falls on a mirror which reflects it at 90°. Finally the reference beam and test beam combine at the second beam splitter where the interference patterns are formed.

These interference patterns can be recorded by a field camera and the analysis is done. Quantitative experiments are possible when the temperature field is uniform parallel to the beam direction. Otherwise the test beam averages the temperature field as it traverses the test cell and only qualitative information can be obtained. The fringe pattern obtained can be directly scanned by a ccd camera coupled with an image processing equipment. The film can be recorded in the memory of computer and can be obtained on the screen of monitor. The analysis can be directly done through software. In the present study all the fringe analysis is done manually using a low magnification microscope.

Testing

Testing in natural convection experiments involved testing of thermocouples and testing of the heater element. Each thermocouple is cleaned and tested against the ideal thermocouple with an ice junction as reference point. A thermocouple showing a widely different response is rejected. Before experiments the heater element is tested several times. It is ensured that the bakelite plate withstands the temperatures encountered during the experiments. This can be as high as 150^{o}C. Proper insulation is provided on the rear side and it was made sure that no significant rise in temperature takes place at the surface of insulating material exposed to the ambient.

In forced convection experiments the testing of the flow apparatus is important. The test cell is examined for the leakages, pressure drop, turbulence level and velocity profile. The openings, slits or holes, if any were sealed properly with the foam packing and tape to prevent any leakage of air from outside.

When tested for pressure drop it is found that the pressure drop was very low across the honey comb. Most of the resistance to flow occurred in the converging adapter and the pipe connecting the adapter to the blower.

The turbulence level was measured using pitot tube connected to a manometer and a rms voltmeter. The maximum turbulence level was 2.5% at the low velocity of 0.24 m/s but as the velocity was increased the turbulence level was found to decrease. At the high velocity of 0.67 m/s the turbulence level was 1.0%. These values of turbulence levels are acceptable at such low velocity ranges. This is because for weak flows it is difficult to protect them from the external influences. This turbulence level includes the flow disturbances due to the movable plate, fluctuations in voltage supply and the vibrations caused by the blower. The table gives the value of turbulence level with velocity. The turbulence level can be seen to be constant in the direction perpendicular to wall.

As the velocity changes the boundary layer thickness changes. At lower velocities the boundary layer thickness is large and the heater is under the influence of boundary layer. It is difficult to estimate the effect of this varying velocity profile on heat transfer. Heat transfer rates are also different over the different parts of heater. Here we have not taken the velocity profile and boundary layer effects into consideration and it is fairly accurate to assume the velocity in the centre of channel as the reference velocity for calculating the Reynolds number over the heater. The reason for this is explained below.

The front face of heater is the region where most of the heat transfer takes place. The upstream region of heater is, to some extent, a stagnant region not affecting the overall heat transfer much. Enveloping of this region inside the boundary layer does reduce the heat transfer but a corresponding increase takes place on the front surface of heater because of increase in velocity as the area reduces in that region. The effect of upstream face of heater being subjected to a reduced velocity is thus compensated. Moreover because of protrusion the front side of heater is subjected to the velocities prevailing in the central portion of channel. Due to the combined effect of these two factors it is reasonable to assume that the velocity in the central part of the channel is the velocity having maximum influence on heat transfer.

This is also the reason of choosing length L of front side as the characteristic length in this work.

The shape of the velocity profile does not seem to affect the heat transfer much. This has been shown by Hsieh et al (1988) in their numerical work. We have also seen similar effects in the numerical calculation of the Nusselt over a flush mounted heater. These results have been presented in the Chapter 4.

Turbulence Measurement

Probe Near the Wall

Velocity m/s	Mean DC voltage	rms voltage	% Turbulence
0.24	0.23	0.006	2.60
0.33	0.30	0.007	2.30
0.37	0.34	0.007	2.00
0.42	0.38	0.0075	1.97
0.47	0.43	0.008	1.86
0.52	0.46	0.0065	1.41
0.57	0.50	0.007	1.40
0.61	0.53	0.006	1.13

Probe in the Middle of the Test Section

Velocity m/s	Mean DC voltage	rms voltage	% Turbulence
0.28	0.24	0.006	2.5
0.32	0.28	0.008	2.85
0.40	0.34	0.006	1.76
0.47	0.41	0.0065	1.58
0.51	0.45	0.007	1.55
0.55	0.50	0.006	1.2
0.60	0.54	0.0065	1.2
0.64	0.56	0.0055	0.98
0.67	0.59	0.006	1.0

The maximum temperature encountered in the experiments is nearly 150^{o}C. So a wide range of ΔT has been covered. In natural convection experiments with a heater of AR = 3, the Rayleigh number varies from 2000 to 70000. With smaller of aspect ratio this range is narrowed. The maximum value of input heat flux is limited by the maximum temperatures reached and the power drawn.

In forced convection experiments with larger heater the range of Reynolds number covered is from 0 to 1050. With

smaller heater the range is reduced from 0 to 600. Maximum velocity encountered is 0.65 m/s.With the protrusion mounted on the opposite wall the resistance to flow is increased and the maximum velocity reached reduces to 0.5 m/s.

The fluid Prandtl number varies from 0.7 to 0.8. Two cases for aspect ratio 2 and 3 have been considered.

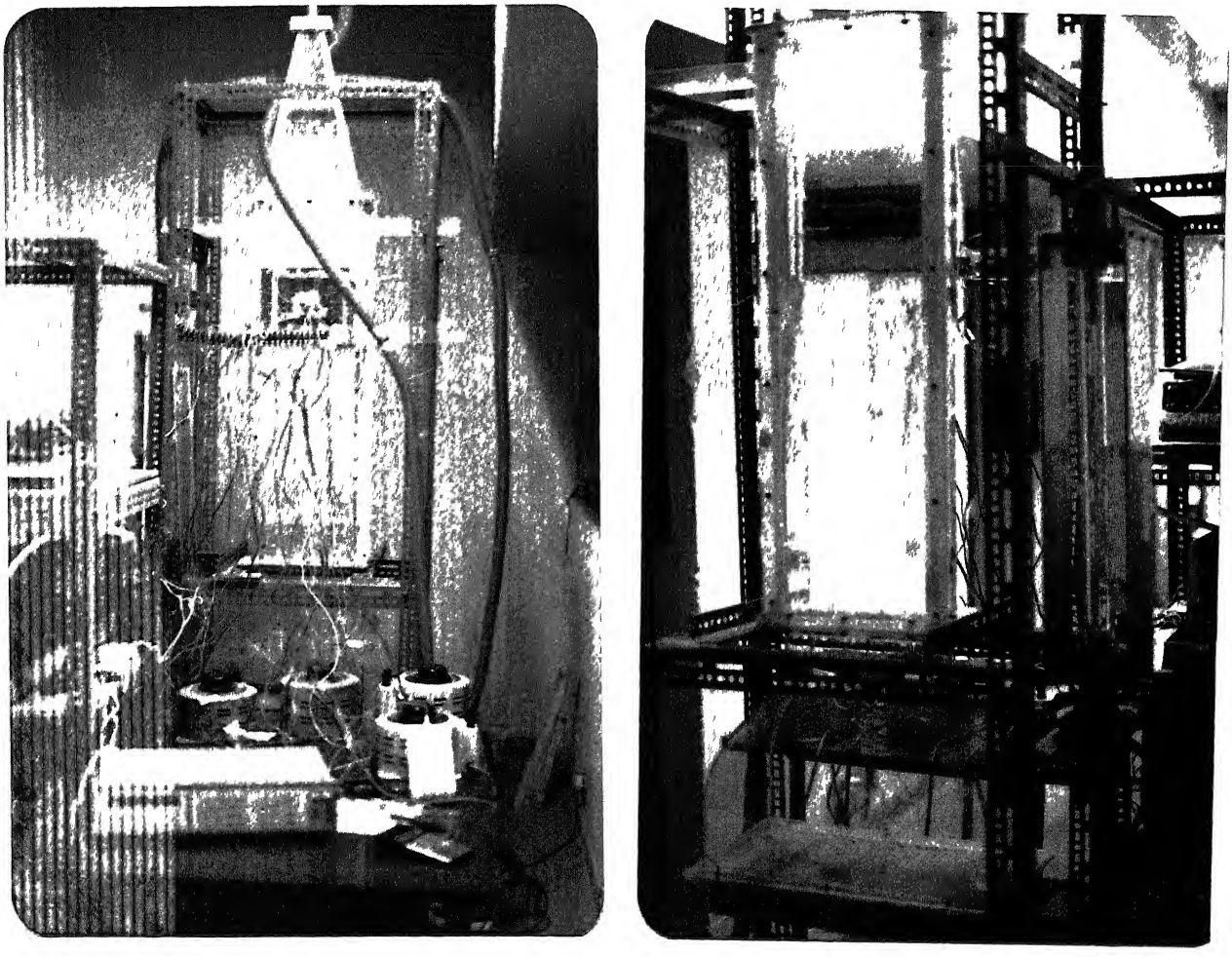

Figure 2 11 : Test cell for forced convection experiments

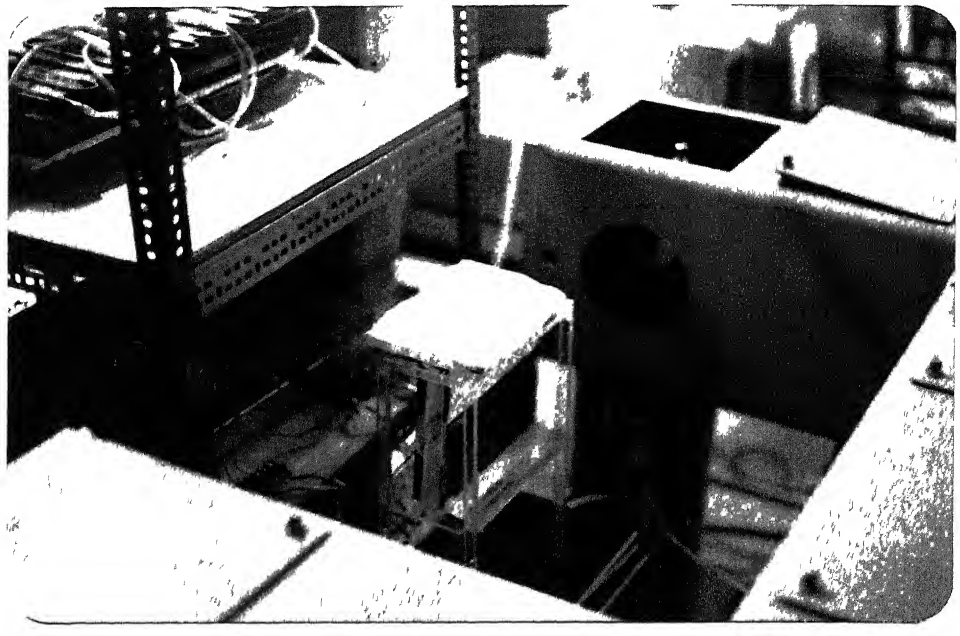

Fig 2.12 Single chip natural convection test cell in the path of test beam

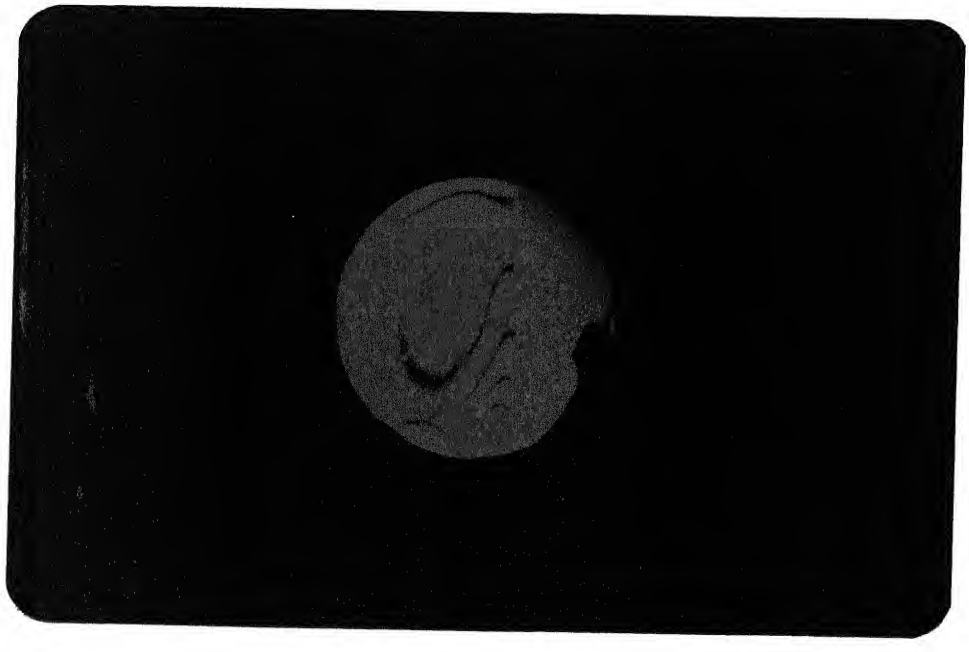

Fig. 2.13 : Fringe pattern obtained on screen

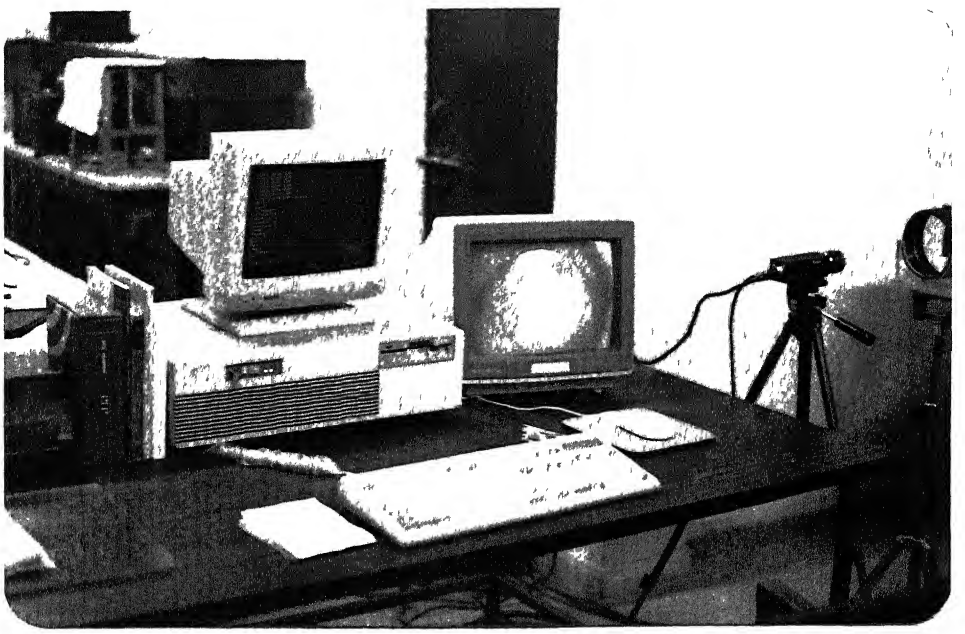

Fig 24. Image Processing

Chapter 3

PROCEDURE AND DATA REDUCTION

We describe below the procedure for natural convection experiments, procedure for forced convection experiments and data reduction for interferometry.

Natural Convection Experiments

The heater located behind the aluminium chip is supplied voltage through a variac connected to a servo-stabilizer. The supply voltage to the heater is kept stable to within $\pm 2\%$. The heater is allowed to reach the steady state. The steady state is reached in approximately 3 hours from a cold start. Steady state is assumed to be reached when the rise in temperature of the chip is less than 0.5% over a half-an-hour period. To accommodate the variations in input supply and variation in response of the individual thermocouple temperatures and voltages are averaged at steady state with data at 5 minute intervals. This averages out minor variations in power input and temperature with time. The strip is instrumented with six thermocouples. The temperature of the strip is taken as the average of all the thermocouple readings. This compensates any variation in temperature over the surface of chip. It can be subsequently assumed to be at a uniform mean temperature. At every step the room temperature is recorded with the digital thermometer. All the experiments are conducted in

an airconditioned room maintaining a fairly constant room temperature. The test cell is protected suitably from the external air currents.

The procedure for multichip experiments is similar to the single chip experiment except that in the case of multichip heater the temperature of all the chips is recorded and the power supplied to the chips is controlled individually.

Forced Convection Experiments

In forced convection experiment the heater plate is mounted in the flow apparatus in a vertical configuration. The electrical power is once again supplied to the heater through the servo-stabilizer variac. The heater is then allowed to reach steady state. All the readings at steady state corresponding to free convection are recoded. The blower is then switched on inducing a flow in the wind tunnel. The blower is made to run at constant speed by controlling its input voltage. This corresponds to a constant mean velocity in the test cell. The temperature of the chip drops due to an increase in heat transfer at its surface. The chip is again allowed to reach steady state. This takes about 2 hours. The temperatures are recorded at steady state as in the natural convection case by averaging over a period of time. Experiments are conducted for various values of the input heat flux for a range of air velocities.

Interferometry

The interferometer is first adjusted in the infinite fringe mode or the wedge fringe mode depending on the requirement. The test enclosure mounted on a stand is placed in the path of the test beam. As the strip gets heated a fringe pattern is obtained on the screen. The photographs are taken during the transient evolution of free convection. The photographic film can be developed in the laboratory itself. The fringe pattern is recorded on an image processor as well. The image can be enlarged and viewed. The fringe pattern has been analyzed in this study under a low magnification microscope. The microscope has a traversing mechanism in two perpendicular directions. The distance between two fringes or the slope of the fringe can be measured and the heat flux can be obtained. Nusselt number obtained by interferometry can act as a cross check for the Nusselt number obtained by the energy balance method. The behaviour of flow and temperature field is also studied in the vicinity of the heated strips using the fringe patterns.

Data Reduction

The resistance of every heater is measured before experiment. Heat input is given by

$$Q = \frac{V^2}{R}, \quad W$$

where V is mean voltage applied (volts), R is resistance of heater (Ohms). Let A (m^2) be the area of strip exposed to ambient. The heat flux q is

$$q = \frac{V^2}{AR} \quad W/m^2$$

Let the temperature of heated strip be T_c and the temperature of ambient be T_{∞}.

Heat transfer coefficient h is determined as,

$$h = q/(T_c - T_{\infty}) \quad W/m^2K$$

Let L be the characteristic length of heater. It is the strip length vertically in the present study.

Let k be thermal conductivity of air. The Nusselt number is calculated as

$$Nu = \frac{hL}{k}$$

The Rayleigh number is calculated as

$$Ra = \frac{g\beta\Delta T\, L^3}{\nu\alpha}$$

Here ρ is the density of air

$\Delta T = T_c - T_{\infty}$

$\beta = 1/(T_c+273)$ $1/K$

ν = Kinematic viscosity of air (m^2/sec).

α = is the thermal diffusivity of air (m^2/sec).

(All the fluid properties are calculated at the mean temperature $(T_{chip} + T_{room})/2$). Further g is the gravitational constant (= 9.81 m/sec^2), and L is the characteristic length of the heater.

In forced convection experiments Reynolds number is calculated along with Nusselt number and Rayleigh number. A calibration curve is drawn between the velocity in the wind

tunnel and the voltage applied to blower. The velocity in the wind tunnel is measured with pitot tube connected to the manometer. Once the calibration is done the pitot tube is taken out.

Reynolds number is calculated as

$$Re = \frac{U.L}{\nu}$$

Nusselt number and Rayleigh number are calculated as in the previous experiments.

Calculation of Nusselt Number by Interferometry

When the initial setting of interferometer is in infinite fringe mode then each fringe obtained on the screen represents an isotherm. The change in temperature for each fringe width spacing is given by

$$T = \lambda / (1 \frac{dn}{dT})$$

n is refractive index of medium, λ is the wavelength of light source (He-Ne laser source in this case). 1 is length of test section parallel to light-beam. In air $|\frac{dn}{dT}| = 0.927 \times 10^{-6}/^{o}C$.

For a He-Ne laser $\lambda = 632.8$ nm. It can be shown that the temperature per fringe shift is

$$T = 0.67/1 \ ^{o}C/m.$$

If ε be the fringe spacing then the local heat flux is given by

$$q(x) = k \frac{0.67/l}{\epsilon(x)}, \quad W/m^2$$

can be measured under a microscope and the average heat flux is

$$\bar{q} = \frac{1}{L} \int_0^L q(x)\, dx$$

where L is the length of the heater vertically.

$$\text{Nusselt Number, } Nu = \frac{\bar{q}}{(T_c - T_\infty)} \frac{L}{k}$$

$$Nu = \frac{1}{(T_c - T_\infty)} \cdot \frac{L}{k} \cdot \frac{1}{L} \int_0^L q(x)\, dx$$

$$Nu = \frac{1}{(T_c - T_\infty)} \frac{L}{k} \frac{1}{L} \int_0^L \frac{k \times 0.67}{\epsilon(x)\, l} dx$$

$$Nu = \frac{0.67}{l\,(T_c - T_\infty)} \int_0^L \frac{dx}{\epsilon(x)}$$

This method is suitable when the number of fringes are small i.e. temperature gradients existing are not very large. When the temperature gradient is large near the hot surface then many fringes are formed at the surface of heated strip. For the calculation of heat flux at the surface the fringe spacing closest to wall is measured. In the case of high temperature gradient the distance is too small to be measured or in other words it becomes difficult to distinguish among fringes. To overcome this problem another approach is used.

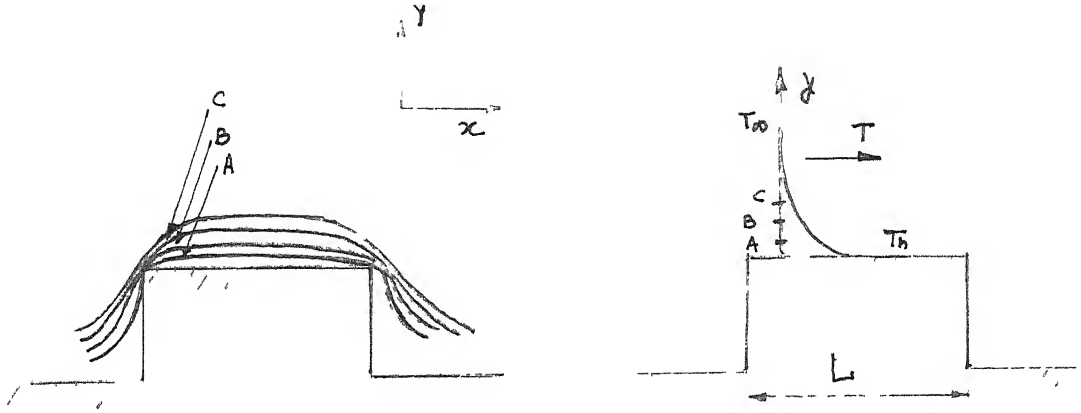

Fig. 3.1

The temperature at the hot surface is known (T_c). Some fringes away from the heated wall are chosen. The fringes are chosen at a point where the fringe spacing can be measured conveniently. Since each fringe width corresponds to a fixed temperature difference, the temperature corresponding to fringe A, B and C can be found out by counting the number of fringes formed from the surface of strip. The temperature T_A, T_B and T_c are known. The distance of the fringes A, B and C is measured from the wall. T_A be the temperature at a distance y_1, T_B be the temperature at a distance y_2, T_c be the temperature at a distance y_3.

A curve can be fitted passing through these points.

Let $T = T_h + ay + by^2 + cy^3$ then

$$T_A = T_h + a y_1 + by_1^2 + cy_1^3 \quad (1)$$

$$T_B = T_h + a y_2 + by_2^2 + cy_2^3 \quad (2)$$

$$T_C = T_h + a y_3 + by_3^2 + cy_3^3 \quad (3)$$

This is a system of simultaneous equation having a, b and c as unknown quantities. These equations can be solved to get the values of a, b and c. The heat flux at the surface is proportional to the temperature gradient at the surface and is given as,

$$q_{surface} = - k \left.\frac{\partial T}{\partial Y}\right|_{y=0} = ka$$

This gives the heat flux locally at any point. To obtain average heat flux

$$\bar{q} = \frac{1}{L} \int_0^L k\, a\, dx$$

$$\bar{q} = \frac{k}{L} \int_0^L a\, dx$$

Nusselt number $$Nu = \frac{\bar{q}}{(T_h - T_\infty)} \quad \frac{L}{k}$$

$$Nu = \frac{\int_0^L a\, dx}{(T_h - T_\infty)}$$

The value of 'a' can be integrated over the whole width L and average value of Nu can be found out.

The table 3.1 presents the values of voltages and temperature taken at steady state. Each voltage reading was taken after 5 minutes.

Mean voltage $V = 10.84$ volts

Mean chip temperature $T_c = 43.15\ ^{o}C$

Mean room temperature $T_{\infty} = 29.67\ ^{o}C$

Resistance of heater = 69.2 Ohm

$$T_m = \frac{T_c + T_{\infty}}{2} = \frac{43.15 + 29.67}{2} = 36.41$$

$$Q = \frac{V^2}{R} = \frac{(10.84)^2}{69.1} = 1.70\ W$$

$$q = \frac{Q}{A}\ ,\ A = 7.985 \times 10^{-3}\ m^2$$

$$q = \frac{1.7}{7.985 \times 10^{-3}} = 212.89\ W/m^2$$

$$h = \frac{212.89}{(T_c - T_{\infty})} = 212.89/13.48 = 15.79$$

$Nu = \frac{hL}{k}$ (k is thermal conductivity of air at mean temperature. The value can be taken from table)

$k = 27.00 \times 10^{-3}$ W/mK

$Nu = 14.618$

$$Ra = \frac{\beta g \Delta T L^3}{\nu \alpha}$$

$\rho = 1.139\ kg/m^3$

$g = 9.81\ m/sec^2$

Table 31:

Ch.No.	V=10.85	V=10.8	V=10.81	V=10.79	V=10.8	V=10.94	V=10.95	Mean V=10.84	V Mear V=10.8
1	42.5	42.7	42.9	43.0	43.0	43.1	43.3	42.92	
2	42.9	43.2	43.3	43.4	43.5	43.6	43.7	43.37	
3	42.6	42.8	42.9	43.0	43.5	43.3	43.3	43.01	Mean Temper
4	42.7	43.0	43.1	43.3	43.4	43.5	43.5	43.21	= 43
5	42.8	43.1	43.1	43.3	43.4	43.4	43.6	43.24	

$$\beta = \frac{1}{T_c} = \frac{1}{(36.41 + 273)} = 3.231 \times 10^{-3}/K$$

$$\nu = 1.661 \times 10^{-5} \ m^2/sec$$

$$\alpha = 2.35 \times 10^{-5} \ m^2/sec$$

$$L = 2.5 \ cm$$

$$Ra = 1.69 \times 10^{4}$$

Forced Convection Experiment

The data for the sample calculation is given in the table 32

$$q = \frac{V^2}{RA} \ W/m^2$$

V(volts) is voltage applied to heater, V = 29.5

$A(m^2)$ is the area of strip exposed to atmosphere

$A = 7.74 \times 10^{-3} \ m^2$

R = 110.8 Ohm

L = 2.5 cm

$$q = \frac{(29.5)^2}{110.8 \times 7.74 \times 10^{-3}} = 1014.7 \ W/m^2$$

Velocity = 0.15 m/s

$T_c = 58.25^{\circ}C$

$T_{\infty} = 19.1^{\circ}C$

$T_{mean} = \frac{58.25 + 19.1}{2} = 38.67^{\circ}C$

$\beta = \frac{1}{331.25} /K$

All the fluid properties are evaluated at mean temperature,

$$Nu = \frac{hL}{k} \quad , \quad h = \frac{q}{\Delta T}$$

$$h = \frac{1014.7}{(58.25-19.1)} = 25.91 \ W/m^2K$$

$$Nu = 23.87$$

$$Ra = \frac{\rho g \Delta T L^3}{\nu \alpha} = 45377.4$$

$$Re = \frac{UL}{\nu} = \frac{0.15 \times 0.025}{1.661 \times 10^{-5}} = 225.6$$

	Heater voltage	Variac voltage	Velocity m/s	Chip temp, ^{o}C	Room temp, ^{o}C	$q = \frac{V^2}{RA}$ W/m^2	Re	Nu	Ra
1	29.6	0	0	63.95	19.0	1021.6	0	20.92	49381.3
2	29.5	75	0.15	58.25	19.1	1014.7	225.6	23.87	45377.4
3	30.2	90	0.22	56.6	19.5	1063.4	330.9	26.45	43532.8
4	29.3	120	0.33	53.5	20.0	1001.0	496.3	27.67	40290.2
5	29.3	140	0.38	53.4	20.7	1001.0	571.6	28.33	39202.0
6	29.1	160	0.43	51.65	21.0	987.4	646.8	29.87	37258.0
7	29.2	180	0.48	53.6	23.63	994.0	722.0	30.24	35713.2
8	28.5	206	0.54	50.45	22.8	947.0	812.2	31.73	33617.3
9	29.8	225	0.595	52.25	24.1	1035.5	895.0	33.93	33423.9
10	29.3	240	0.63	51.9	24.6	1001.0	947.6	33.82	32421.2

Calculation of Nusselt Number by Interferometry

We do a sample calculation for obtaining the temperature profile and thereby the Nusselt number through curve fitting.

The power input $q = 564.72 \ W/m^2$

Temperature of heated surface $T_c = 48.7^{\circ}C$

Ambient temperature $= 18.1^{\circ}C$

Three fringes away from the heater are selected where the fringe spacing can be conveniently measured. The temperature change per fringe shift is $3.2^{\circ}C$.

Temperature corresponding to fringe 1 = 39.1, fringe 2 = 35.9, fringe 3 = 32.7. The fringe width is calculated at 6 locations along the vertical length of the heater.

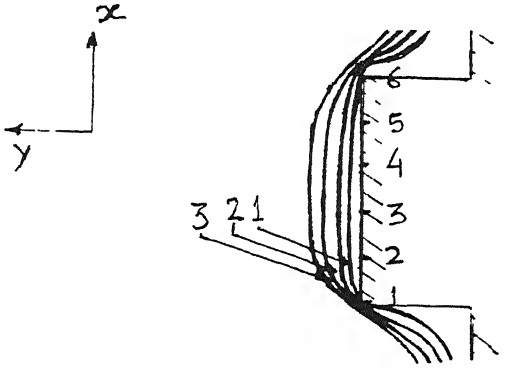

Fig. 3.2

The fringe width at these points is given below:

Location	x^{mm} mm	y_1 mm	y_2 mm	y_3 mm	a_x	Nu_x
1	0	0.15	0.75	2.85	-78.76	64.34
2	5	0.375	1.65	3.75	-30.04	24.54
3	10	0.45	1.80	3.90	-25.53	20.85
4	15	0.525	1.80	3.90	-22.45	18.40
5	20	0.525	1.725	3.75	-22.59	18.44
6	25	0.30	1.50	3.30	-36.82	30.08

y_1, y_2 and y_3 are the fringe widths for the fringes 1,2 and 3 respectively.

We have $T = T_c + ay + by^2 + cy^3$

Substituting the values for T_1, T_2, T_3 and corresponding fringe widths in the above equation we get for location 1.

$$33.1 = 48.7 + a\,(0.15) + b\,(0.15)^2 + c(0.15)^3$$
$$35.9 = 48.7 + a\,(0.75) + b\,(0.75)^2 + c(0.75)^3$$
$$32.7 = 48.7 + a\,(2.85) + b\,(2.85)^2 + c(2.85)^3$$

These three equations can be solved to give the value of a, b, and c. Similarly the value is obtained for all the points along the length of heater surface.

As we have said earlier

$$\frac{\partial T}{\partial y}\Big|_{y=0} = a_x$$

The value of temperature gradient at chip surface is known

$$q_x = -k \frac{\partial T}{\partial y}\Big|_{y=0} = -k\, a_x$$

$$(k = 27 \times 10^{-3}\ W/mk)$$

$$Nu_x = \frac{-a_x L}{(T_c - T_\infty)}$$

The average Nusselt number is obtained by integrating these values over the entire length of the heater

$$Nu = \frac{-\int_0^L a_x\, dx}{(T_c - T_\infty)}$$

Using trapezoidal rule we evaluate the average value of heat flux and Nusselt number as

Chapter 4

RESULTS AND DISCUSSION

The results are presented below for the following configurations.

Single chip natural convection.

Three-chip natural convection.

Single chip forced convection.

Three chip forced convection.

Qualitative and Quantitative analysis by interferometry

Single Chip Natural Convection

In these experiments the variation of Nusselt number with Rayleigh number has been studied. The chips are made of aluminium. In view of the high thermal conductivity of aluminium these can be assumed to be at a uniform temperature over their surfaces. Direct calculations show a negligible temperature drop from the thermocouple bead position to the chip surface. The effect of placing of neighbouring passive wall has also been determined. The role of heat conduction to the supporting bakelite plate and the effect of radiation losses has been investigated and eliminated to a large extent. Hence the Nusselt number reported here corresponds entirely to the convection mechanism in the fluid phase.

The Nusselt number shows an increase with the increase in the chip temperature and hence the Rayleigh number. Table (4.1) gives data for an enclosure that is kept open at the top and bottom. The distance between the active plate and neighbouring passive plate is 3H where H is the height of protruded heater. Figure 4.3 compares the data for an enclosure that is closed at the top and bottom with an enclosure that is open on these sides.

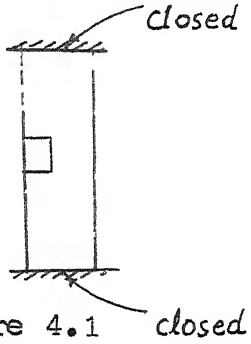

Figure 4.1

Nu increases with Ra in general but in case of a closed enclosure the Nusselt number obtained is less than that in an open enclosure. The possible mechanisms that lead to this result are as follows. When the enclosure is open air movement is free and uninterrupted. Owing to buoyancy air rises from the lower side and leaves the top of the enclosure in a vertically upward direction.

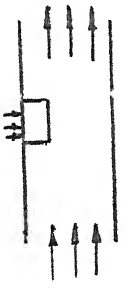

Fig. 4.2 : Buoyant flow through open enclosure

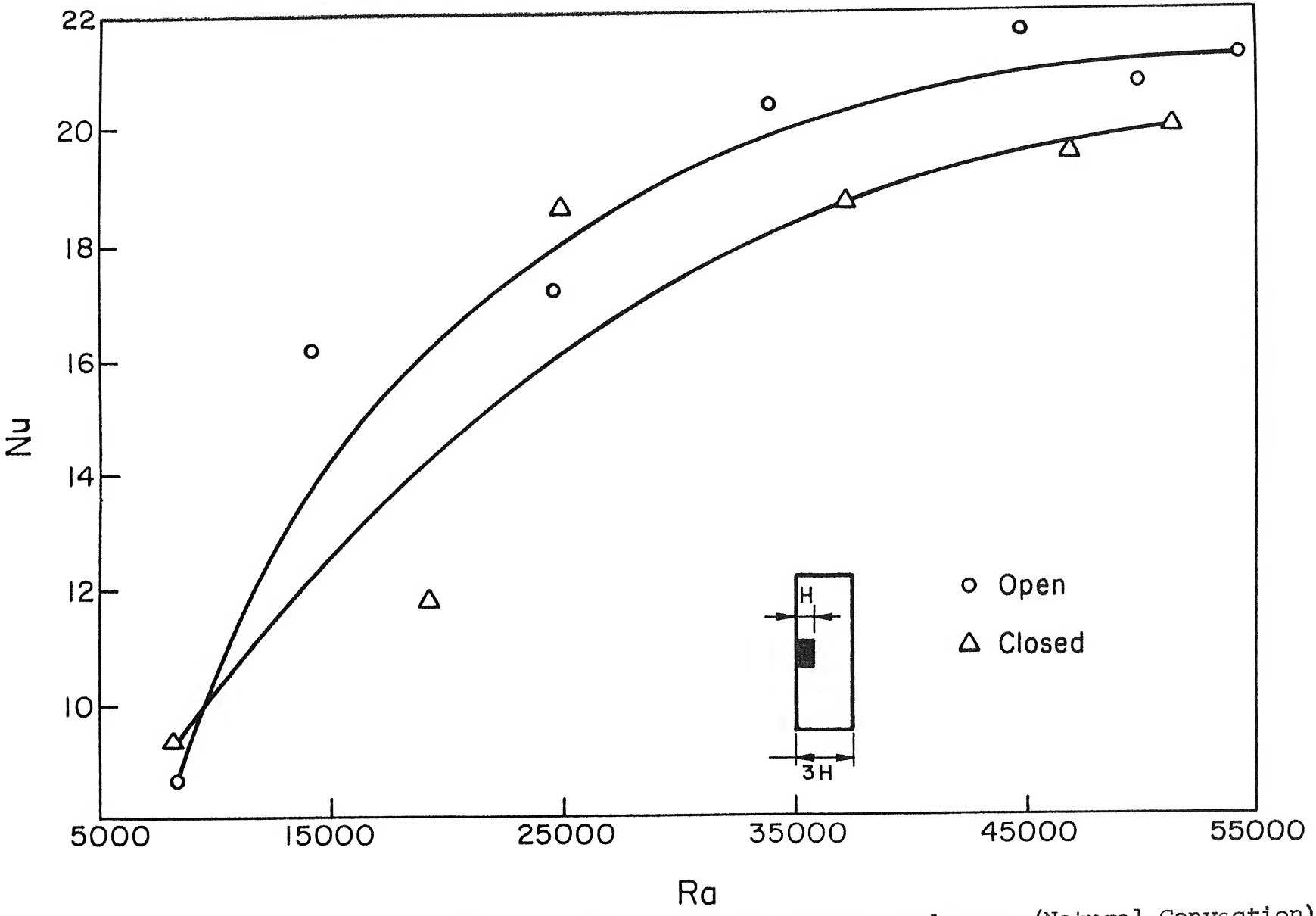

Fig. 4.3 : Comparison between open and closed enclosure (Natural Convection)

When the enclosure is closed at the top and bottom faces, the cold air from the lower portion of enclosure rises but can not exit from the top face. Hot air gets accumulated in upper portion of the enclosure and results in an increase in overall temperature of the enclosure. The possible air flow paths are shown below. This is a case of combined horizontal and natural convection. Air is taken in from the lower sides of the enclosure and leaves the enclosure on a combined horizontal and vertical path. The absence of accumulation of heated air in the

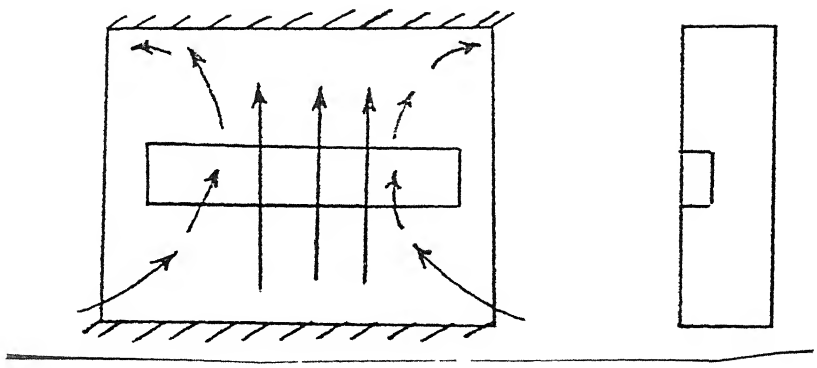

Fig. 4.4 : Flow mechanism in a closed enclosure

upper portion of enclosure and a shorter, more vigorous air flow mechanism results in heat transfer being better in the case of an open enclosure. This emphasizes the need of proper ventilation in cabinets having many circuit boards. The systems having natural convection cooling should have sufficient space below and above the heated elements.

Table 4.2 presents data for the closed enclosure with the passive plate kept at a distance of 2H from active plate. On comparing Tables 4.2 and 4.3, it can be seen that the position of passive plate hardly affects heat transfer. The distance between the two plates is not a critical parameter unless it is made excessively small. The observation can be explained as follows. In natural convection there is a formation of a boundary layer over the heater. The length of the heater parallel to this flow is quite small. Hence the thickness of the boundary layer is also small. Since all the temperature drop takes place within the boundary layer and the fluid outside the boundary layer is at the ambient temperature, the neighbouring plate does not disturb the boundary layer. As a result the heat transfer rates are not affected. If the neighbouring plate is kept very close to the heater it decreases the Nusselt number. This is due to the unavailability of a sufficient amount of cold air in the vicinity of the chip.

The effect of a sharp protrusion kept close to the heater to divert the flow towards the heater has also been studied. The effect of the protrusion is studied for two values of heat flux. The Table 4.4 shows the effect of protrusion placed at various positions. The different positions are shown in Figure 4a.

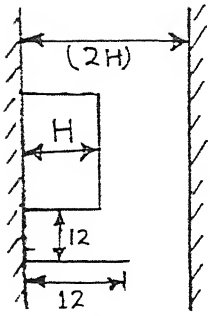

a

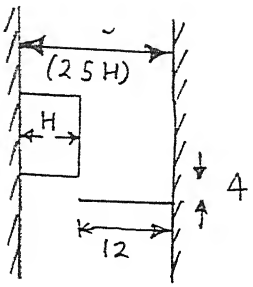

b

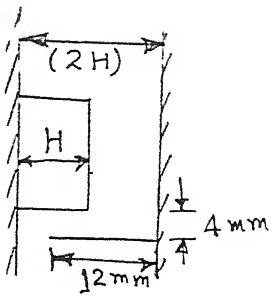

c

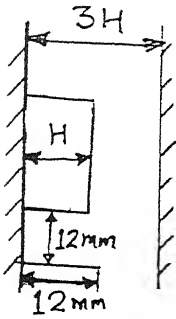

d

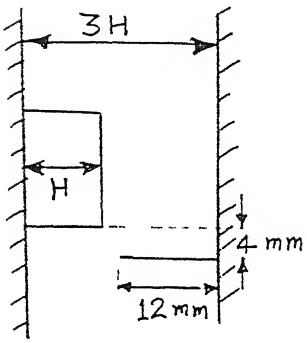

e

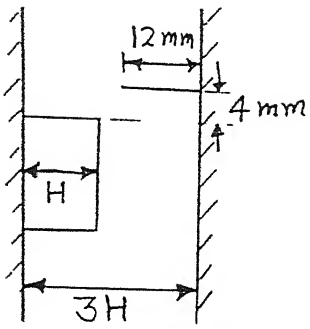

f

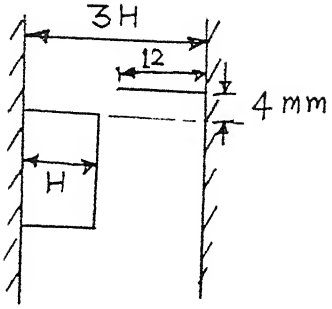

g

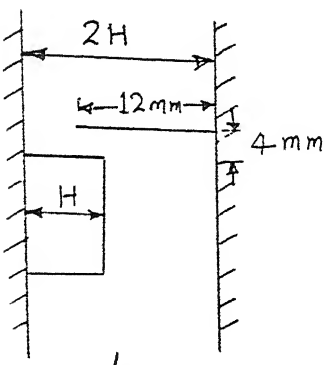

h

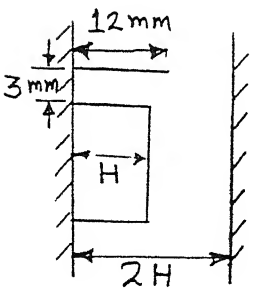

i

H = 8 mm

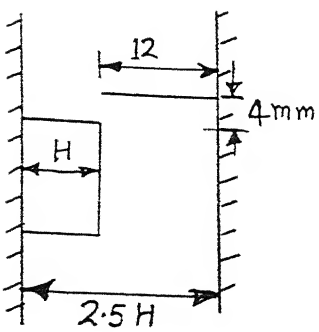

j

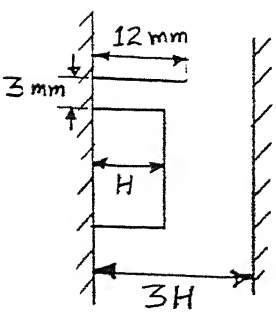

k

It can be seen from the data presented in this table (4.4) that Nusselt number is lowered when the disturbing strip is placed in the path of the flow. The protrusion tends to block the flow resulting in an increased resistance and a reduction in average air velocity. For a given heat flux the Nusselt number obtained without protrusion is higher and hence the maximum temperature reached on the chip is lowered.

Effect of Radiation from the Chip

To estimate the amount of radiation losses the experiments were separately carried out in a white enclosure and a black enclosure. In a white enclosure all the radiation falling on the walls is assumed to be reflected back to the heated chip while in case of black enclosure all the radiant energy falling on the walls is assumed to be absorbed completely.

It can be seen from the Fig. 4.5 that for given Ra, Nu is higher in case of a black enclosure. Here the heated metallic strip loses a part of its energy by radiation. This results in a lower surface temperature. In case of a white enclosure the radiation mechanism is not available and all the energy released goes to the ambient air by convection only. This leads to a higher chip temperature and subsequently lower Nusselt number. The amount of losses due to radiation for the test cell used in this study are approximately 10% of the total input heat flux. Appendix A.3

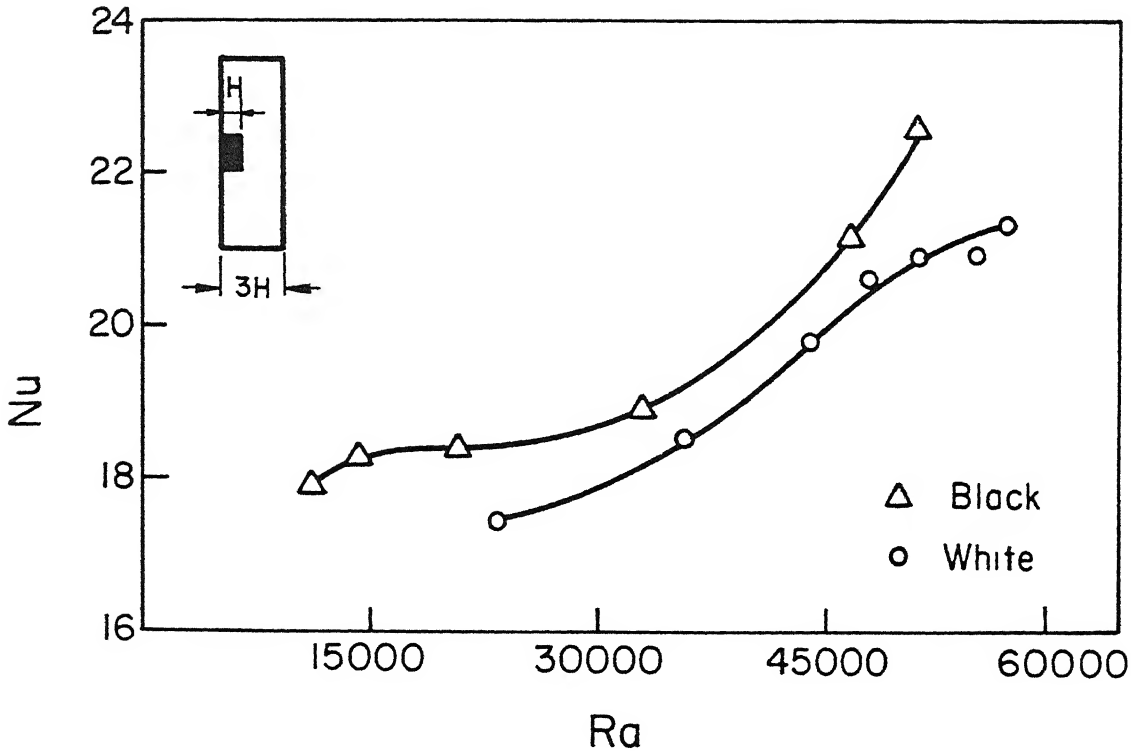

Fig.4.5 : Effect of Radiation from the chip

gives the detailed method of calculating the radiation losses.

The Table 4.7 gives the values of radiation loss in a black enclosure. If experiments are done in a black enclosure then the data free of radiation effects can be obtained as 90% of the measured Nusselt number. In present study we have used white enclosure for all the natural convection experiments and this correction is not necessary.

Wall Conduction Effects

As the temperature of the strip increases the temperature of the wall on which the strip is mounted, also increases because of conduction. This changes the temperature profile over the bakelite sheet and precludes the assumption of discrete heater. This change in temperature profile affects the overall heat transfer rate. Air

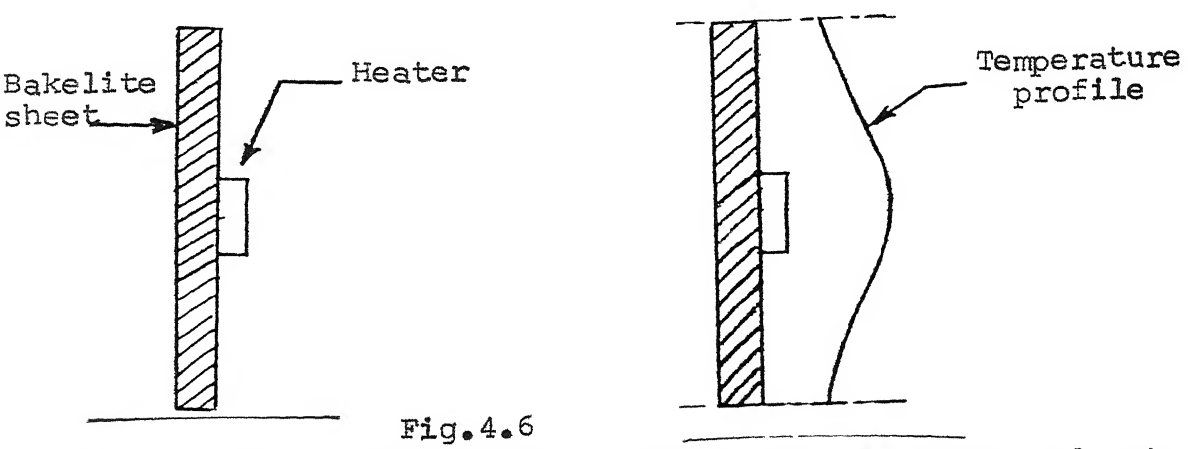

Fig.4.6

rising upwards comes in contact with the wall first and gets pre-heated before it reaches the heater. The Nusselt number calculated on the basis of the assumption, that all the heat supplied is lost to ambient through the strip only, is

likely to be higher than the Nusselt number in which end-conduction is present.

To minimize the effect of conduction, experiments are carried out in a test cell having an air gap between the heated strip and the supporting bakelite sheet. Two bakelite pieces are fixed at the ends of strip to avoid three dimensional effects.

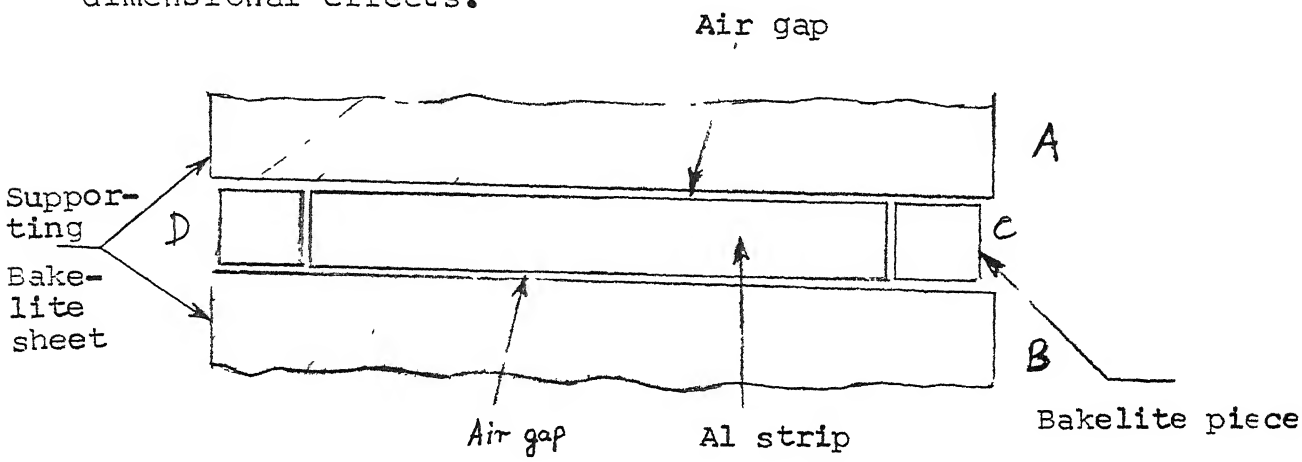

Fig.4.7 : Air gap to prevent conduction

Figure 4.8 shows that the effective Nusselt number obtained in the setup with a slit is less than that obtained without a slit. The two values differ by 5-10%. This result is expected as explained earlier. At Higher Rayleigh number this difference increases. The temperature of heater increases linearly with an increase in the heat flux.

Ravine and Richards [1988] present experimental data for a flush heater mounted on a vertical wall. The heater length is l and channel separation is b in their study.

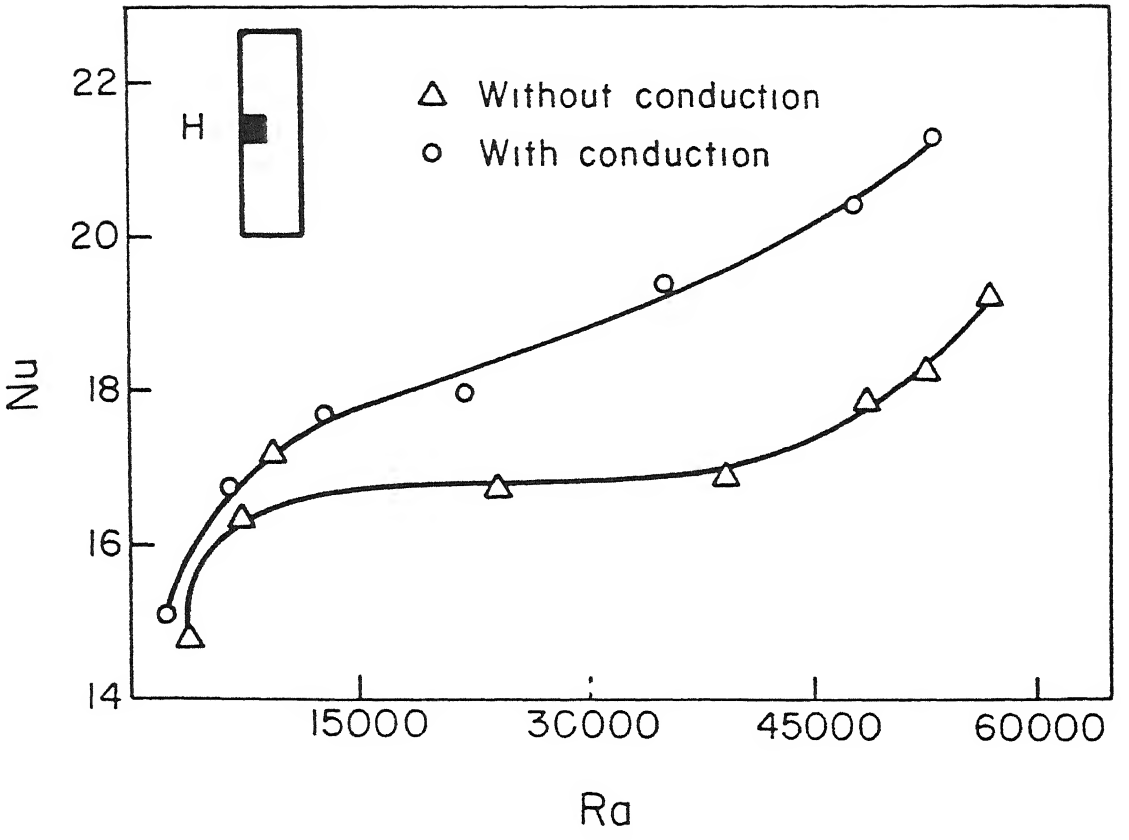

Fig. 4.8 : Effect of conduction to the supporting plate

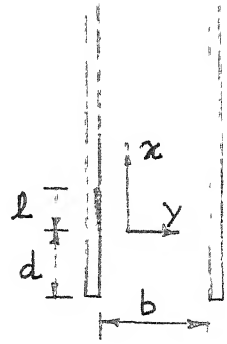

Fig.4.9

x is measured from the leading edge of the heater.

For $b/l \geq 1$ they report

$$\frac{Nu_x}{(Ra_x)^{0.25}} \sim 0.4$$

In the present study this ratio varies from 0.9 to 1.6. The protruded heater does not show strict similarity as in the case of a flush heater. The protruded heater generates a non-parallel flow field and hence a higher Nusselt number.

Aspect Ratio Effects

The aspect ratio has been defined as L/H in this work. Two cases for aspect ratio 2 and 3 have been considered. Figure 4.10 shows a plot of temperature versus heat flux for heaters with aspect ratios 2 and 3. Results for a three dimensional heater are also shown here. The heater with larger aspect ratio shows a higher temperature rise than for a heater with smaller aspect ratio. Figure 4.11 shows variation of a $Nu/(AR)$ with $Ra/(AR)^3$. The axes have been taken as $Nu/(AR)$ and $Ra/(AR)^3$ so as to have the same characteristic length for the two heaters.

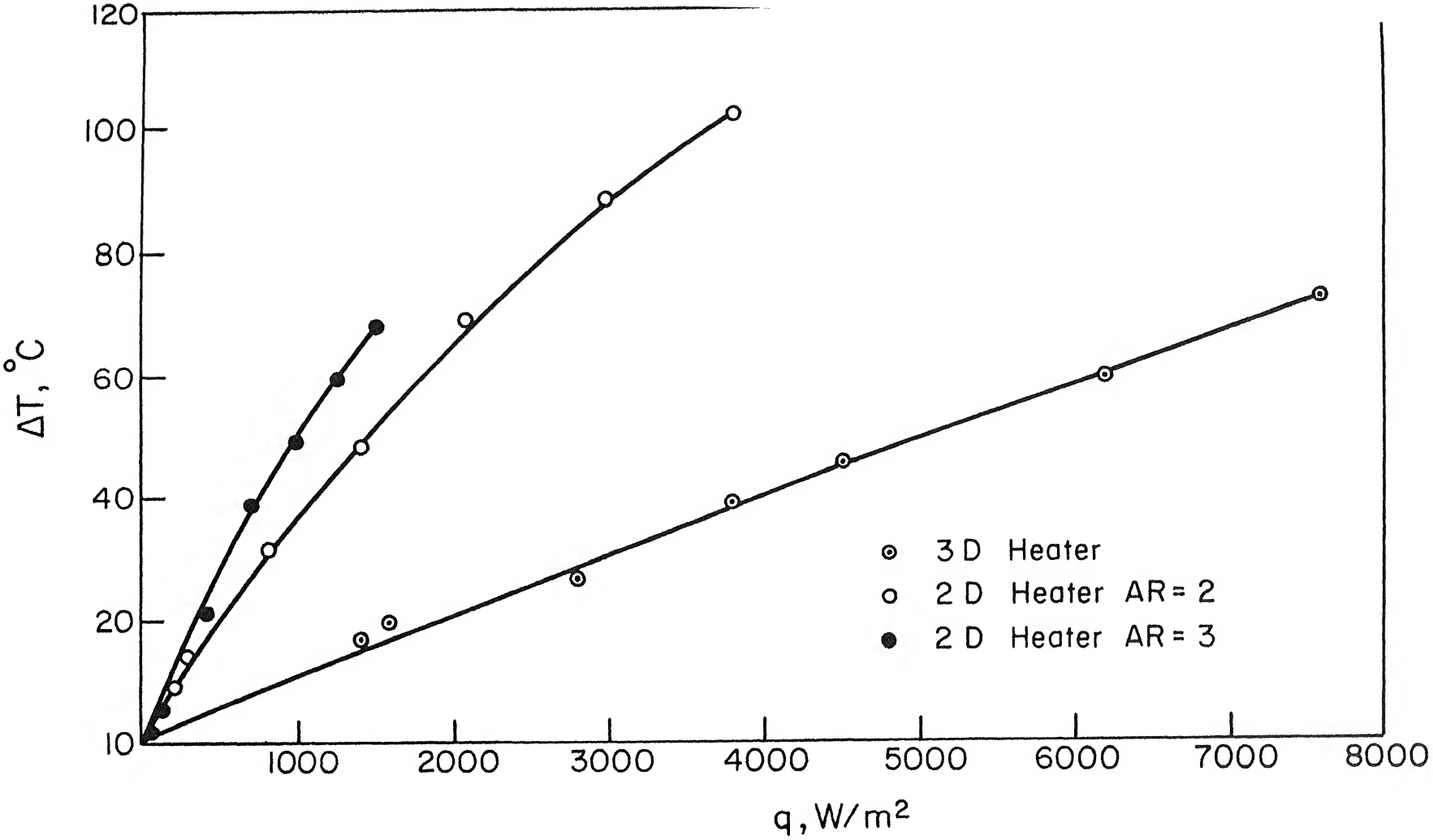

Fig. 4.10 : Temperature rise with heat flux

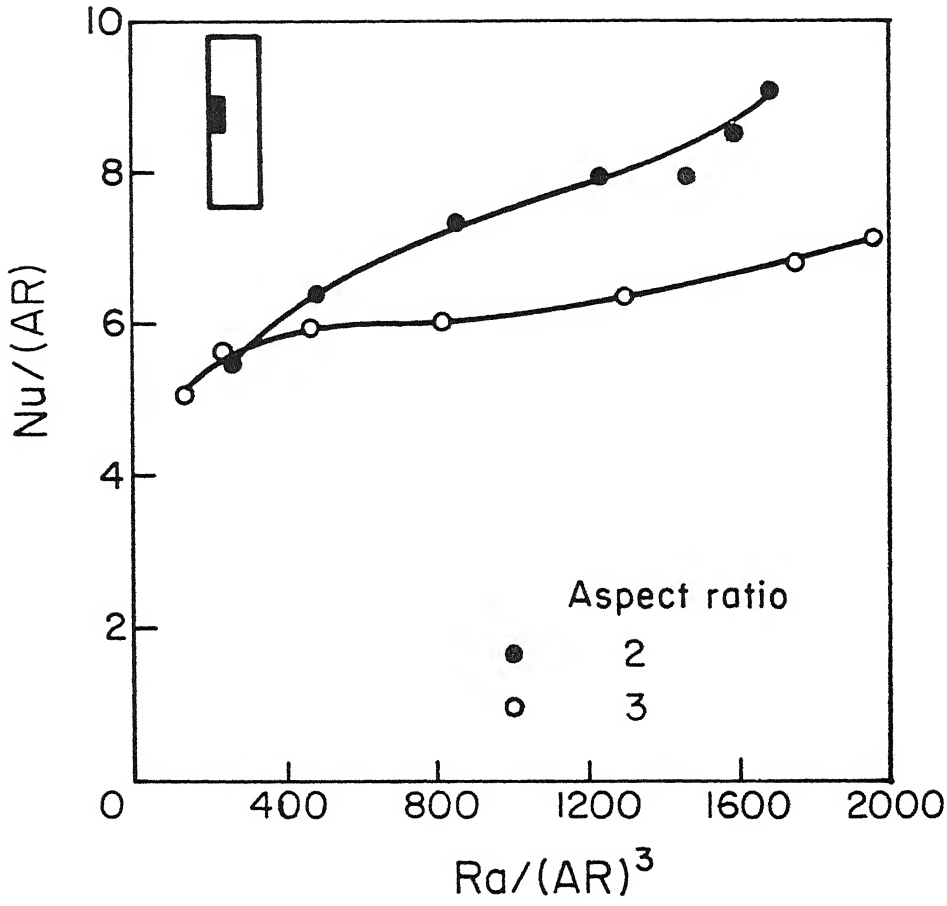

Fig. 4.11 : Aspect ratio effect (Natural Convection)

It is evident from the two figures that the heat transfer rate is higher in case of heater with smaller aspect ratio. This is because the heater with smaller aspect ratio is closer to a point source. The point source and a uniformly heated flat plate are the maximum and minimum limits for heat transfer.

As the size of source becomes smaller the flow field becomes three dimensional. We present results for a three dimensional copper heater with a square cross-section mounted on a bakelite plate.

Experiments show that the Nusselt number for a horizontal configuration is smaller than that for the vertical configuration. Since the heater size is small the variation in Rayleigh number is also small ($10^3 < Ra < 10^4$) and flow remains close to laminar. The corresponding change in Nusselt number is also small. From Fig. 4.10 it can be seen that the temperature rise for a 3-dimensional heater is less than that for a 2-dimensional heater. Correspondingly the Nusselt number obtained with a three dimensional heater is considerably larger than for a two dimensional heater. The effect of placing a wall in the proximity of the heater does not significantly affect the heat transfer rate.

Radiation losses are found to be insignificant in case of a three dimensional heater. At a heater temperature of $53^{o}C$ the radiation loss is found to be 1.4% of input heat flux. For two dimensional heater, a larger surface area and a large chip temperature leads to radiation losses as high as 10% of the input energy. Since the Rayleigh number for a

small heater is small the flow is likely to be easily affected by external influences. The experiments dedicated to scatter show scatter as large as 10% with a 3D heater. This explains the slight inconsistency in the value of Nusselt number with increasing Rayleigh number. A detailed scatter analysis is given later.

Since the heat transfer rate for a two dimensional chip is the smallest, the modelling of an IC chip as a two dimensional heater will give the worst thermal performance of an electronic system. This will help in designing the system on the basis of the worst conditions.

Multichip Natural Convection Experiments

The aim of these experiments is to study thermal interaction among the heating elements mounted on a vertical wall. The presence of an unpowered heater close to a powered heater can also affect the heat transfer characteristics. Experiments have been carried out with three similar heaters mounted on a bakelite sheet. In these experiments we have used heaters with a small aspect ratio to simulate closely the electronic components. The height of the protrusion is same as in the case of single chip heater but the width has been reduced to 15 mm.

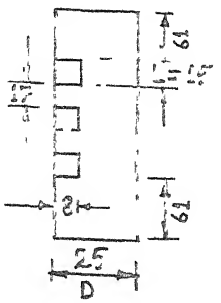

Fig. 4.12

The three heaters are controlled separately. Various combinations of cold and heated strips are possible. We have studied interaction effects for the three configurations shown below.

1.

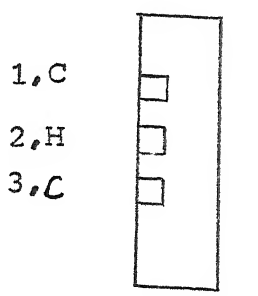

C-H-C Configuration

2.

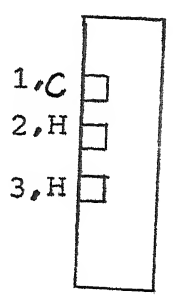

C-H-H Configuration

3.

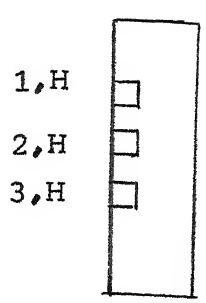

H-H-H- Configuration

Fig. 4.13

Middle Chip Heated

In this configuration energy is supplied to the central chip only. Table 4.14 gives the value of relevant heat transfer parameters for this case. The Nusselt number increases with the Rayleigh number for the middle chip as shown in the Figure 4.14 .

Figure 4.15 shows the variation of temperature beyond the ambient for all the three chips. The lower chip is found to be barely affected by the presence of the heated central chip. The temperature of upper chip increases significantly. This shows that the presence of a powered component does not significantly change the temperature of a component below on a circuit board. If the same powered component is mounted below, the rise in temperature of the chip above is significant.

As seen in the case of a single chip heater, the open enclosure leads to improved cooling in the case of multichip heaters. The comparison between two cases is shown in Fig. 4.16 . For a given Rayleigh number the value of Nusselt number is higher in an enclosure open from the top. This is, as explained earlier, due to vigorous ventilation in an open enclosure.

Lower Two Chips are Heated

In this configuration energy is supplied to the chips 2 and 3. The effect of a powered component below and a

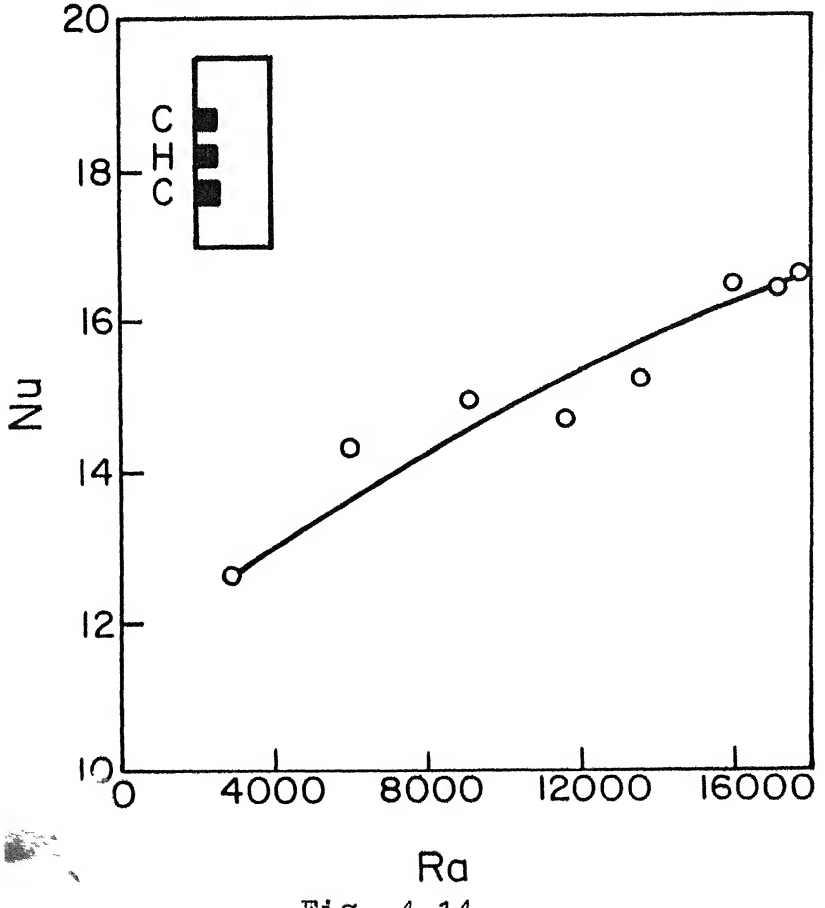

Fig. 4.14

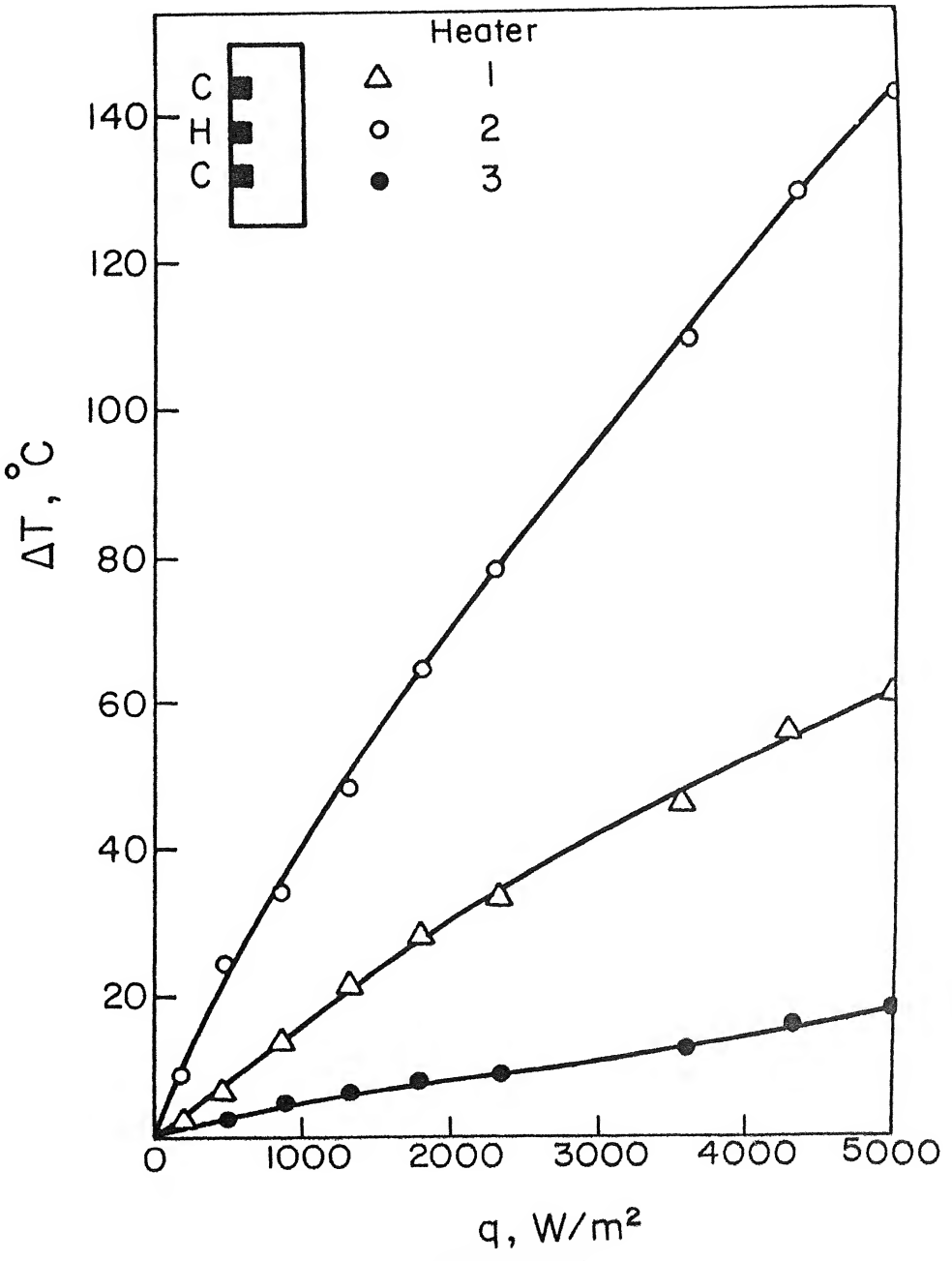

Fig.4.15

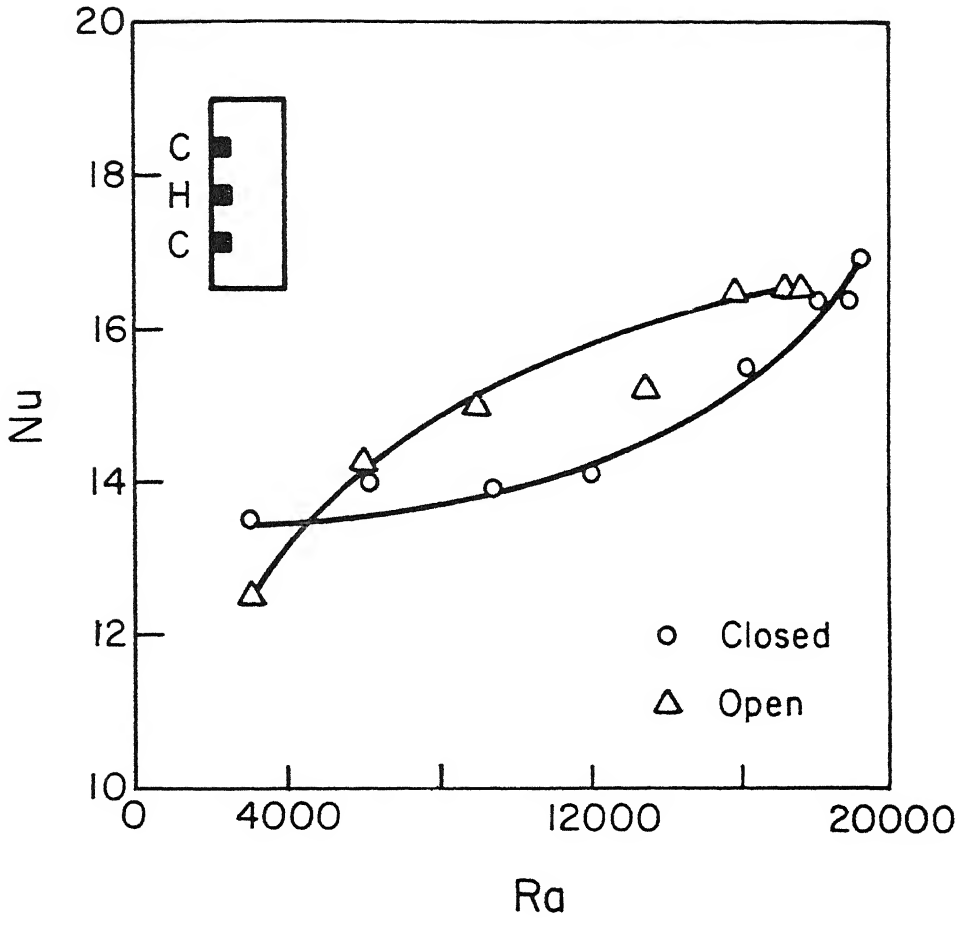

Fig.4.16 : Comparison between open and closed enclosure for a multichip heater (Natural Convection)

unpowered component above has been studied. The lower chip is found to have a higher Nusselt number than the central chi This is because for the lower chip the cold ambient air is available drawn from the bottom of the enclosure. The presence of a heated chip below reduces the heat transfer rate at the middle chip. This happens because of the heating of air before it comes in contact with the central chip. The lower chip acts as a disturbance for the upward flow of air, but since the natural convection velocities are very small this does not distort the flow sufficiently to have any augmentation in heat transfer for the central chip. The effect of pre-heating continues to dominate for the range of Rayleigh numbers studied here, resulting in a lowering of its Nusselt number. Figure 4.17 gives the variation of Nusselt number for the two heaters. Figure 4.18 gives the rise in temperature for all the three heaters for this configuration. Maximum temperature rise occurs over the central chip. If we compare the temperature rise curves for the heater 1 in C-H-C and C-H-H configuration, it can be seen that rise in temperature is greater in case of C-H-H configuration. This is due to the presence of two heaters below the passive heater.

These experiments show that on a circuit board, the components which are sensitive to temperature should be mounted as close to the base as possible. Powered components in series should be avoided even if they have low heat dissipation.

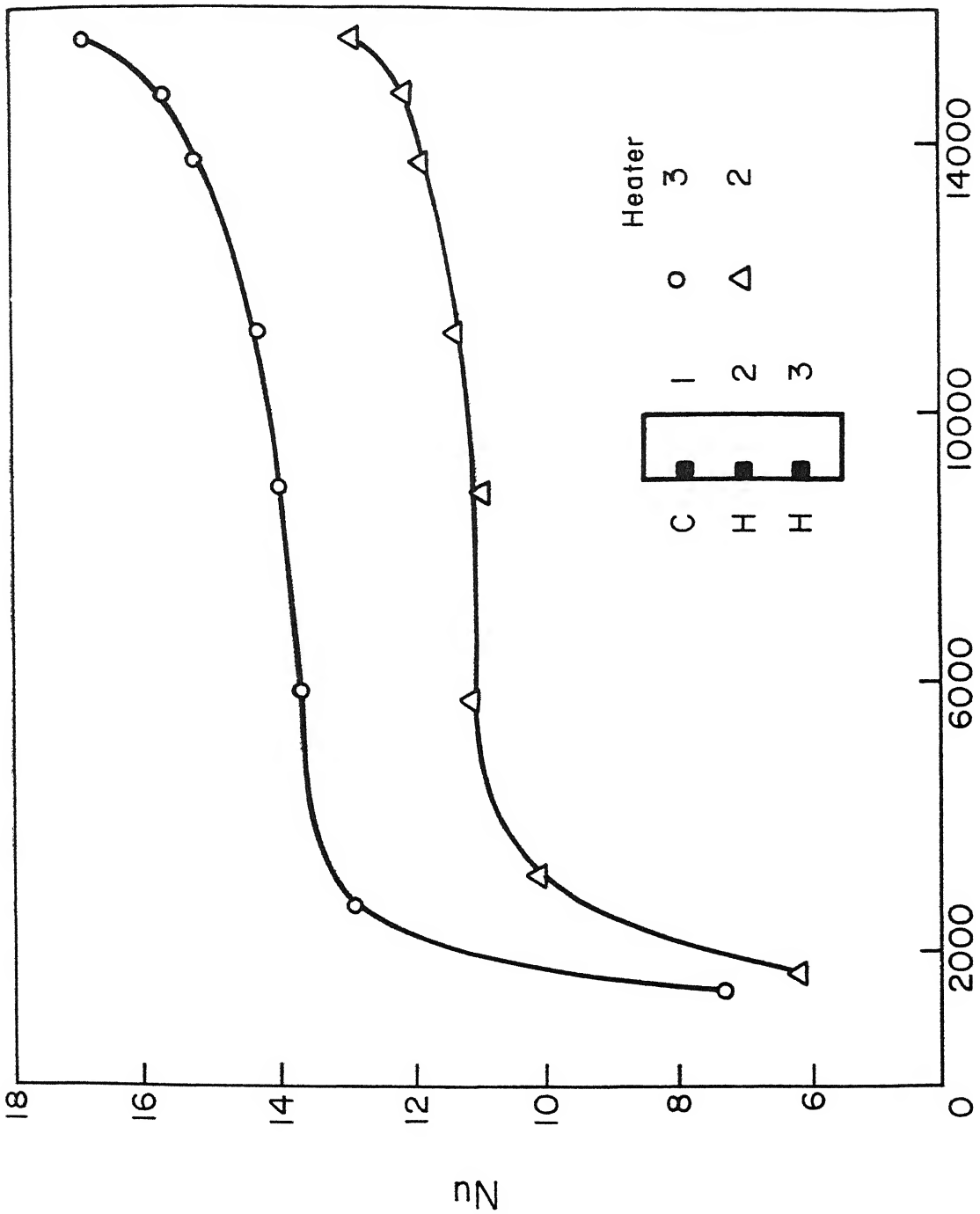

Fig. 4.17

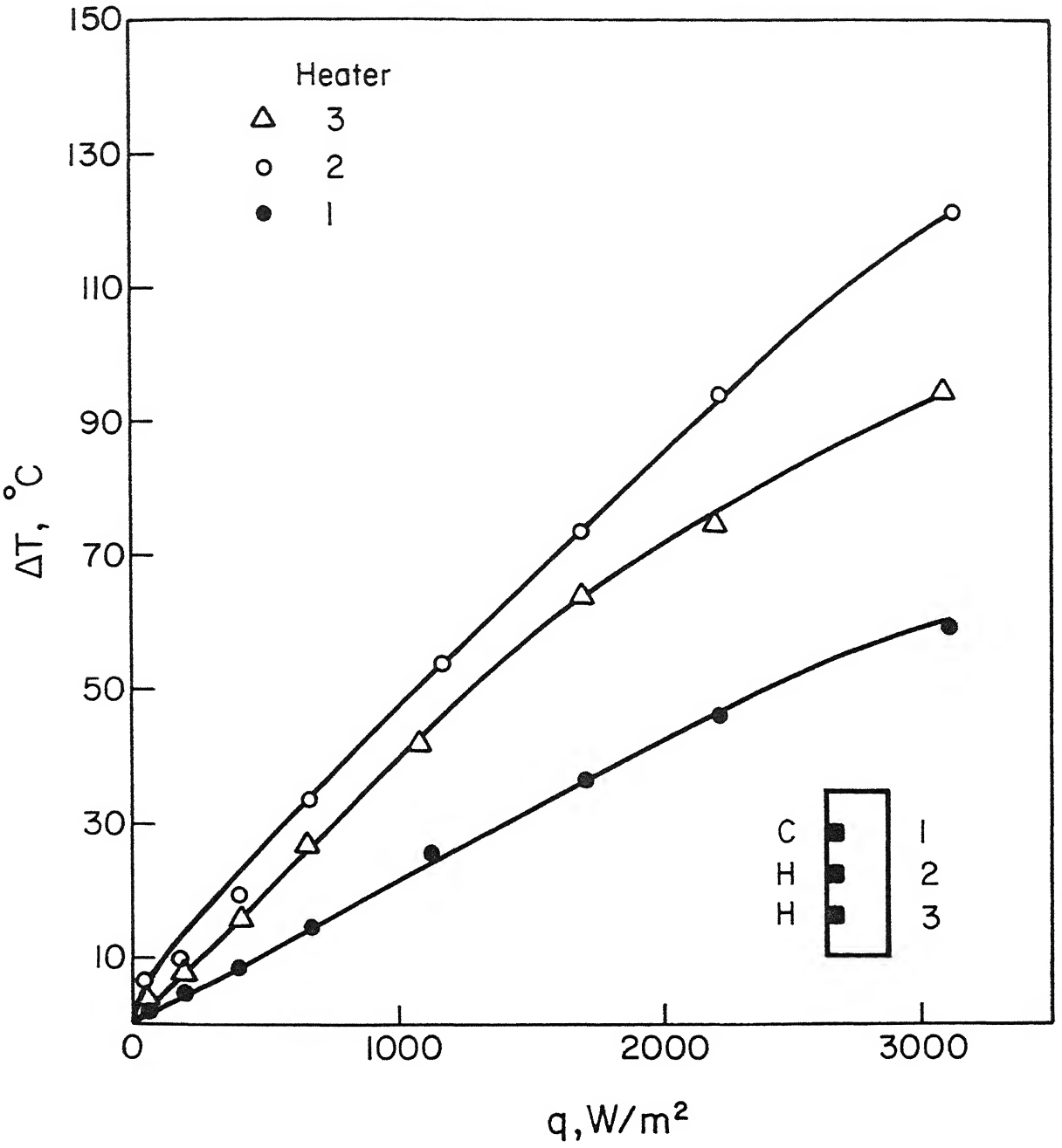
150
130
110
90
70
50
30
10
ΔT, °C
Heater
3
2
1
0
1000
2000
3000
q, W/m²
C
H
H
1
2
3

Fig. 4.18

The presence of a heated lower chip not only reduces the Nusselt number over the middle heater, but also flatens the Nu-Ra curve. Hence it is preferable to operate chip 2 at a lower heat flux because for any increase in heat flux the corresponding increase in Nu will not be significant. The lower chip does show a gradual increase in Nu with Ra and hence can be operated even at higher heat fluxes. The change in the position of the neighbouring passive plate does not have any effect on Nusselt numbers reported here.

All the Three Chips Heated

Energy is supplied to all the three chips in this configuration. Experiments have been done for a wall spacing of 3H.

Figure 4.19 shows the variation of Nusselt number for all the three heaters for this configuration. The maximum Nusselt number occurs over the lowest chip as in the case of C-H-H configuration. This is again due to availability of cold ambient air for the lower chip. In this case also the middle chip has a lower value of Nusselt number and a comparatively flat Nu-Ra curve. The upper chip is found to have the same Nusselt numbers as the middle chip. This is because air rising from the lower chip passes over the middle chip, accelerates resulting in the velocity increasing to a large extent. Hence there is an increase in the heat transfer coefficient over the upper chip. This increase in velocity compensates for the rise in temperature of air and the

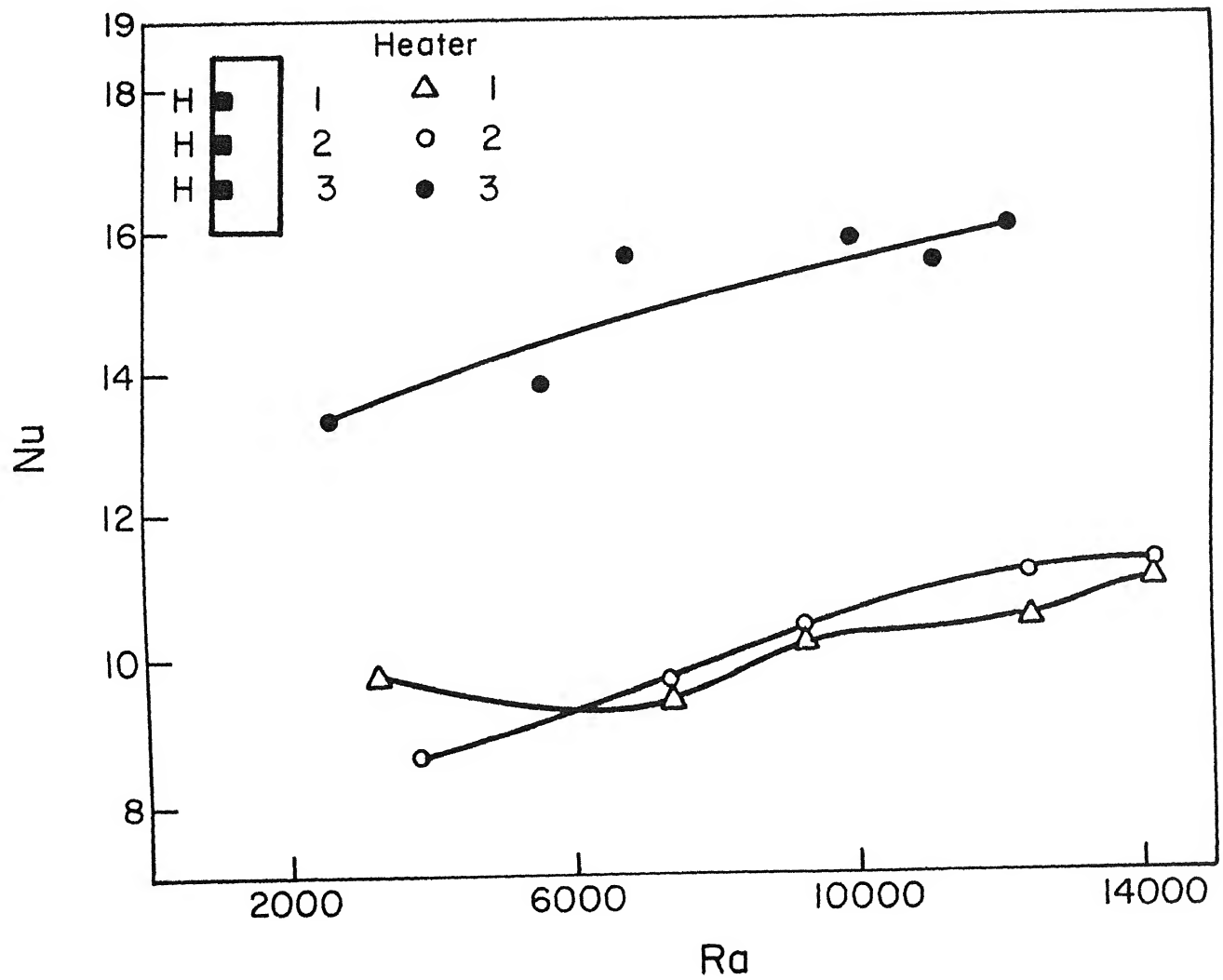
Heater
H
H
H
1
2
3
1
2
3
Nu
19
18
16
14
12
10
8
2000
6000
10000
14000
Ra

Fig. 4.19

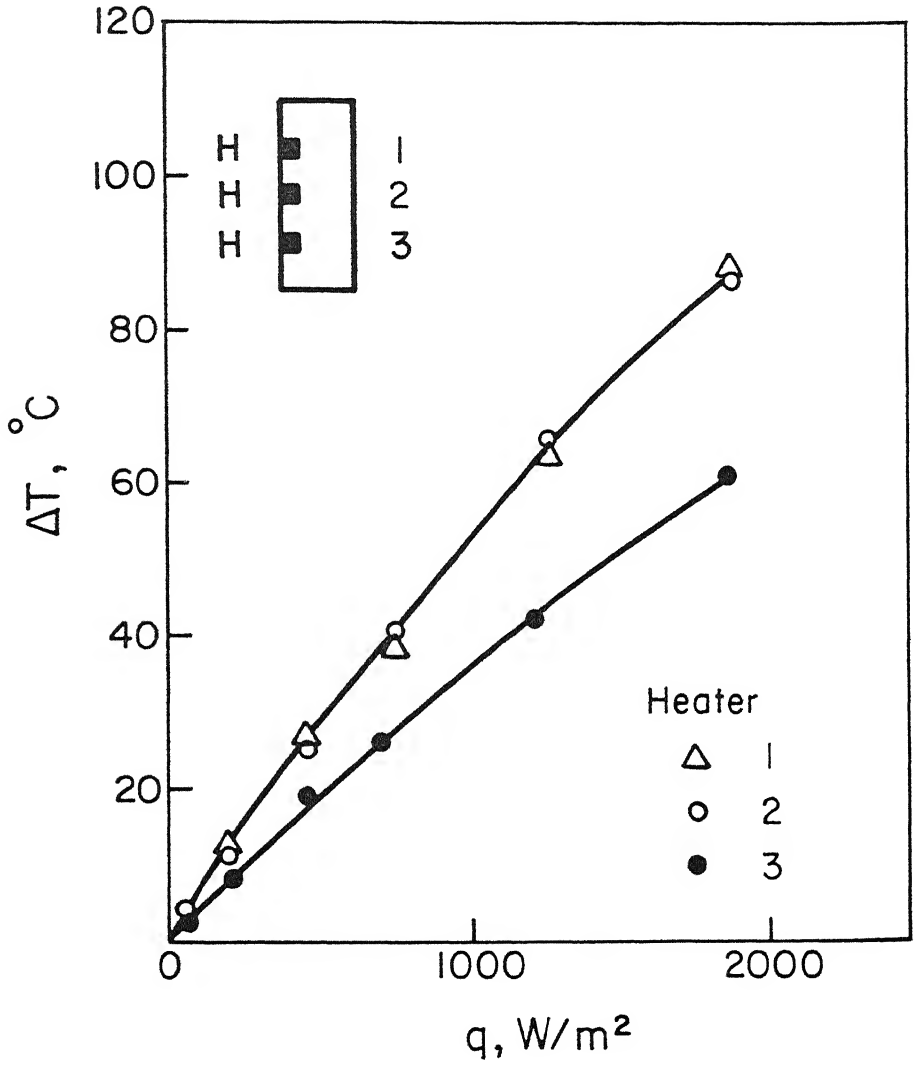

Fig. 4.20 : Temperature rise with heat flux. All chips heated

Nusselt number for the upper heater does not fall further.

We observe that a drop in heat transfer rate is not always necessary for a component if a few powered components are mounted below it. This gives an idea about the placement of IC chips dissipating different amounts of thermal energy on a circuit board. The most crucial component, highly sensitive to temperature rise, can be mounted on the lower side. In electronic systems there are always some components present which dissipate a large amount of energy but can tolerate a reasonably high rise in temperature. Such components can be mounted at the top as the energy released by components below will not have any significant effect on them. Further large temperature rise for such components will not deteriorate the performance of the system.

Comparison with Existing Work

Afrid and Zebib (1987) have carried out a numerical analysis for a two dimensional single and multiple uniformly heated devices mounted on an insulated wall. A two dimensional, conjugate, laminar flow model has been used and solid and fluid physical properties are assumed constant. They have reported the results for a heater with AR = 2. The Rayleigh number defined in their study is,

$$Ra = g \frac{q}{L^5} \frac{\beta}{(K_s \alpha \gamma)}$$

where,

q is heat input per unit volume

K_s is thermal conductivity of solid

α is thermal diffusivity

ν is kinematic viscosity

L is distance from the first component to leading edge of channel

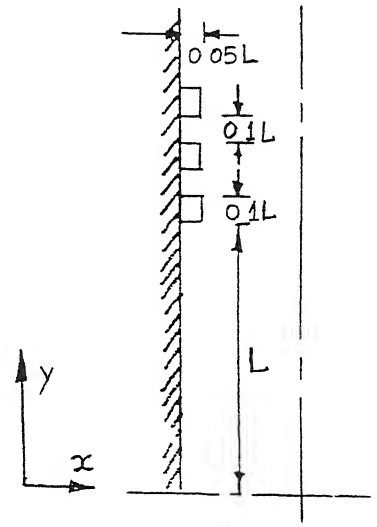

Fig.4.21 : Configuration used by Afrid and Zebib

If we define Rayleigh number as mentioned above the range of Ra for a single heater with AR = 2 in present case varies from 0.25×10^6 to 0.52×10^6. The corresponding variation of Nu is from 10.75 to 18.19. The value of Nu obtained by Afrid and Zebib varies from 26 to 42 for a variation of Ra from 4×10^6 to 33×10^6. In present case the value of Ra is limited by the temperature rise and power drawn by the heater. If we fit a curve, $Nu = cRa^m$ and and calculate the constants c and m for their data the value Nu for our Ra range varies from 15 to 16. In present experime study we have obtained a larger increase in Nu with Ra. The reason might be that the slope of Nu-Ra curve decreases with

increase in Ra and the exponents obtained on the basis of higher Ra will give a smaller slope.

Afrid and Zebib also show the effect of spacing between the components and the role of non-powered and highly powered components. They have noticed that when all the three components are heated the temperature rise between upper two components is smaller than the rise between the lower and the middle component. These results have also been obtained in the present experimental study. Experimental work by Ortega and Moffat (1985) also confirms this result. They report no change of temperature of the device after the fourth row of a set of 10 rows of aluminium components. Numerical analysis of Afrid and Zebib shows that the temperature rise varies almost linearly with the heat input for a single heater. This is exactly what has been found in the present work.

Forced Convection Experiments

Single Chip

Here we present results for a single heater with aspect ratio AR = 3, mounted on the wall of the flow apparatus. The range of Reynolds number covered is from 0 - 1050. This range of Reynolds number has been studied because the velocities encountered in the electronic equipment are small even in the presence of a fan. The range of Rayleigh number covered is 3000-65000.

In the forced flow experiments different regimes such as forced convection, mixed convection and strong mixed convection regimes are encountered. These regimes can be distinguished on the basis of the parameter Ra/Re^2. On the basis of the value of Ra/Re^2 we classify,

$Ra/Re^2 < 0.1$ as forced convection,

$0.1 < Ra/Re^2 < 1$ as mixed convection,

and $Ra/Re^2 > 1$ as strong mixed convection.

Heat transfer rate increases substantially in the presence of an imposed flow. Fig.4.22,4.23,4.24 and 4.25 show the variation of Nusselt number with Reynolds number and different flow regimes at varying levels of input heat flux.

At a low heating level, the Rayleigh number is small and buoyancy effects are insignificant. The heater goes into the forced convection regime, just after initiation of flow.

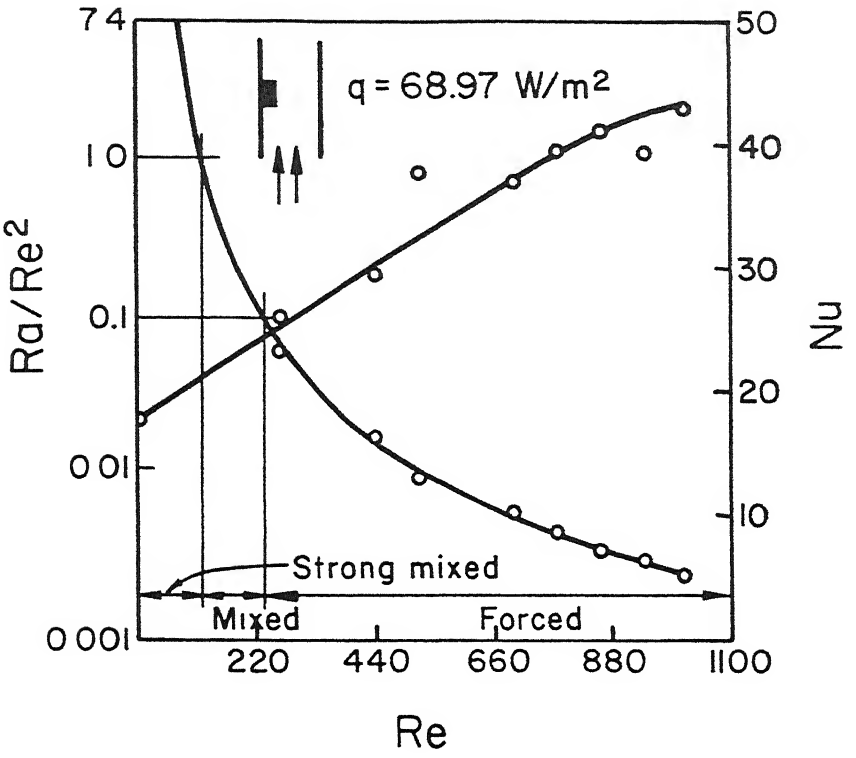

Fig. 4.22

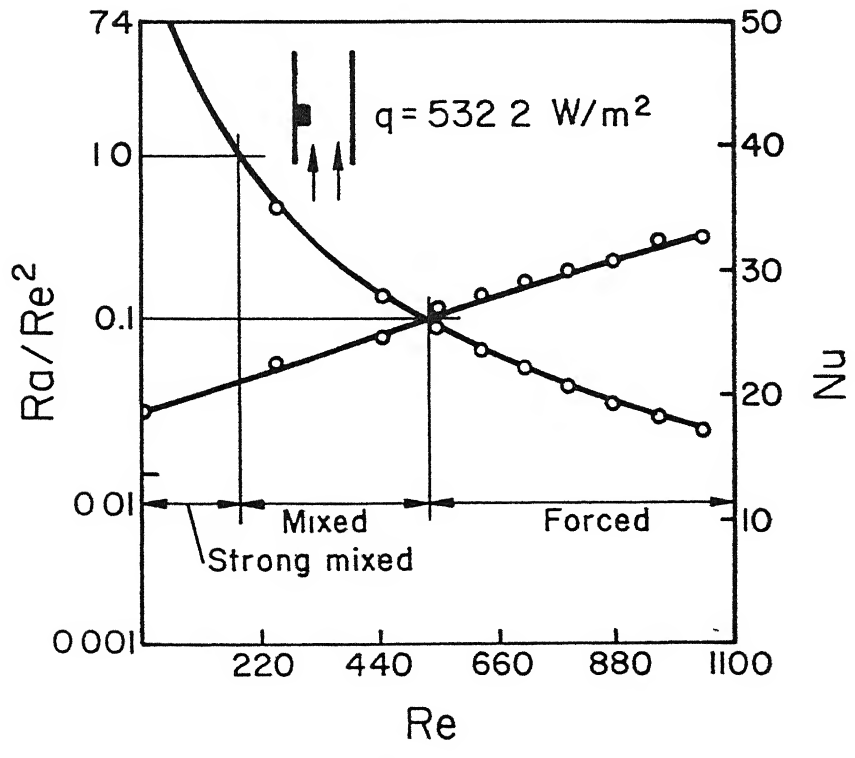

Fig. 4.23

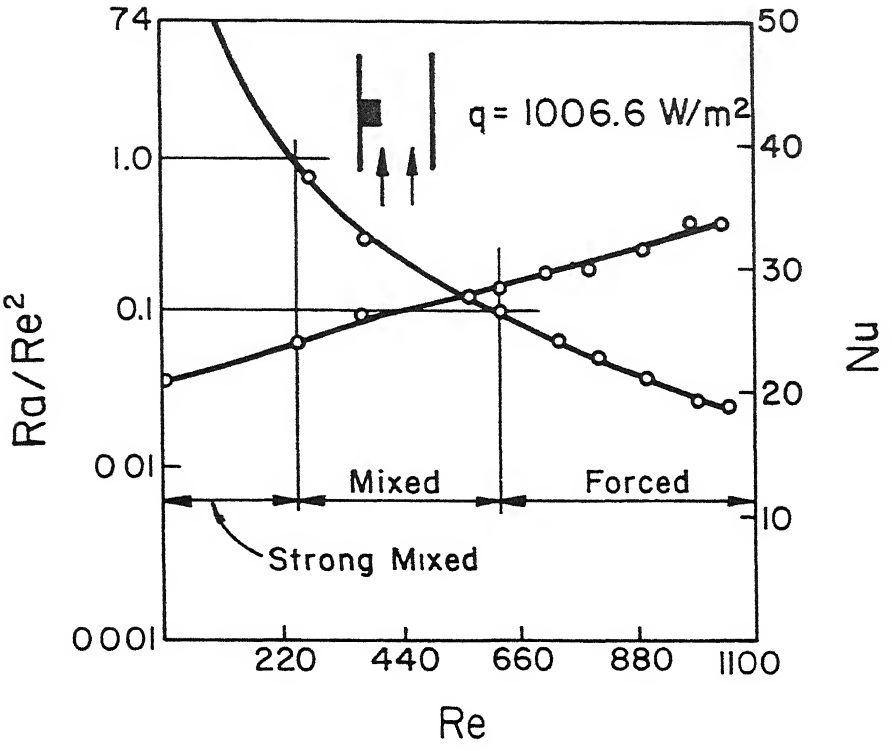

Fig. 4.24

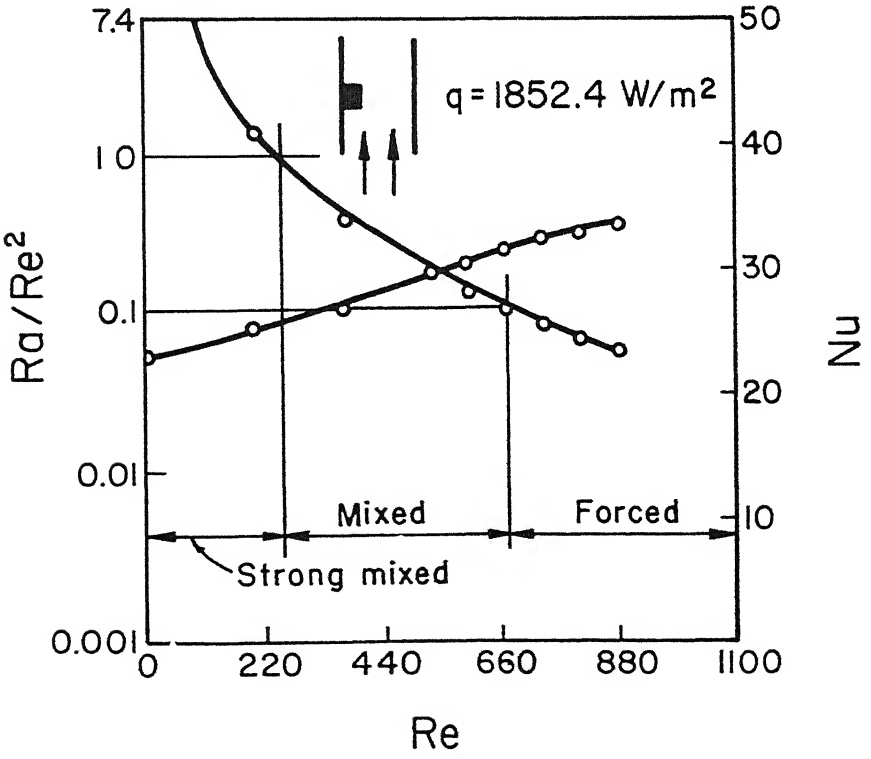

Fig.4.25

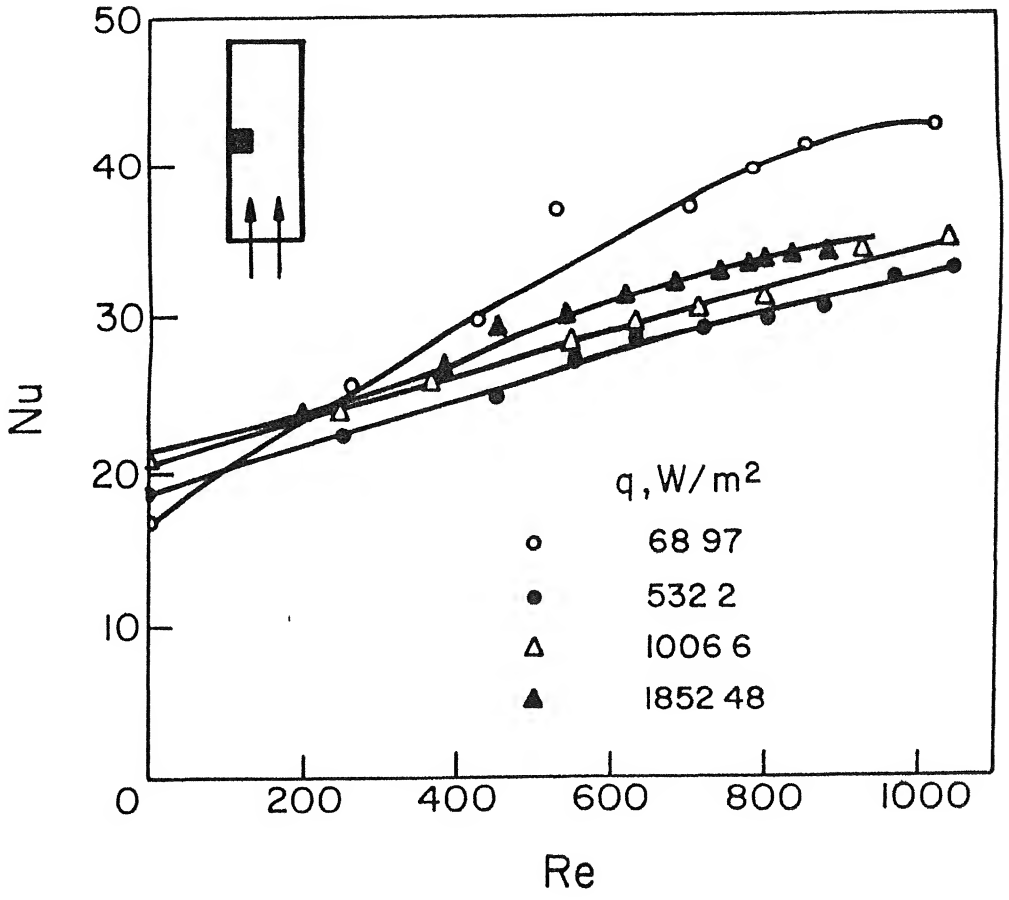

Fig.4.26 : Comparison at different heating levels

The slope of Nu-Re curve in this region is high and the increase in Nu with Re is large. As the input heat flux increases the Nu-Re curve becomes flat reducing the increase in Nu with Re. When heating levels are sufficiently high buoyancy effects become significant. Initial value of Ra at $q = 532.2\ W/m^2$ is 34517.4. This is the point beyond which buoyancy seems to augment the flow and hence heat transfer. Figure 4.26 shows the comparison Nu-Re variation at different heat fluxes.

If we compare the variation of Nu at q = 68.97 and $q = 532.2\ W/m^2$, it can be seen that beyond Re = 200 the value of Nu for $q = 68.97\ W/m^2$ is more than the value of Nu for $q = 532.2\ W/m^2$. This is because at $q = 68.97\ W/m^2$, heater is mostly in the forced convection regime and the slope of the curve is high. At $q = 532.2\ W/m^2$ the heater is in mixed convection having a flat Nu-Re curve. If the curves are compared in the same flow regime, the magnitude of Nu will be seen to be larger at higher heat inputs. This is seen in values below Re = 200 when both the heaters are nearly in same flow regime.

At q higher than $532.2\ W/m^2$ the buoyancy effects are important and we observe an increase in Nu with increasing heat flux. This can be seen from the curves for q = 532.2, 1006.6 and $1852.48\ W/m^2$.

This behaviour is different from what is known to occur in flush mounted heaters. The phenomena of heat transfer from a protruded heater is complicated. In such a flow field two regions of separation exist. The first region starts from the upstream wall and reattaches at the leading edge of heater. The second region starts from the trailing edge and reattaches on the downstream side of the wall. Heat transfer characteristics depend very much on the behaviour of these recirculation regions. These are affected by relative magnitudes of Rayleigh and Reynolds number. At low heating levels the buoyancy effects are small. The eddy size in the recirculation zone beyond the heater is small and weak. As the Reynolds number increases the size and strength of eddies on the upstream and down stream side of the heater increases. The large eddy gives better mixing with the colder fluid resulting in a higher rates of heat transfer. The flow in the upstream side separates from the wall and reattaches on the leading edge of heater. The leading edge is subjected to a colder fluid because of better heat transfer in the recirculation zone before the heater. The thermal boundary layer thickness starts from zero at the leading edge. As the Reynolds number increases, these phenomenon become stronger and stronger resulting in a higher heat transfer rates.

At a high heat input the initial Rayleigh number is large and buoyancy effects are important. The buoyancy force suppresses eddies in the upstream and downstream side. The

reattachment length on the downstream side reduces. The strength of vortex beyond the heater increases but because of a smaller size it results in poor mixing with the cold fluid away from the heater. When reverse flow occurs at the heated supporting wall, energy is transferred to the main flow. This results in elevated temperatures in the recirculation zone and a reduced heat transfer coefficient. The eddy on the upstream side is also suppressed. Hot air gets trapped just below the heater. This heated film of air is stably stratified and reduces heat transfer. The approaching cold fluid is also affected by the trapped heated air and its temperature increases. The leading edge of the heater is now subjected to heated air and the thermal boundary layer over the heater does not start from zero as initial thickness. This results in reduced heat transfer over the vertical front surface of heater. The buoyancy force does tend to increase the velocity over the heater but the net augmentation in the heat transfer is less. A larger thermal boundary-layer thickness results in small temperature gradients normal to the mean flow direction and a weakening of the buoyancy force hence the heat transfer is less than that obtained in forced convection regime. This is the main reason due to which a higher Nusselt number is obtained in the forced and weakly mixed convection regime.

As the input heat flux is increased beyond a certain point buoyancy effects begin to dominate and improvement in Nusselt number is seen. This explains the increase in Nu when

the heater is in a higher Ra/Re^2 range for q = 1006.6 and q = 1852.4 W/m^2.

Similar behaviour has been reported by Habchi and Acharya (1985) in their numerical work on laminar mixed convection in a partially blocked, vertical channel. They have investigated the flow and temperature field numerically at different Rayleigh numbers for different values of Ra/Re^2. They report that at a given Ra, the recirculation region above the blockage becomes stronger and smaller as Ra/Re^2 increases. At a high Rayleigh number, Nu along the upper surface of the blockage increases as Ra/Re^2 increases due to an increase in the recirculating eddy strength. At a lower Rayleigh number ($Ra = 10^3$) they observe a decrease in Nu along the upper surface as Ra/Re^2 is increased because of very small and weak recirculating eddy beyond the blockage. They have also reported the values of average Nusselt number. It is found to increase with increasing Ra/Re^2 at high Rayleigh numbers. At low Ra and Re, the recirculation zone is very small and its effect is not seen on average Nusselt number.

Shou-Shing Hsieh, Huei-Jan Shih and Ying-Jong Hong (1988) have presented the results for laminar forced convection from surface mounted ribs in a horizontal channel. They numerically study the low speed forced convection heat transfer near two dimensional transverse ribs in which the walls are held at a uniform temperature.

They define the average Nusselt and the Reynolds number on the basis of heater depth H. They have also considered

for the cases when mixed convection effects are negligible (at q = 40.64, 68.97, 102.05 and 126.96 W/m^2) the Nusselt number is found to vary within the range of 6.89 at Re_H = 84 to nearly 14 at Re_H = 333. The range of Nusselt number calculated experimentally in our case is found to agree well with the results presented by Hsieh et al. despite the present study being applicable for a vertical configuration. The thermal boundary layer thickness over the heater in case of forced convevection is small than in natural convection. Any increase in the distance between the heater and the passive plate beyond 2H does not affect the heat transfer.

Since Nu increases with increasing Re and the increase in Nu is greater in forced convection regime, it is preferable to operate with a large Re to have good cooling performance rather than rely on augmentation due to mixed convection.

Effect of a Protrusion on the Opposite Wall

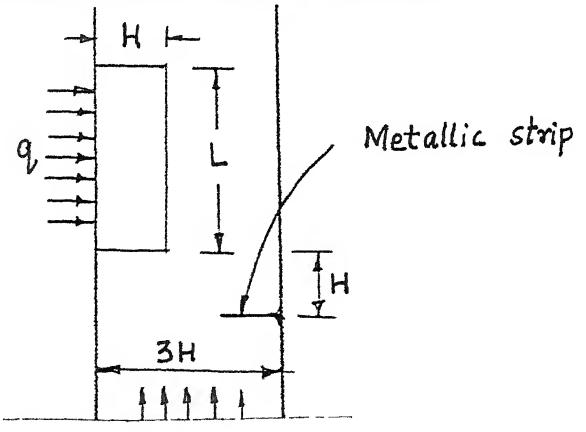

Fig.4.27 :

We have studied the effect of a baffle mounted on the opposite wall in case of forced convection experiments with single heater. We present data for the three values of heat

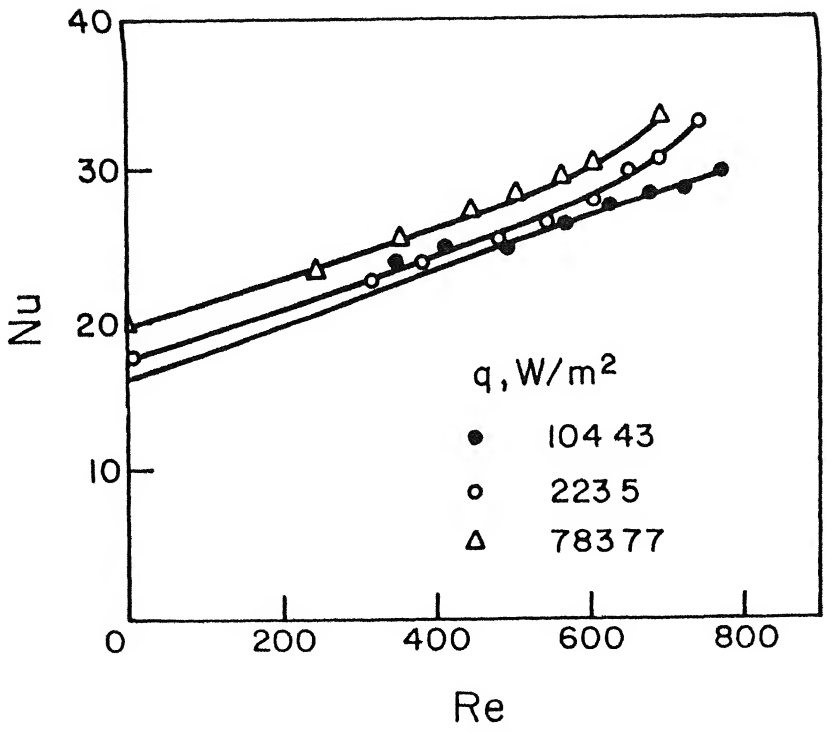

Fig.4.28: Forced convection, Protrusion mounted on opposite wall

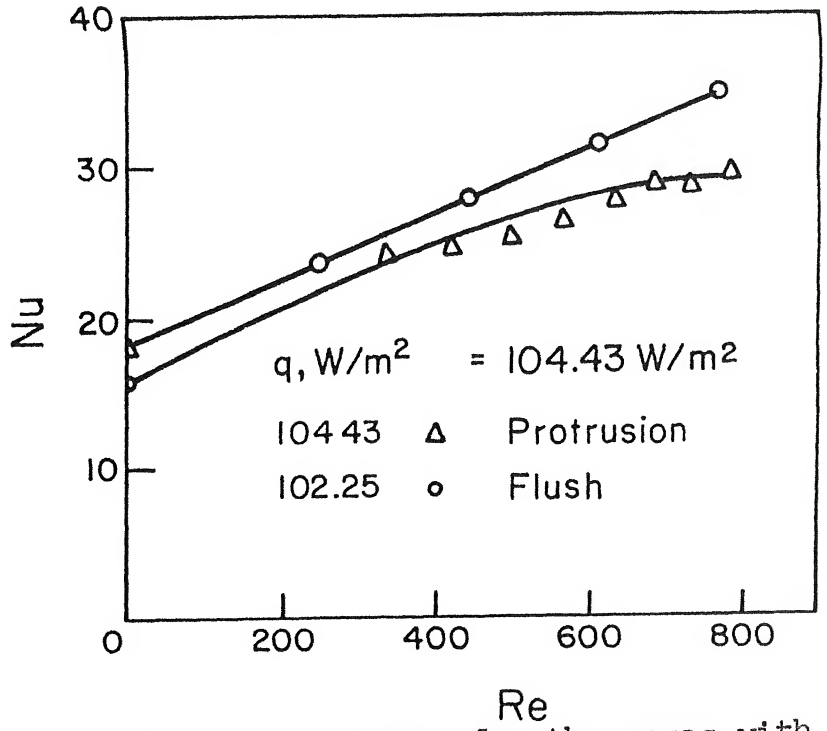

Fig.4.29 : Curves for the cases with and without protrusion on opposit wall

fluxes (q = 104.43, q = 222.5, q = 783.77 W/m^2). With a sharp protrusion in the way of flow the resistance to flow increases. Hence the maximum velocity in the test cell is reduced limiting the largest Reynolds number to 780.

From Figure 4.28 it can be seen that the buoyancy augments the heat transfer more clearly with a baffle. No improvement in the Nusselt number is observed at q = 104.43 W/m if the results are compared with those for a heater without protrusion on the opposite wall. This can be seen from the Figure 4.29 when the two heaters are at nearly equal heat input. Figures 4.30 and 4.31 show the comparison between the two cases at higher heat flux. (Note that there is some difference in the energy input between a flush and a protruded heater).

At higher heat fluxes the Nusselt number with and without a baffle is found to be nearly equal. If we look at the curves the value of q for heater with protrusion is 222.5 W/m^2 and for heater without protrusion on opposite wall is 532.2 W/m^2. Because of reduced buoyancy effects the expected Nu-Re curve at q = 222.5 W/m^2 in case of heater without protrusion is likely to fall on the curve for the heater with a protrusion on the opposite wall. By a similar reasoning the expected curve for q = 783.77 W/m^2 for heater without protrusion will fall almost on the curve for heater with protrusion.

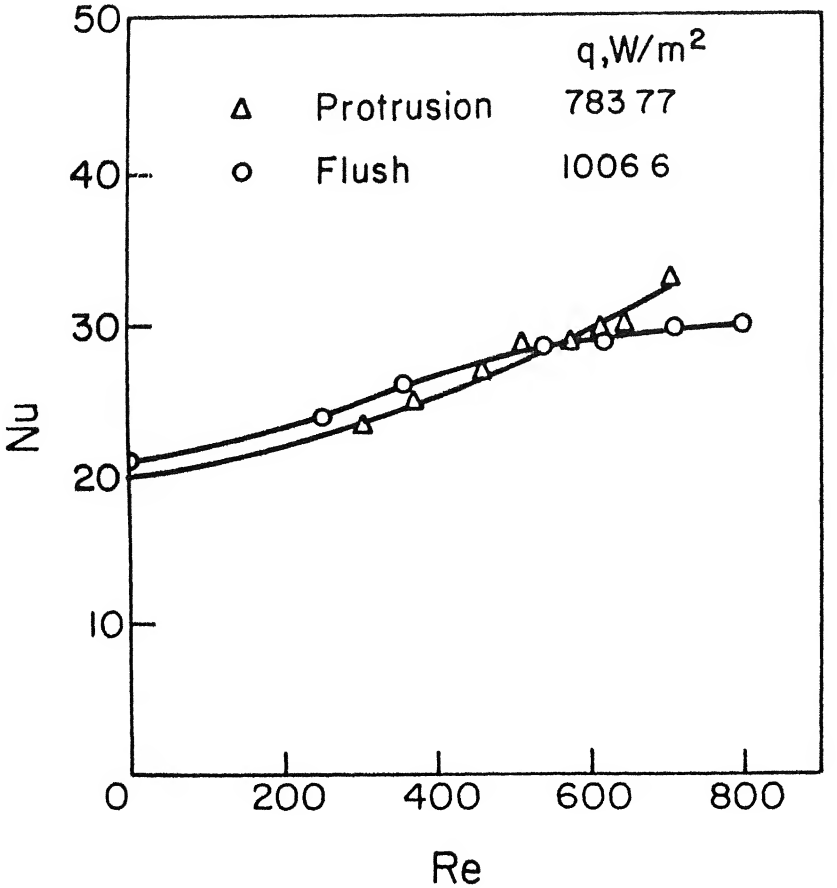

Fig. 4.31

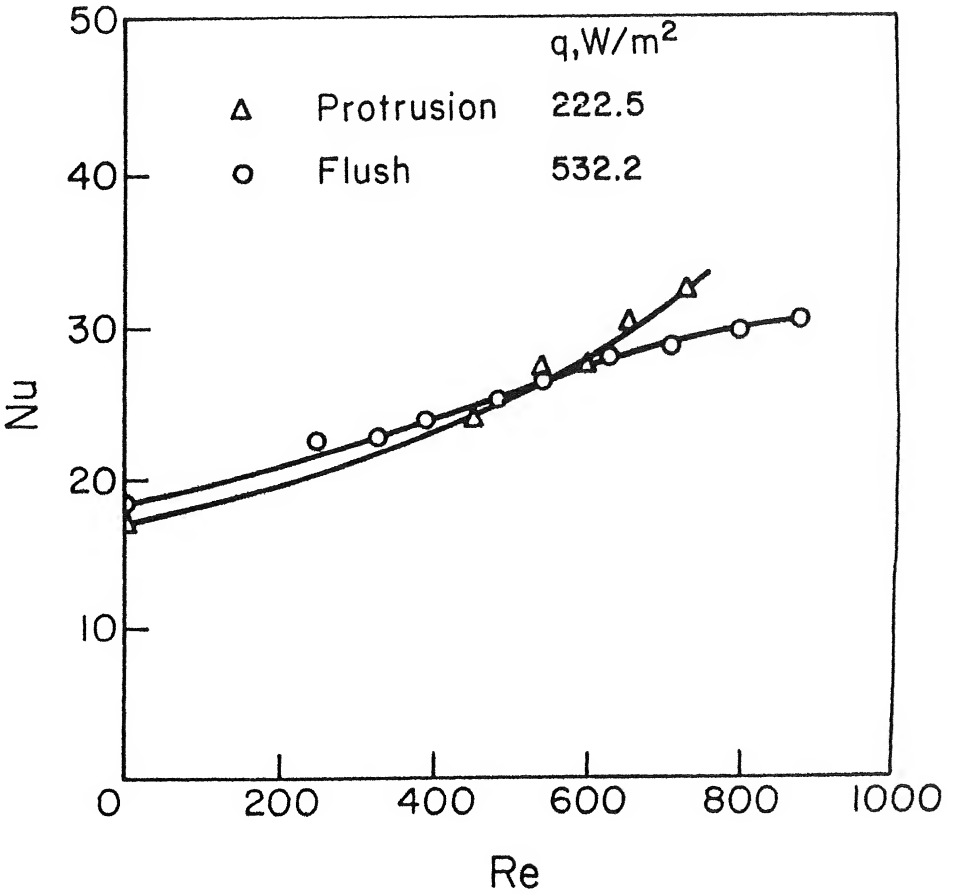

Fig. 4.30

Curves for the cases with and without protrusion on opposite wall

The absence of augmentation in heat transfer in the presence of a protrusion on the opposite wall can be explained as follows.

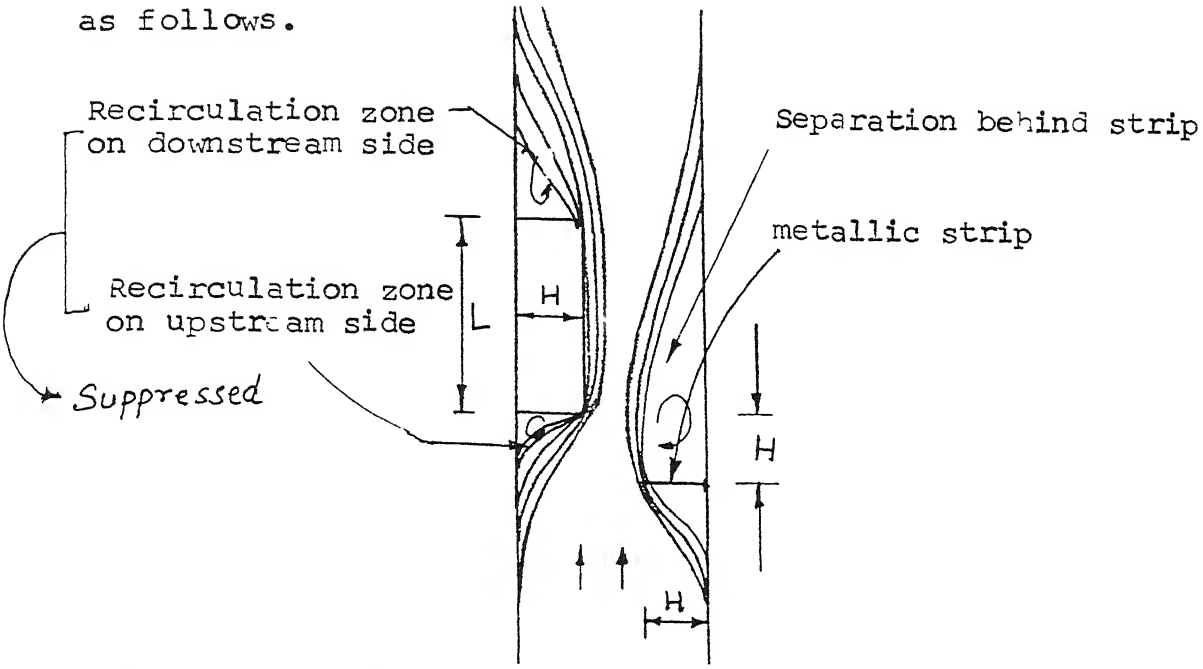

Fig.4.32: Flow pattern with protrusion on opposite wall

Fluid rising in the channel is diverted towards the heater in the presence of the protrusion on the opposite wall. This diversion of fluid is likely to have suppressed the vortex in recirculation zone on the upstream and downstream side of heater. Though the velocity near the heater increases because of reduced area, the lower heat transfer from the upper and lower sides of heater may be the reason for no augmentation in Nusselt number.

Since the fluid flowing is closely packed near the vertical surface buoyancy seems to have a stronger effect in this case showing a clearer rise in Nu with increased heat flux. The recirculation regions being already suppressed in case of heater with protrusion an increase in the slope of Nu-Re curve is not seen at low

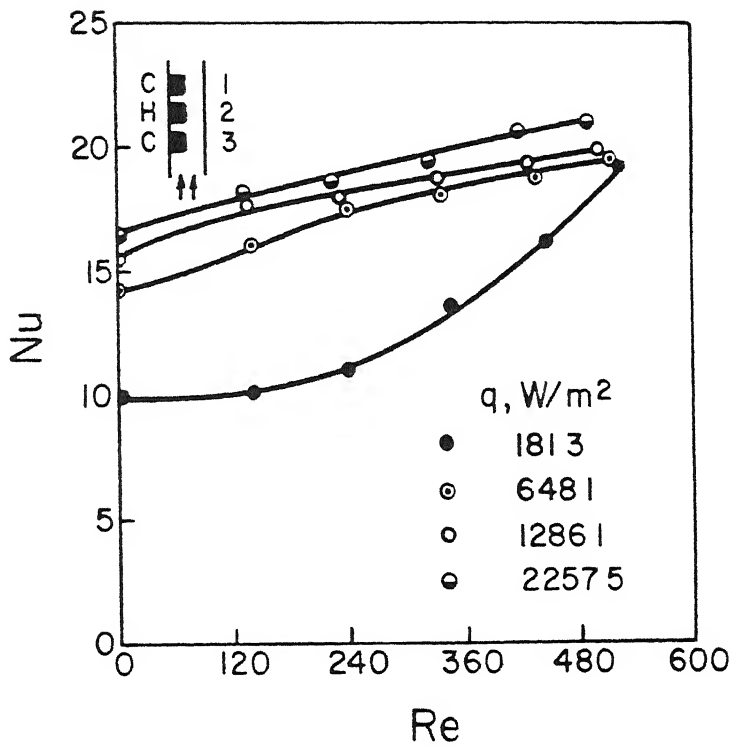
25
20
15
10
5
0
Nu
C
H
C
1
2
3
q, W/m2
1813
6481
12861
22575
0
120
240
360
480
600
Re

Fig. 4.33

heating levels.

The placement and the size of baffle will have an effect on heat transfer from the heater. The presence of protrusion increases the resistance to flow substantially. Hence it may not be really economical unless there is marked improvement in Nusselt number. This aspect must be investigated in detail in future studies.

Multichip Forced Convection Experiments

In these experiments forced convection studies over a multichip heater have been carried out. The configurations considered are:

Central chip heated

Upper and lower chip heated

All the three chips heated

Upper two chips heated.

In these experiments,due to increased resistance to the flow and the reduced size of heater, the range of Reynolds number is reduced to 550. The variation of Rayleigh number is up to 15000. Maximum temperature encountered is nearly $100^{o}C$. Four different heat flux levels have been considered. The aspect ratio for these heaters is 2.

Central Chip Heated

Figure 4.33 shows the variation of the Nusselt number with Reynolds number at different heat fluxes for the central heater.

At q = 181.3 W/m^2 the curve is initially flat and then rises as the Reynolds number is increased. The other curves are in the mixed convection regime having a flatter response with Re. The range of Re is from 0 to 550 only. At these low Reynolds numbers buoyancy will have a stronger effect. It is also due to differences in the flow pattern in comparison to a single chip heater. In the valley between the lower and the middle chip a recirculation zone exists because of flow separation over the lower chip. This

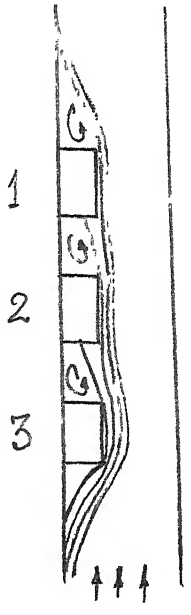

Fig.4.34 : Flow pattern for multichip heater

recirculation zone will lead to a better mixing of fluid in this region and an improved heat transfer. This is to be contrasted with a single chip heater where a hot stagnant film is formed downstream. Similarly the vortex in the region between the upper and middle chip is also not suppressed by increase in buoyant force as its strength primarily depends on the strength of flow. At higher Reynolds number the mixed

convection effects become insignificant and all the curves tend to merge.

Upper and Lower Chip Heated

The problem has been considered for 4 different heating levels. It is seen that the Nusselt number for the heater 1 is more than the Nusselt number for heater 3 and the difference reduces at higher heating levels. This can be seen from Figs. 4.35 and 4.36.The lower and middle chip disturb the flow and an increase in heat transfer over the upper heater is obtained. At higher heating levels the temperature of fluid goes up when it passes over the lower heater and hence the difference between the Nusselt number for the two heaters is reduced.

Fig.4.37 and 4.38 present the variation of Nu with Re at various heating levels for heater 1 and 3. Since the Re range is small, buoyancy effects are clearly seen. For heater 1, the augmentation due to buoyancy decreases as the heat flux increases. At a high input heat flux the temperature of fluid passing over the heater 1 is sufficiently high and uniform because of heat gain from the lower heater. This reduces the temperature gradients in the direction perpendicular to the heater. Subsequently there is reduction in augmentation due to buoyancy.

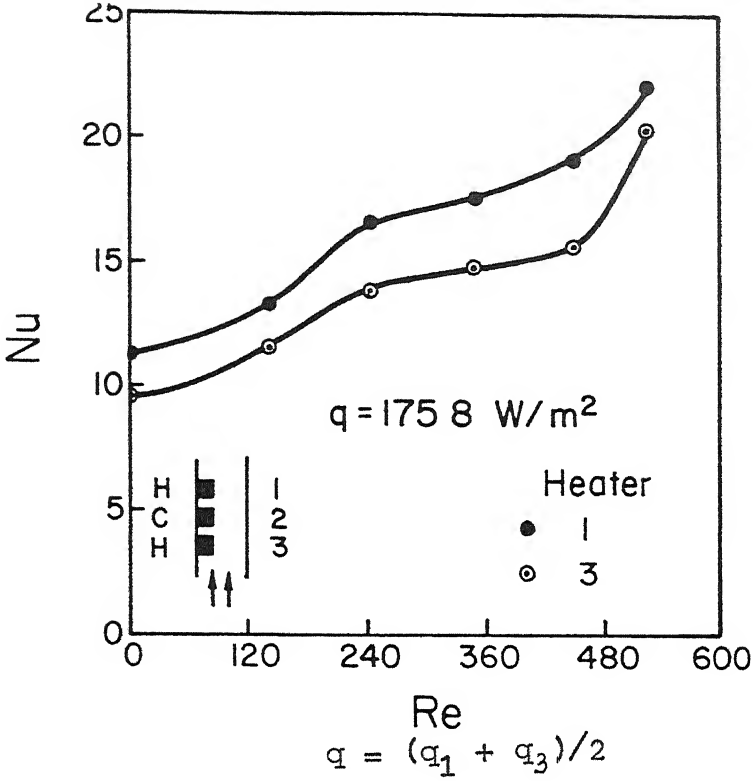

$q = (q_1 + q_3)/2$

Fig. 4.35

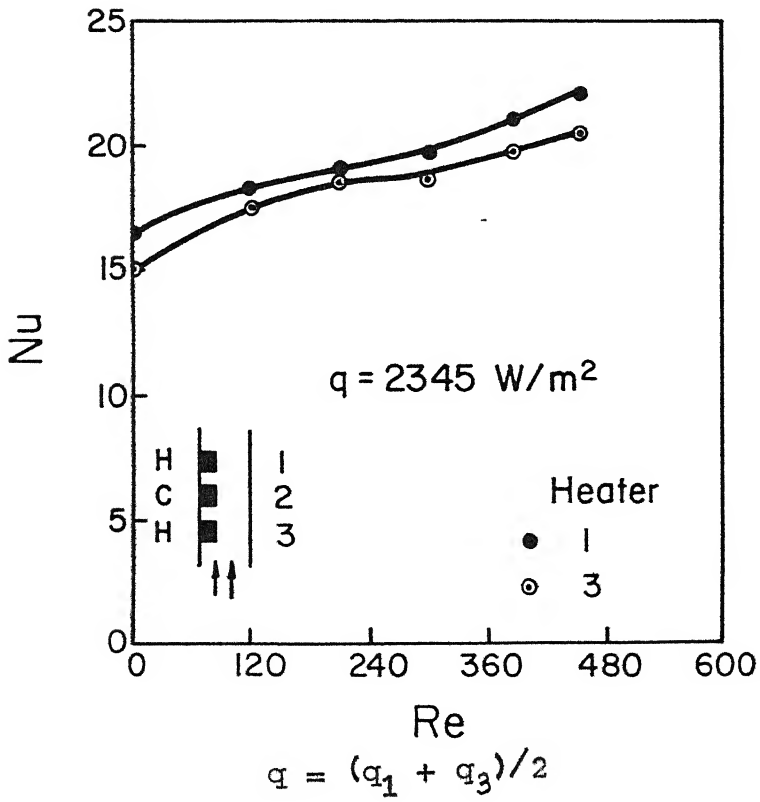

$q = (q_1 + q_3)/2$

Fig. 4.36

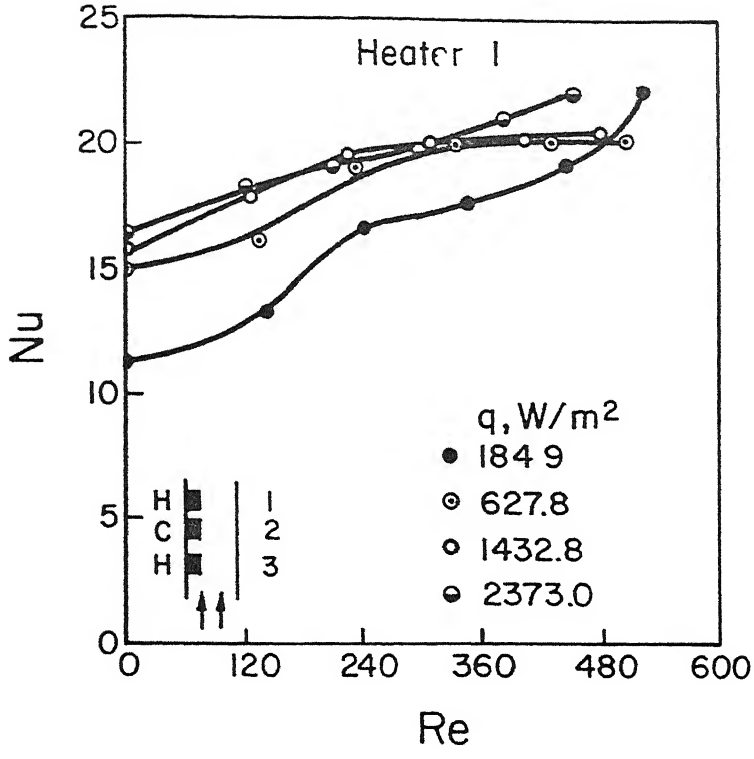

Fig. 4.37

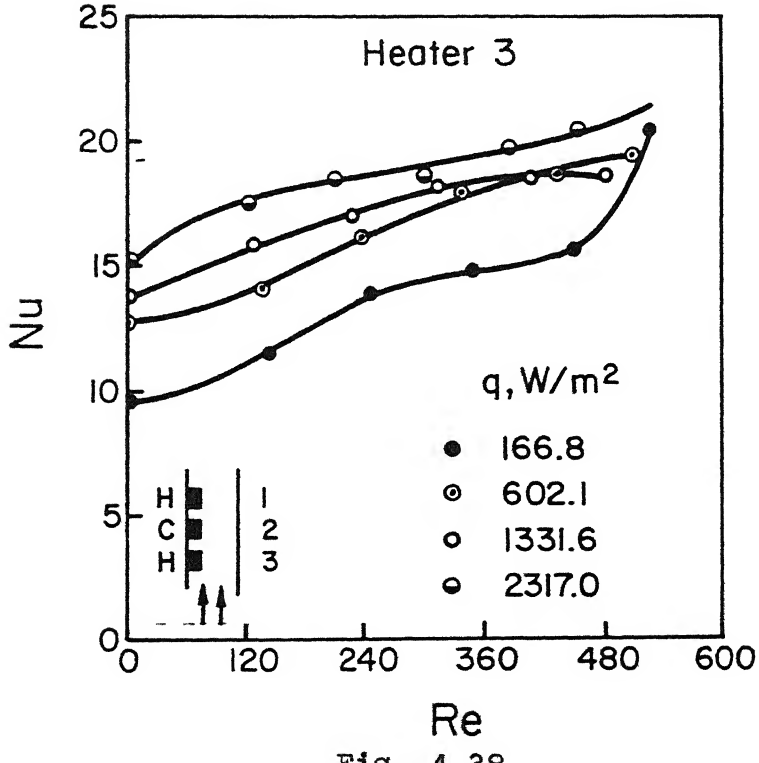

Fig. 4.38

All the Chips are Heated

We have studied this configuration for three heating levels. Figs.4.39 to 4.41 give the comparison of Nusselt number for the three heaters at different heat flux. In all the cases it is seen that the heater 2 has the lowest Nusselt number. Heater 3 is found to have the highest Nusselt number as it is subjected to the cold ambient fluid. The lower heater increases the disturbance in the flow over the middle heater but the temperature of fluid also increases. Since the value of Re is low the effect of rise in temperature of fluid is predominant and the Nusselt number over the middle heater drops a little. As the fluid passes over the central heater the disturbance to the flow increases significantly resulting in a better heat transfer over the heater 1. Nusselt number of heater 1 is nearly equal to that of heater 3 at q = 192.7 and 634.5 W/m^2. At a further increase in heat flu the temperature effects are important for heater 1 resulting in its Nusselt number being equal to that of heater 2.

Figures 4.42 to 4.44 show the Nu-Re variation individually for the three heaters at different heating levels. Augmentation due to buoyancy can be seen for all the three heaters. As the Reynolds number increases, the forced convection becomes significant and the curves seem to merge. For the upper heater, as in case of H-C-H configuration, the effect of buoyancy seems to reduce because of the reasons given earlier.

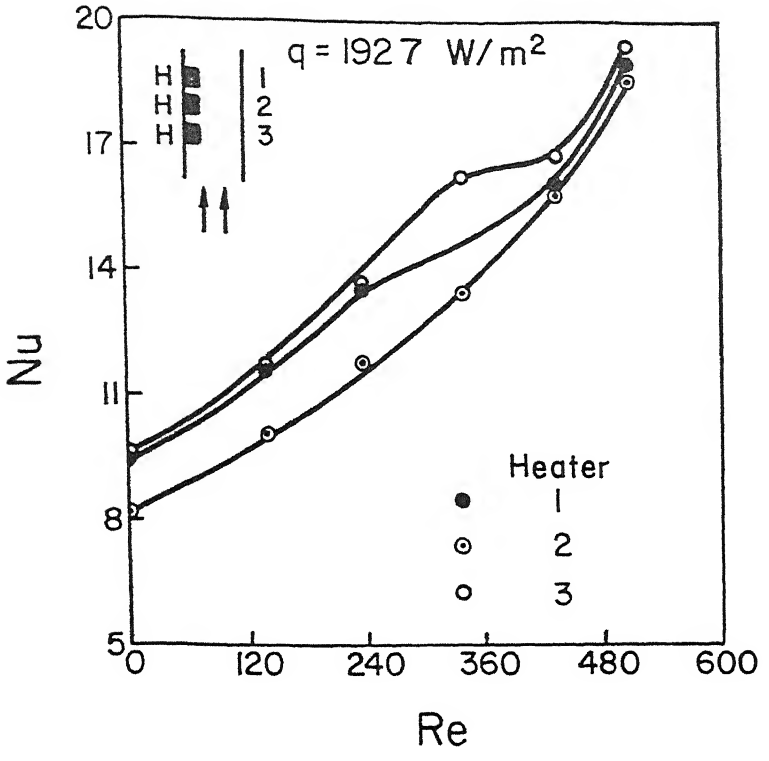

$$q = (q_1 + q_2 + q_3) / 3$$

Fig. 4.39

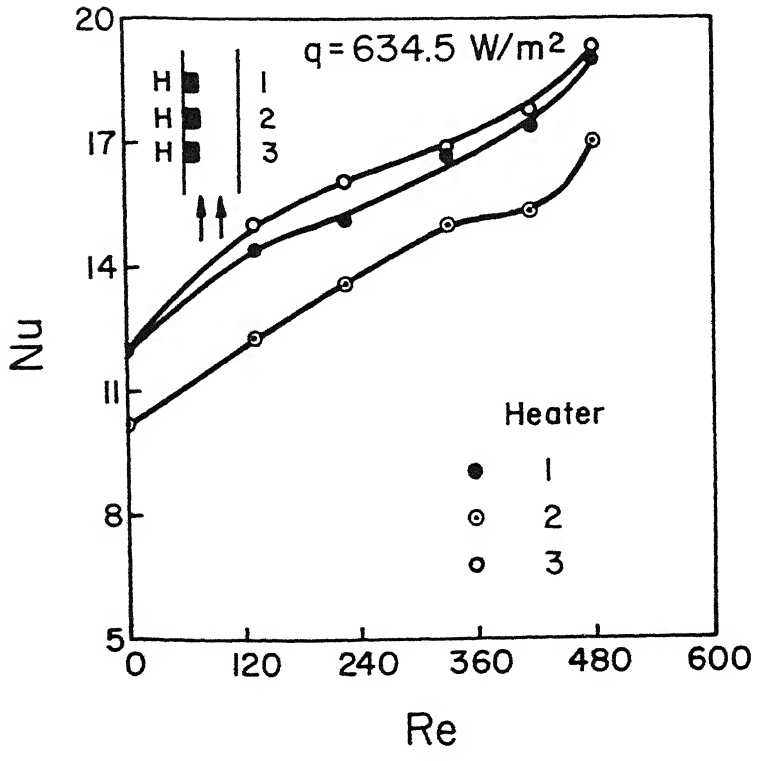

$$q = (q_1 + q_2 + q_3) / 3$$

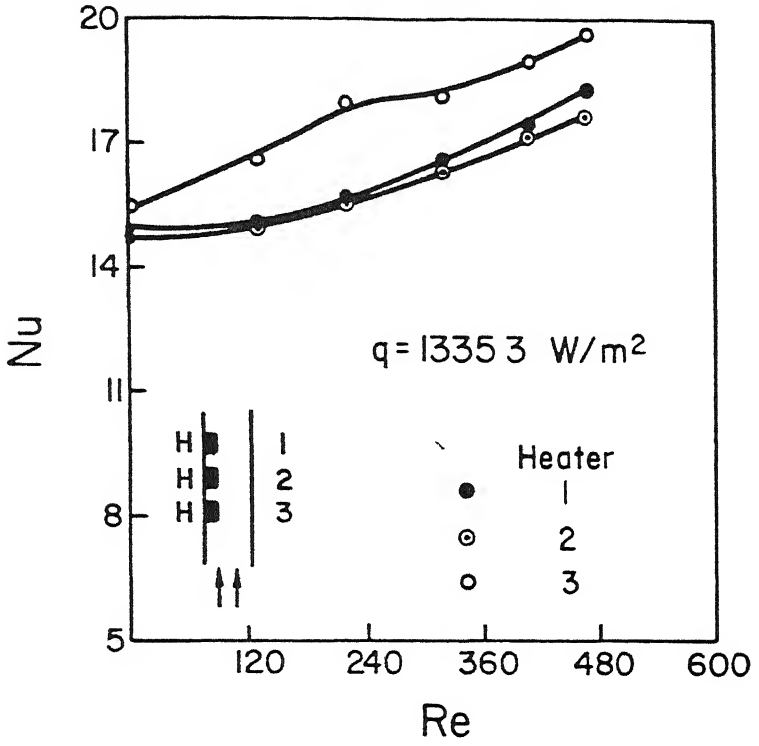

$$q = (q_1 + q_2 + q_3) / 3$$

Fig. 4.41

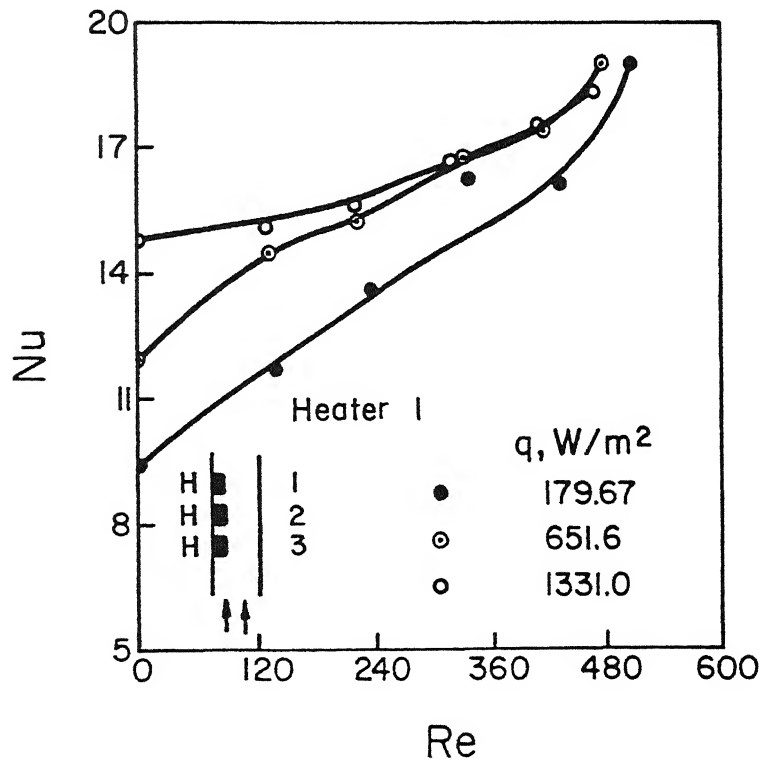

Fig. 4.42

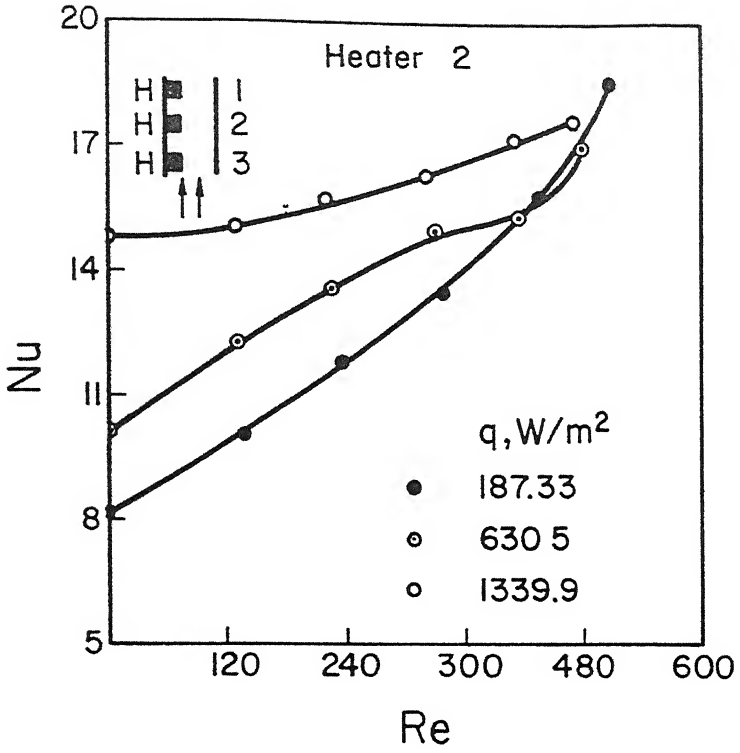

Fig. 4.43

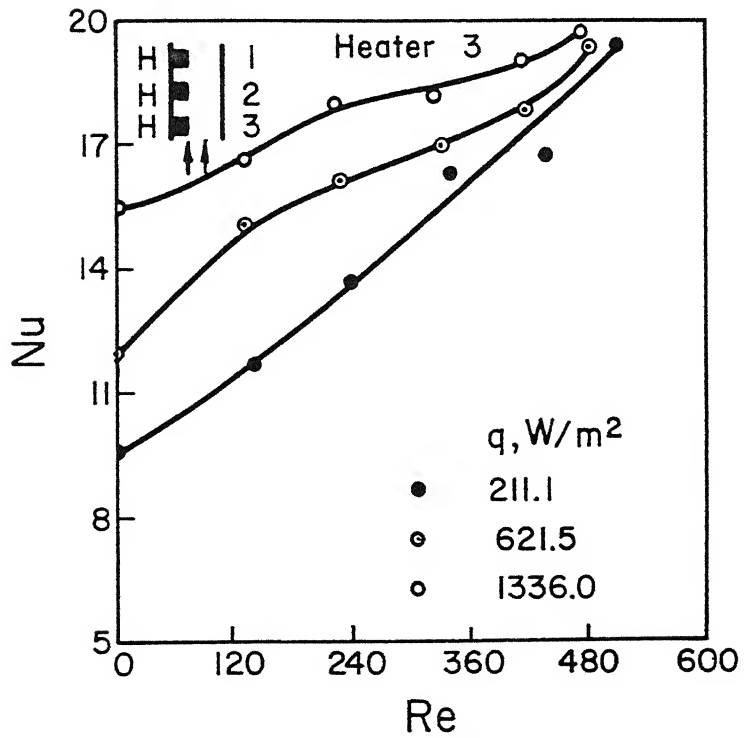

Fig. 4.44

McEntire and Webb (1988) have studied experimentally forced convective heat transfer from protruding and flush-mounted two dimensional discrete heat sources. They have measured local heat transfer coefficients within the range of $1000 \leq Re \leq 10000$. For the protruded heaters, they find enhanced heat transfer for the second and subsequent heaters. This is explained by the flow separation and associated venna contracta effects, with eventual downstream transition to turbulent flow induced by the presence of protruding heater.

Similar disturbing effects have been seen in the present study. Since in our case the range of Reynolds number is small the temperature effects are also significant and we do not see any transition to turbulence. This is the reason for slight lowering of heat transfer coefficient over the second heater (heater 2). The heat transfer coefficient for the third heater (heater 1) is nearly equal to that for the first heater (heater 3) which shows that at higher Reynolds numbers the disturbance initiated by the first heater will increase and subsequently an enhancement in heat transfer coefficient for downstream heaters will be obtained.

Upper Two Chips Heated

From the Figure 4.45 it is clear that the Nusselt number for the heater 1 is more than that for heater 2. In this case the heating level is low and temperature effects are small. The flow passes over the lower two heaters and the

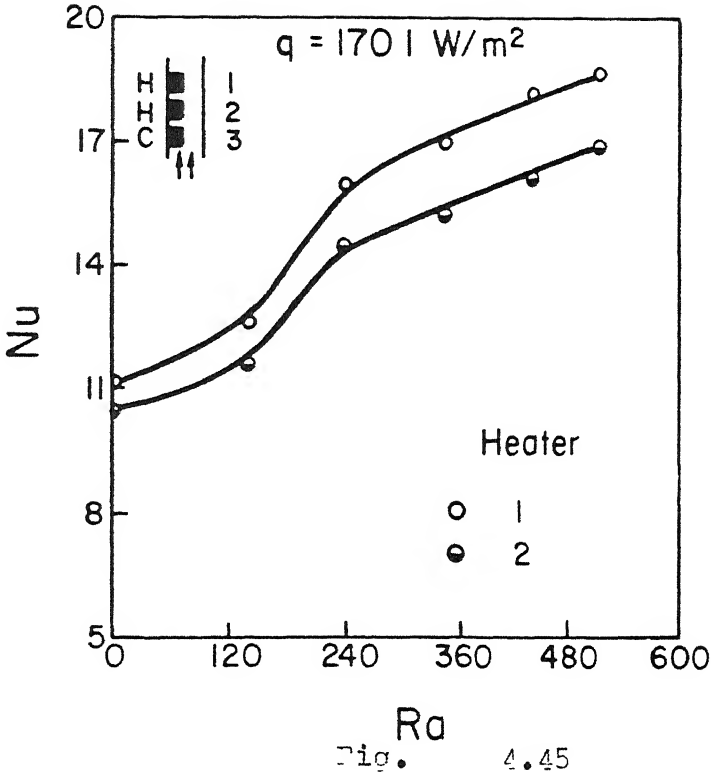
q = 1701 W/m²
H
H
C
1
2
3
Heater
1
2
Nu
Ra
20
17
14
11
8
5
0
120
240
360
480
600

Fig. 4.45

disturbance is high enough to enhance the heat transfer over the upper heater. Since we do not have data for a higher heat flux, we can not present the exact behaviour in this configuration but the difference between the Nusselt numbers for two heaters is expected to reduce because of increasing temperature effects at higher heating levels.

Let us consider the effect of a cold protrusion mounted before a heater. For this study we look at heater 2 in C-H-C combination. This heater is subjected to an unheated protrusion and cold ambient flow. The Nusselt number variation for this heater can be compared with that for the heater 3 in H-H-H and H-C-H configuration. The heater 3 in these configurations is exposed to cold ambient flow directly. The value of Nu_2 for C-H-C configuration is in general higher than Nu_3 for H-H-H and H-C-H configurations if compared for nearly same heat flux and Reynolds number.

This shows that the presence of a cold protrusion in the path of flow before the heater increases the disturbance and hence heat transfer. This suggests that the placing of an unpowered component before a powered component will lead to a better thermal performance of the electronic system.

On comparing the value of Nu_3 for H-C-H and H-H-H configuration, it can be seen that the placing of cold component above a powered component does not have any significant effect on the heat transfer.

If we compare the Nu_1 in H-C-H, H-H-H and H-H-C configurations, it is seen that maximum Nusselt number is obtained in case of H-C-H configuration in general. This gives a design idea about the placement and spacing of components in an electronic system. In these configurations the heater is subjected to disturbance created by two protrusions on the upstream side. Nu_1 in H-C-H is more than Nu_1 in H-H-H because a cold chip is placed between the two heated chips reducing the heating effects of the lower chip. Nu_1 in H-H-C is more than Nu_1 in H-H-H as in the former the heater 1 is preceeded by one heated protrusion. In H-H-H heater 1 is preceeded by two heated protrusions. Heat transfer will increase if an unpowered component is mounted between two powered components. Alternatively the distance between the two is increased which will result in a better mixing with an entrainment of cold ambient fluid.

Let us compare H-H-H configuration in forced and natural convection. In both cases the maximum Nusselt number occurs over heater 3. In natural convection the difference between Nu_3 and Nu_2 is large and then the Nusselt number becomes nearly constant for further heaters located downstream. Owing to disturbance in the flow the difference between the Nu_3 and Nu_2 is small in forced convection. The Nusselt number increases further for the heater 1. It is expected to rise further for the heaters located further downstream. This signifies the complicated flow phenomena and role of disturbance in the flow initiated by the heaters mounted on the upstream side

in forced flows. In both cases location, spacing and size of components are quite important. In forced convection flow is complex over and between the heaters. Besides mixed convection effects, recirculation and separated regions exist and analysis and interpretation of data are more involved.

Qualitative Analysis by Interferometry

In this section we present a qualitative description of the thermal field over a single chip and multi-chip heater. When the interferometer is initially in the infinite fringe setting, each fringe is an isotherm. These isotherms give the idea about the thermal boundary layer. To a limited extent flow pattern, recirculation and flow separation can also be predicted. In the present study each isotherm corresponds to a change in temperature of 3.20 °C.

For a single chip heater all the photographs have been taken from the monitor of image processing system with a highly sophisticated camera (Canon T90) with a 400 ASA film. Some of the pictures are pseudo-coloured to show a clear contrast between fringes. Another advantage of pseudo-colouring is that different temperature zones can have different colours and thus one can have a clear observation of the temperature field. In present study we have not made use of this facility and the colouring has been done only to make the picture sharp.

For the multichip heater, the photographs have been taken by the field camera and the film is developed in the laboratory itself. This causes some of the pictures to be not very sharp. Moreover thermocouple wires in the path of the light beam also distort the image by producing their own dispersive optical effects.

Single Chip Heater

Both the transient and the steady temperature field inside the enclosure have been visualized using interferometry. Figures 4.46 & 4.47 show the isotherm over the heater during the transient and steady state respectively. The first film has been taken 20 minutes after the cold initial state. The number of fringes is fewer and the fringe spacing is large. This shows low temperature gradients and hence a low Nusselt number during the transient. The number of fringes at steady state is fairly large. These are closely packed, indicating a large temperature gradient and a high Nusselt number. Thermal boundary layer can be seen in the Figure 2. The thickness of the thermal boundary layer is small at the leading edge of chip and increases over the heater. This shows that the highest value of the Nusselt number occurs at the leading edge. The air outside the boundary layer is cold as seen by the absence of fringes in that region.

Figures 4.48 and 4.49 show the trailing side of heater for a low and a high input heat flux respectively. The thickness of fringes increase near the trailing edge due to a reduction in heat transfer in that region. On the downstream side of heater, the fringe spacing is increased which is a region of low velocity and low heat transfer. The deviation of the outer fringe indicates the existence of a

recirculation zone. Further downstream the deviation of the outer fringes towards the passive wall is also observed. The isotherms remain attached to the passive wall beyond the trailing edge. Hence we expect the temperature in this region to be higher. If cooling is provided here then the thermal performance of the circuit board can certainly improve.

Figure 4.50 shows the isotherms in the upper region of the enclosure when the top of the enclosure is open. Here a wall plume like behaviour is seen and the thermal energy is lost to the ambient from the top instead of accumulating on the side wall as in the case of a closed enclosure.

Figure 4.51 shows the initial cold state with the interferometer set in the wedge fringe mode. Subsequent deviations of the isotherms at steady state is shown in Figure 4.52 . Here again a boundary-layer can be seen whose thickness is equal to that in the infinite fringe setting for a given input heat flux.

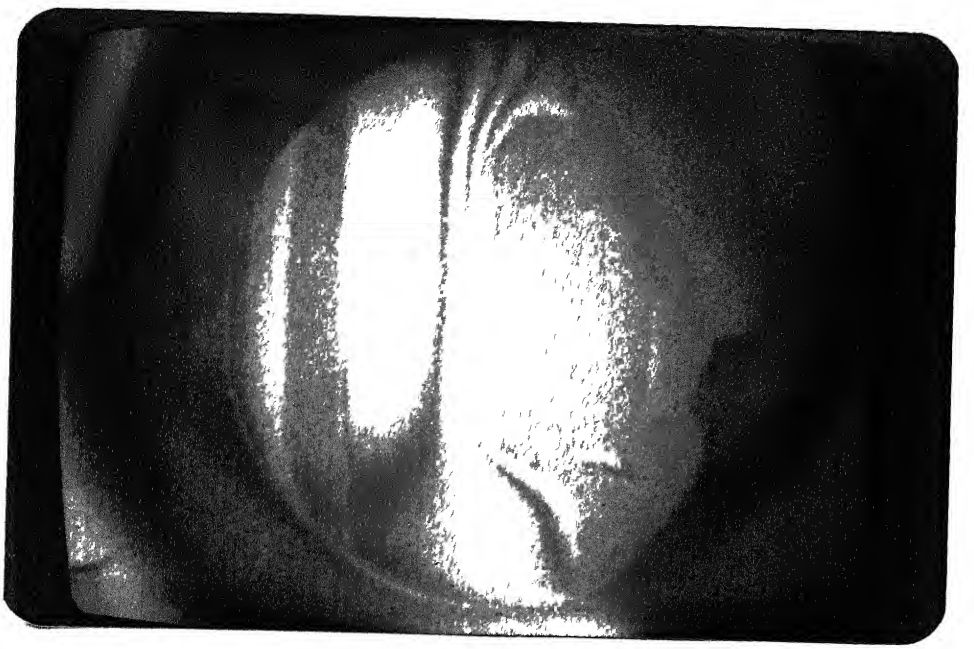

Fig. 4.46 : Isotherms in transient

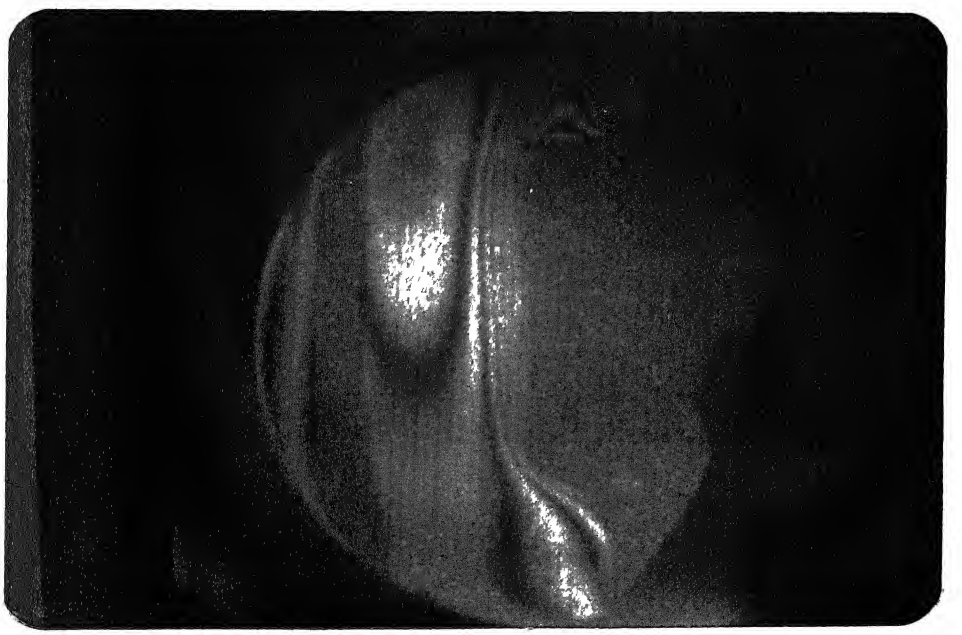

Fig. 4.47 : Isotherms in steady state

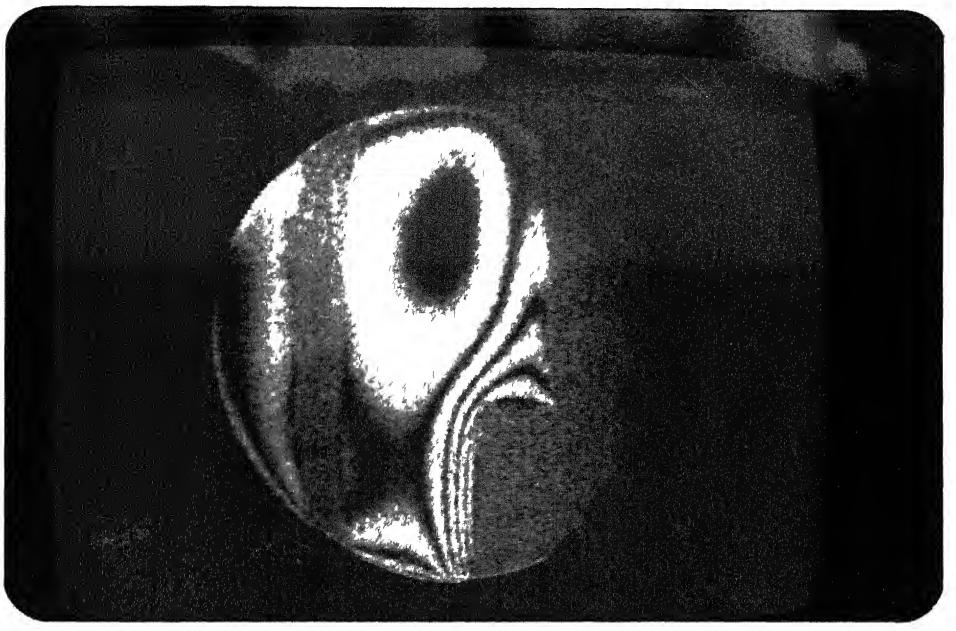

Fig. 4.48 : Isotherms downstream the heater at low heat flux

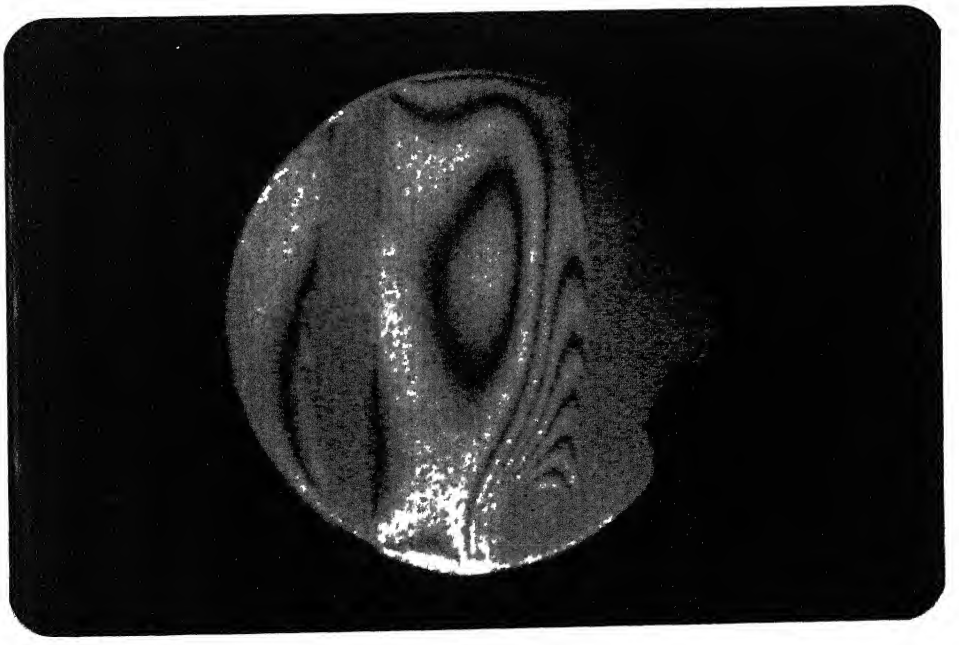

Fig. 4.49 : Isotherms downstream the heater at high heat flux

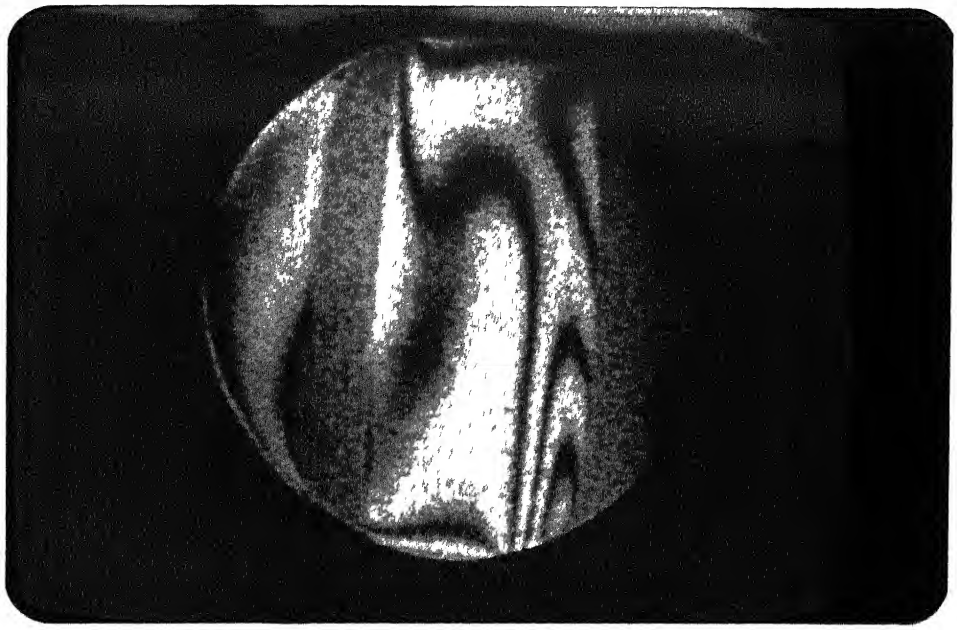

Fig.4.50 : Isotherms in the upper region of an open enclosure

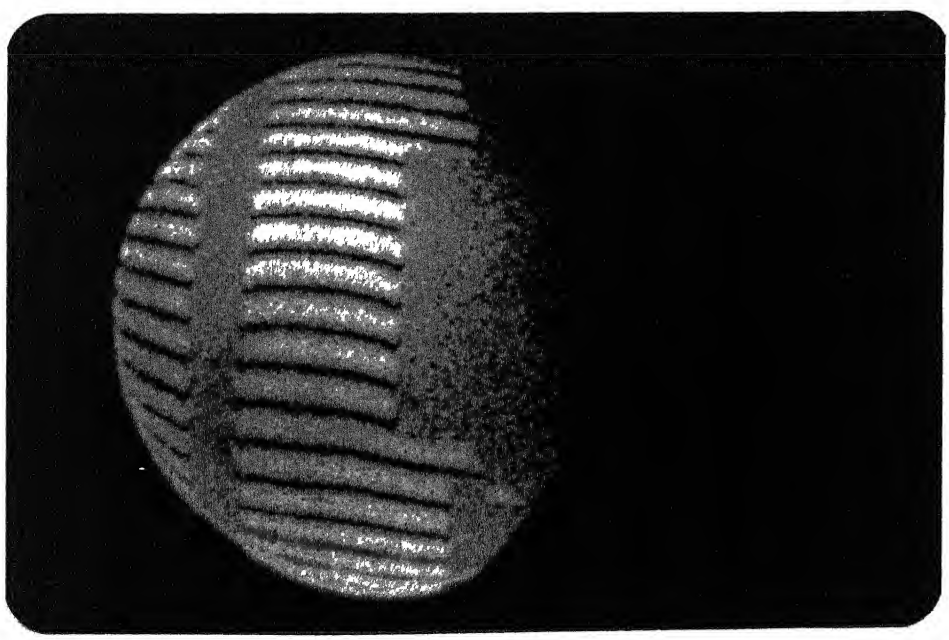

Fig. 4.51: Initial setting of interferometer in wedge fringe mode

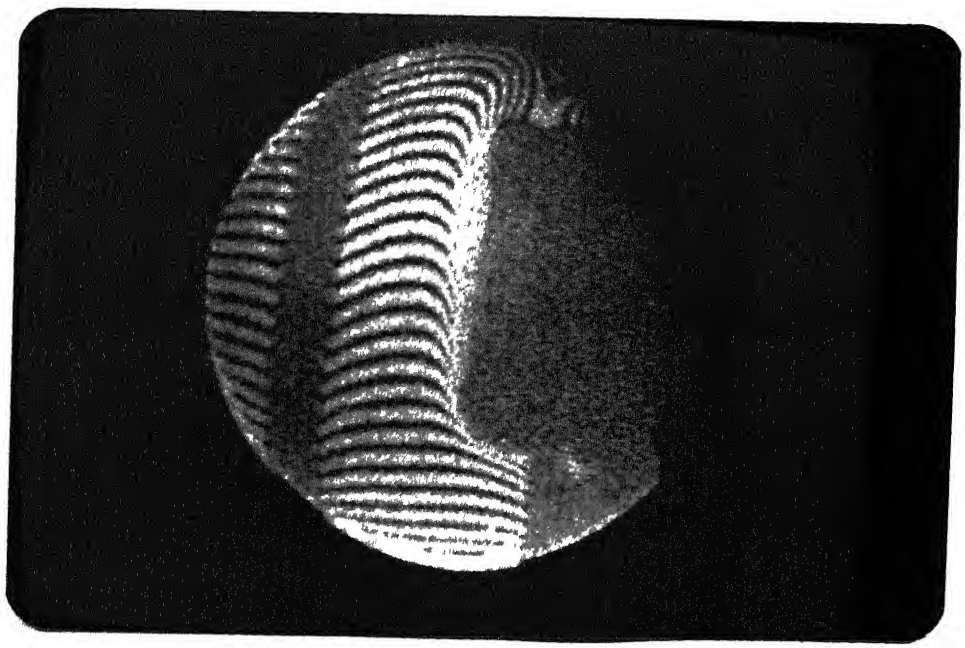

Fig. 4.52 : Wedge fringes at steady state

Mulichip Heater

The problem can be divided into 3 configurations.

(a) Central chip heated

(b) Lower two chips are heated

(c) All the three chips are heated.

Central Chip Heated

The heat flux applied is $q = 709\ W/m^2$ and temperatures are $T_c = 53^{\circ}C$ and $T_{\infty} = 27^{\circ}C$. The transient state can be seen in Figures 4.53 and 4.54 . In the initial stages the isotherms tend to tilt away from the heated strip because of weak flow. As the temperature of chip increases the buoyancy force increases and the natural convective flow in the vicinity of chip becomes more parallel.

Figure 4.55 shows the middle chip at the steady state. The growth of thermal boundary layer in the vertical direction can be seen here.

Figure 4.56 shows the lower chip and the spacing between middle and lower chip. Since the lower chip is unheated only one fringe is formed on its surface. Most of the fringes can be seen originating from the wall which shows the heating of wall close to the chip. The absence of fringes in the lower portion of enclosure indicates a cooler region as expected.

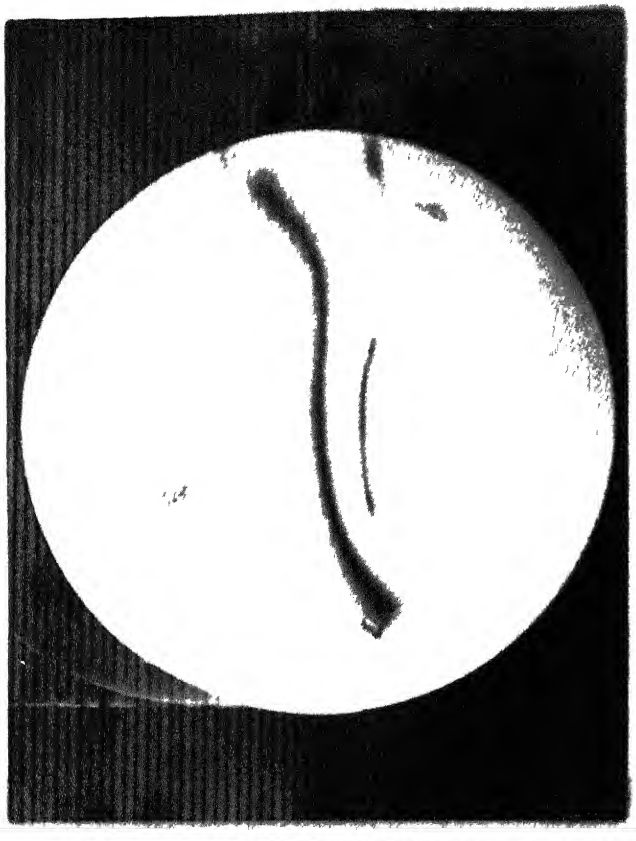

Fig.4.53

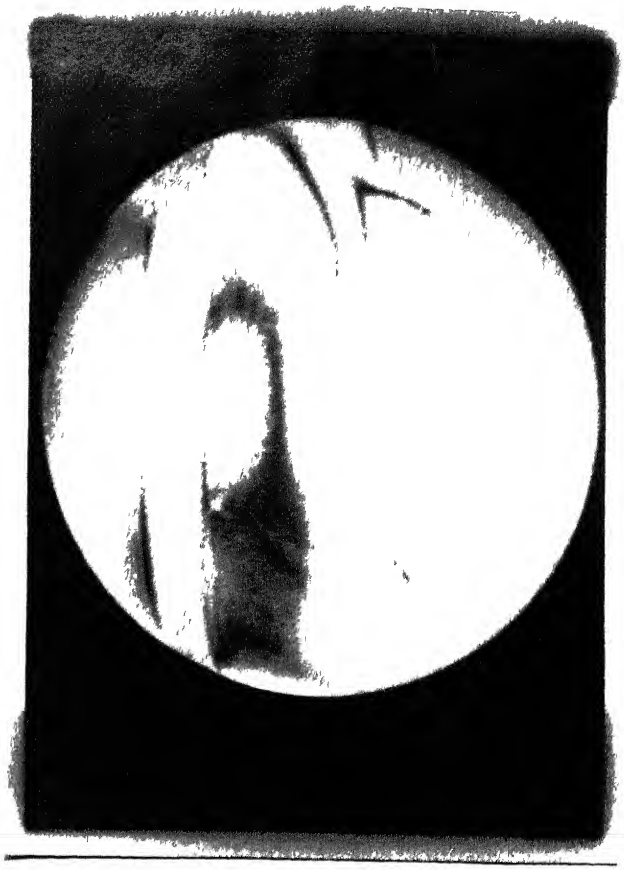

Fig.4.54

Isotherms over central chip in transient state

Figure 4.57 shows the isotherms in the region between upper and middle chip. The isotherms very close to the heated chip merge in the region close to the trailing edge of the chip. This shows that the temperature of chip is much higher than temperature of the supporting wall which indicates that conductive heat transfer to the bakelite sheet is low. The upper strip is also unheated except by the plume coming from below. Hence it does not have many isotherms.

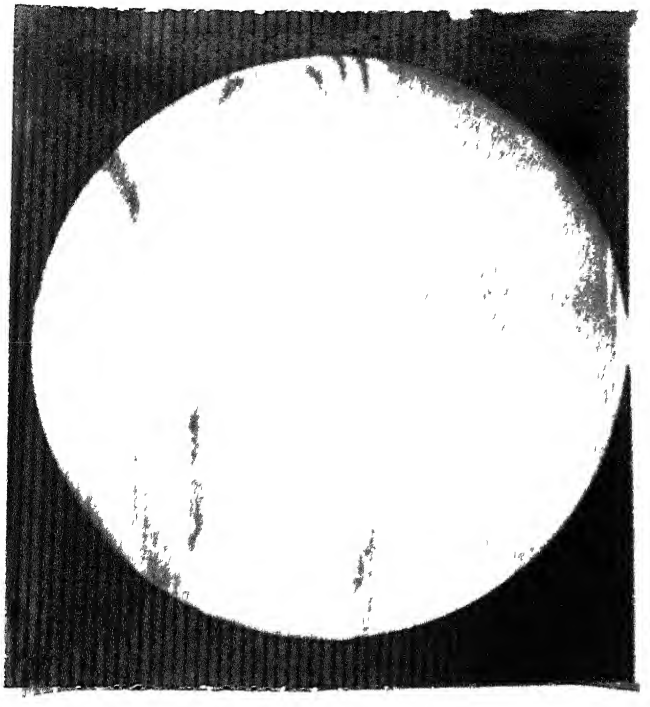

Fig.4.55 : Isotherms at steady state

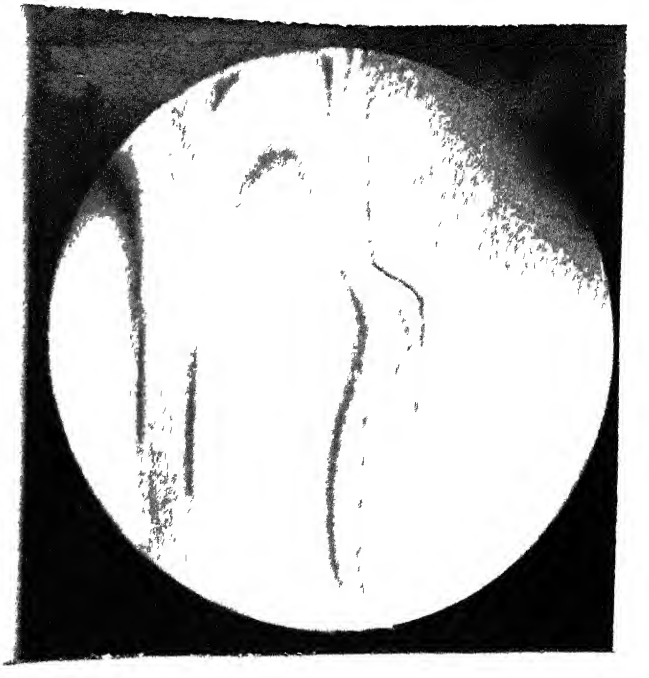

Fig.4.56 : Spacing between middle and lower chip

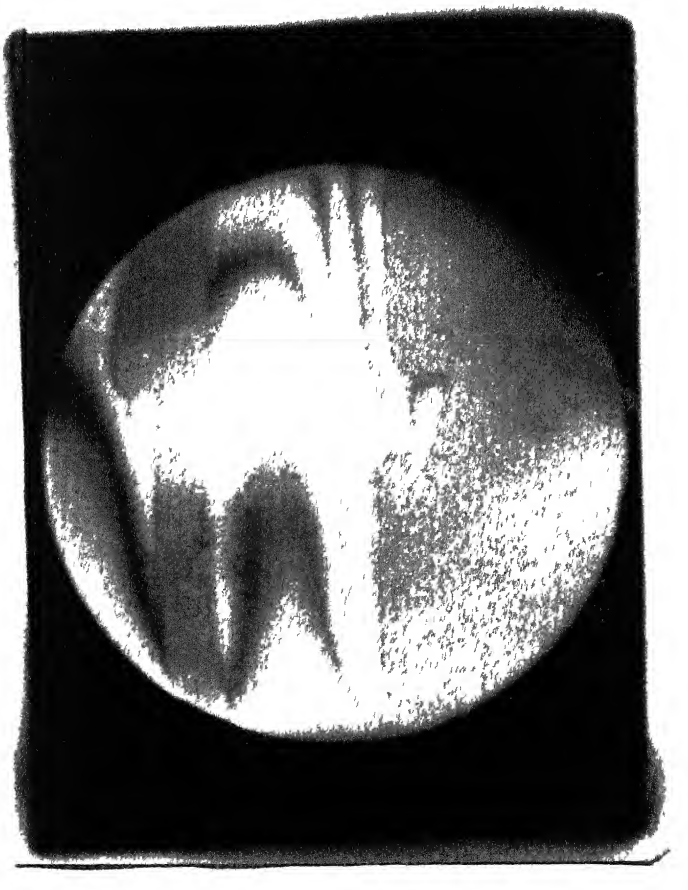

Fig. 4.57 : Isotherms in spacing between upper and middle chip

The presence of a few isotherms however does show the temperature of upper chip is higher than the ambient temperature. Since the upper chip does not dissipate any heat flux the isotherms are fairly away from the chip. No significant thermal boundary layer growth is seen. The number of isotherms in the lower region of enclosure being less than that in the upper region clearly indicates the difference between the heat transfer mechanisms to lower and upper heater and the direction of mean buoyant flow. The lower chip gets heated because of diffusion only and it is reasonable to expect the wall conduction to be insignificant.

Lower Two Chips are Heated

In this configuration the middle and the lower chip are dissipating heat. The chips are subjected to only moderate heat flux levels so that the fringes formed on them can be seen clearly. The figures 4.58 to 4.61 show the thermal field close to the lower chips in transient state. Figure 4.58 corresponds to initial infinite fringe setting of interferometer. Figure 4.59 shows the beginning of the formation of isotherms. This film has been taken after 50 minutes from initial cold state. Figure 4.61 shows the fringes at steady state. In this configuration the heat flux on central chip is $q_2 = 202.6\ W/m^2$ and on lower chip is $q_3 = 208.4\ W/m^2$.

$T_1 = 28.8^oC$, $T_2 = 34.72^oC$, $T_3 = 31.96^oC$ and $T_\infty = 18.3^oC$.

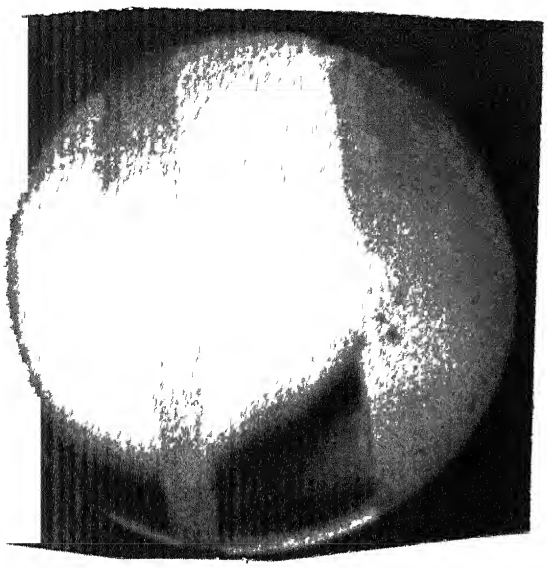

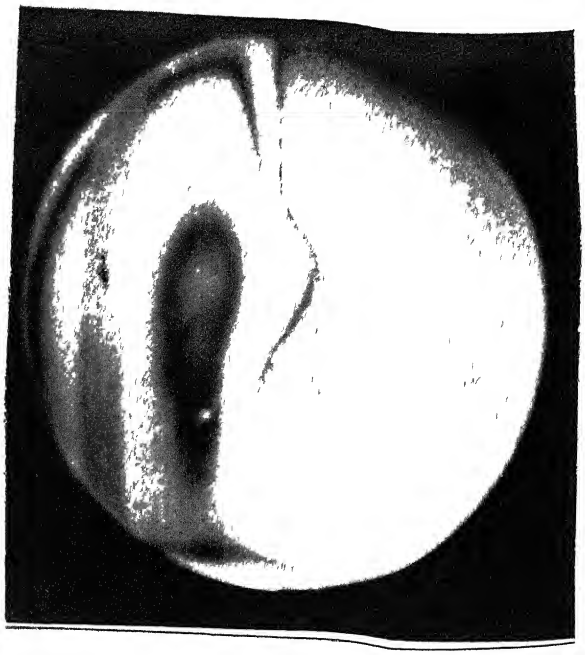

Fig.4.58:Initial infinite [illegible]

Fig.4.59: Transient [illegible]

The isotherm closest to the heater follows the wall along the heater surface. It follows the wall in the valley also between the two chips. Since in this case the heat flux is low, the flow is weak and separates from the heater surface. Higher order fringes show early separation by tilting away from the wall.

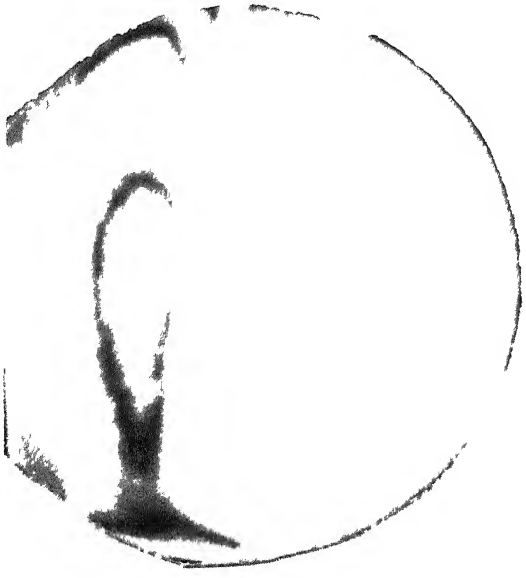

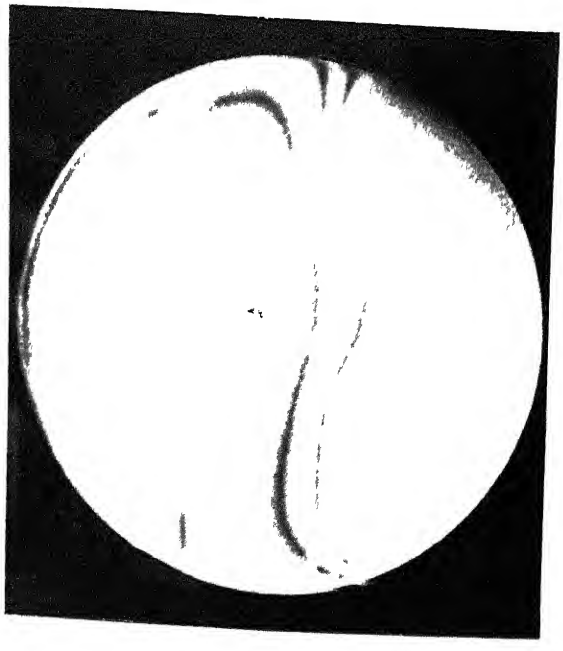

Fig.4.60: Transient state Fig.4.61 : Steady state

It can be seen from the Figure 4.61 that rate of heat transfer and subsequently the Nusselt number is highest at the leading edge of the lower chip. The central chip does not come in direct contact with cold air. This is seen from the isotherm that begins from the lower chip and envelopes the middle chip. This explains the lowering of Nusselt number over the central chip.

The Figure 4.62 shows the isotherms in the region between middle heated and upper unheated chip. Since the upper chip is unheated, separation occurs right at the trailing edge of the central heater. It can be explained as follows. Consider the isotherm which follows, the wall and the valley between the two heated chips. It begins to

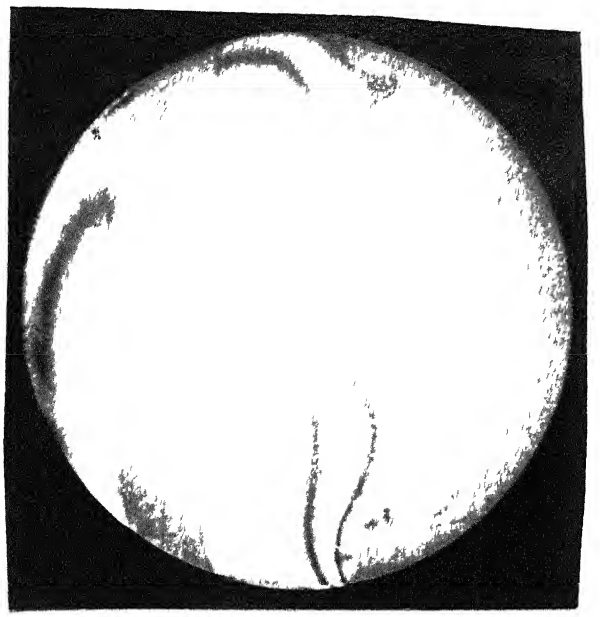

Fig. 4.62 : Separation of isotherms at the trailing edge of central heater

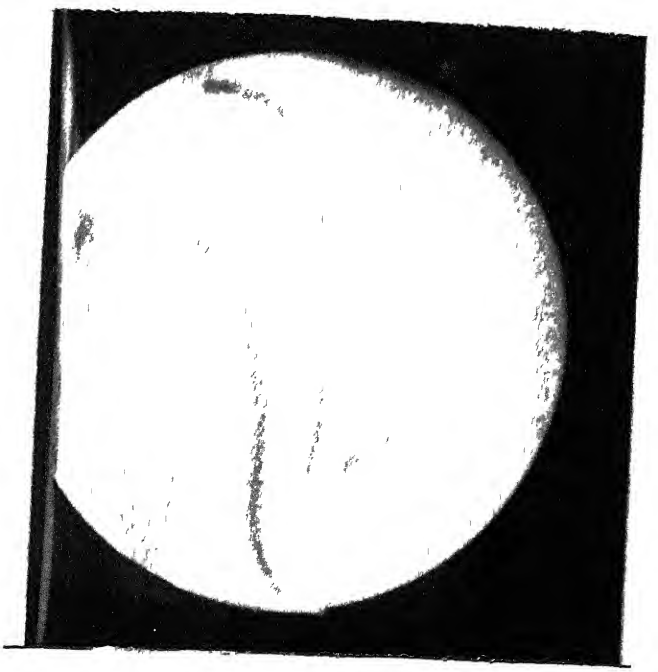

Fig.4.63 : Deviation of fringe due to unheated upper heater

separate at the end of central heater.

The Figure 4.63 shows isotherms in the upper region of enclosure. As the upper chip is unheated the isotherms show a deviation towards the neighbouring wall and accumulation of hot air in the upper region. It can be seen that the upper cold chip acts as a disturbance to the thermal plume rising from the central chip resulting in the isotherms get deviated towards the opposite wall. This energy can be absorbed efficiently if the cooling and ventilation are provided on the opposite wall.

All The Three Chips are Heated

In this case the chips were subjected to a higher heat flux. As can be seen from the figures that the fringe density is very high close to the chips. As in the earlier configurations the maximum Nusselt number occurs at the leading edge of the lower chip since the thermal boundary layer thickness is a minimum at this point. The heat flux and temperature levels are-

$$q_1 = 1334.6 \text{ W/m}^2 ; q_2 = 1319.0 \text{ W/m}^2$$

$$q_3 = 1300.5 \text{ W/m}^2$$

$$T_1 = 87.02^{\circ}\text{C} ; T_2 = 86.8^{\circ}\text{C} ; T_3 = 64.16^{\circ}\text{C}$$

$$T_{oo} = 21.8^{\circ}\text{C}$$

Figure 4.64 shows the isotherms over the lower and central chip. The region between the two chips also becomes hot.

The lower order isotherms close to the heater follow the contour of the heater and the valley between heaters.

Figure 4.65 shows the region between the central and upper heater. It can be seen from this figure that the temperature of air inside the enclosure increases as we move upwards. Figure 4.66 shows the isotherms in the upper portion of the enclosure. The separation of isotherms from the wall is seen here. The deviation of isotherms and congestion in the upper region indicates hot air accumulation and some amount of air-circulation.

The lower region of enclosure is shown in Figure 4.67 . It can be observed that the temperature of the enclosure in this region has not risen much above the ambient temperature. It is only beyond the middle of the central heater that the mean temperature of air inside the enclosure rises substantially.

As we begin to move up in the enclosure, it can be seen that the higher order fringes follow the wall upto a point and then separate and deviates towards the neighbouring wall. Their thickness also increases along the path. The fringe pattern near the opposite wall indicates some amount of recirculation in the enclosure as the hot air on the active wall rises up and pushes the air trapped in the upper portion.

The thermal boundary layer formed over the central and upper heater are seen to be nearly equal in thickness. Hence the heat transfer rates and Nusselt number over the two heaters are nearly equal. This is in conformance with the result obtained in the energy balance experiments. There is a variation in Nusselt number over the heater length and this can be seen from the variation in the fringe density over the heater length.

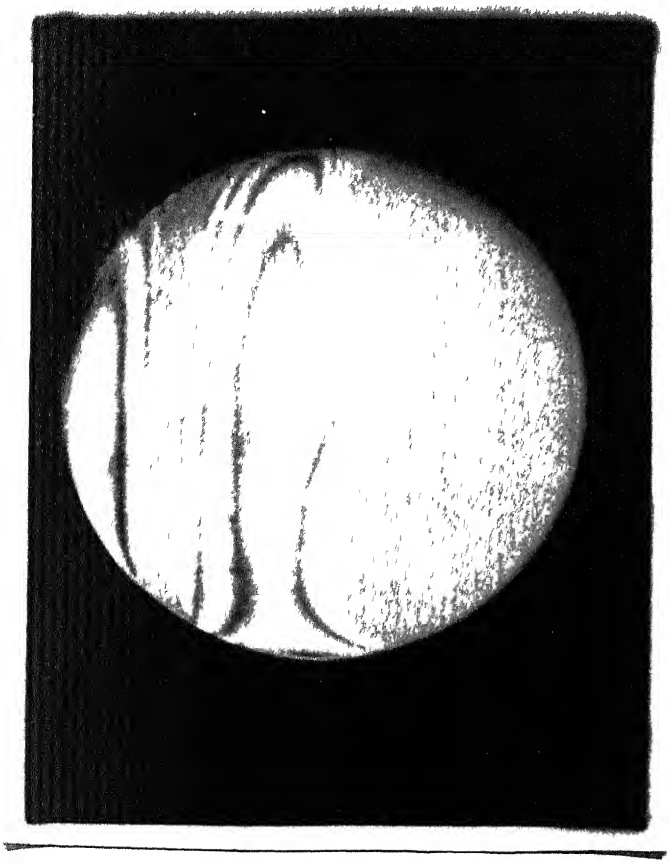

Fig.4.64 : Isotherms between lower two chips

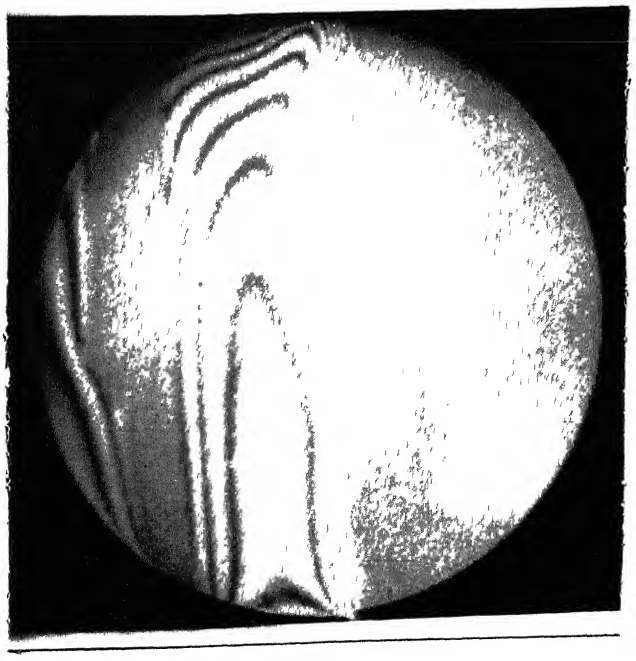

Fig. 4.65 : Isotherms over upper heater

Quantitative Analysis by Interferometry

We have calculated the value of Nusselt number by interferometry for a few cases to cross check the results obtained by using energy balance. Here we present results for two cases. The method used to calculate the Nusselt number is based on curve fitting referred earlier in Chapter 3.

Case 1:

The heater aspect ratio is 3.

Input heat flux $q = 564.72\ W/m^2$

Temperature of chip $T_c = 48.7^{\circ}C$

Ambient temperature $T_{\infty} = 18.1^{\circ}C$

The Nusselt number through conventional method = 18.1.

The Nusselt number through interferometry = 20.71.

Case 2:

The heater aspect ratio is 2.

Input heat flux $q = 799\ W/m^2$

Chip temperature $T_c = 53^{\circ}C$

Ambient temperature $T_{\infty} = 27^{\circ}C$

The Nusselt number through conventional method = 14.3.

The Nusselt number through interferometry = 16.1.

The Nusselt numbers obtained by the two methods are close but the value obtained using interferometry is higher.

[illegible] the test section length being small the estimated [illegible] not negligible at the chip surface. This is [illegible] to temperature gradients near the heated wall. [illegible] temperature gradient reduces away from the chip surface. [illegible] points chosen to determine the temperature profile [illegible] from the chip surfaces the temperature gradients [illegible] the error due to refraction at those points [illegible] and can be neglected. The accuracy of this method depends on the number of points chosen and their distance from the heated surface. More the number of points better will be the fitted curve. The points taken near the heated surface will give a better approximation to the actual temperature profile in the vicinity of the heater. Measurement of fringe spacing manually through the negative of a photographic film also involves some amount of error and approximation.

Considering all these factors, the results obtained by the two methods can be considered to be close within experimental limits.

Calculation of the Nusselt Number (Numerical)

In the Table 4.53 we present the results for a flush heater mounted on the wall of a vertical channel as calculated numerically. The basic scheme is described in Muralidhar and Kulacki (1987). Here the results have been obtained with some modifications in the boundary conditions. The data presented gives an idea about the Nusselt numbers with a flush heater in mixed and forced convection regime.

Free convection has not been considered in numerical calculation. For configuration and detailed numerical analysis refer Appendix 4 .

It can be observed that the Nusselt numbers with a flush heater are lower than that with a protruded heater (as calculated experimentally in this study). This result is expected because of better heat transfer rates obtained with a protruded heater. It is clear that as the Rayleigh number increases the Nusselt number increases for the same Reynolds number. Flow patterns are simple and the buoyancy has a clear augmentating effect on the Nusselt number for a flush heater. Some amount of recirculation on the opposite wall has been observed at high Rayleigh numbers. Experiments with protruded heater show a different behaviour because of complex mechanisms of flow and heat transfer.

Numerical results have been obtained for flat and parabolic velocity profile in the channel. The Nusselt number obtained with a flat velocity profile is little higher than with a parabolic velocity profile. But the velocity profile does not affect the Nusselt number too significantly.

Table 4.1 : Single Chip Natural Convection

Open Enclosure

q	T_c	T_∞	Ra	Nu
60.99	36.4	30.1	8333	8.732
208.27	41.88	30.2	14687	16.2
411.55	51.95	30.2	24992	17.2
756.04	63.6	30.0	34911	20.45
1178.46	79.2	30.1	44663	21.6
1396.5	90.89	30.3	49993	20.75
1752.9	104.1	30.5	54547	21.4

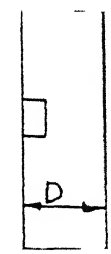

D = 3H , AR = 3

Table 4.2 : Single Chip Natural Convection
Closed Enclosure

q	T_c	T_∞	Ra	Nu
63.49	35.17	31.0	5458.9	14.2
212.9	43.15	29.6	16904.2	14.61
432.56	52.88	33.0	20313.5	19.66
775.08	66.65	30.3	36728.4	19.1
1176.71	83.60	29.3	47828.7	19.0
1388.35	91.84	29.1	51702.4	19.0

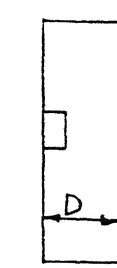

D = 2H, AR = 3.

Table 4.3 : Single Chip Natural Convection
Closed Enclosure

q	T_c	T_∞	Ra	Nu
62.6	36.3	30.1	8208	9.4
208.4	46.5	30.3	19529	11.8
451.9	55.09	33.3	23926	18.75
774.3	67.40	30.2	37367	18.6
1211.0	84.90	30.6	46982	19.5
1390.6	93.75	30.2	51258	18.9

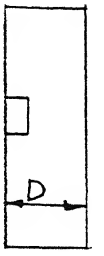

D = 3H, AR = 3.

Table 4.4 : Single Chip Natural Convection
With a protrusion mounted in the path of fluid. Location of protrusion is shown in Figure (4a)

Position of disturbing strip case	q	T_c	T_∞	Ra	Nu
a	440.45	56.76	33.83	24751	17.33
b	435.45	58.49	34.26	25687.1	16.11
c	439.3	58.42	31.52	28982.9	14.74
d	439.3	58.31	31.31	29153.11	14.74
e	437.0	57.92	31.8	28220.3	15.15
f	434.32	58.30	31.14	29357.1	14.47
g	435.44	58.12	31.0	29383.4	14.53
h	437.07	57.33	30.5	29354.2	14.75
i	1169.3	86.32	31.9	46211.0	18.59
j	1173.8	86.95	32.5	45848.6	18.65
k	1169.3	87.01	32.1	46313.6	18.48

AR = 3

Table 4.5 : Single Chip Natural Convection

White Enclosure

q	T_c	T_∞	Ra	Nu
387.9	50.27	29.95	23799.8	17.5
716.6	65.55	30.9	35223.5	18.55
1153.4	82.43	31.81	44407.2	19.91
1487.5	95.21	33.3	48536.8	20.67
1482.4	91.41	29.51	51075.9	20.82
1497.8	94.82	31.3	50493.3	20.36
1838.45	104.66	29.85	55388.3	20.965
2213.77	115.98	30.26	57945.8	21.45

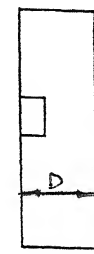

D = 3H, AR = 3

Table 4.6 : Single Chip Natural Convection

Black Enclosure

q	T_c	T_∞	Ra	Nu
179.3	38.73	29.5	11993.6	17.94
202.8	38.22	28.1	13321.7	18.3
341.15	46.43	29.25	20851.7	18.35
719.47	67.78	33.87	33261.5	18.95
1167.31	80.39	34.11	40776.2	22.104
1509.7	95.62	34.47	47485.8	21.20
1928.99	106.19	33.93	51733.6	22.62

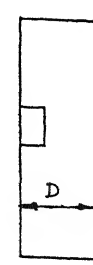

AR = 3, D = 3H.

Table 4.7 : Single Chip Natural Convection
Radiative Heat Loss

Chip temp. ^{o}C	Power input watts	Radiation losses watts	% Radiation losses
38.73	1.434	0.1433	9.99
46.43	2.72	0.2797	10.2
67.7	5.745	0.6436	11.83
80.38	9.321	0.9748	10.45
95.2	12.05	1.533	12.7

D = 3H, AR = 3.

Table 4.8 : Single Chip Natural Convection
Setup without Slit

(With Conduction to supporting plate)

q	T_c	T_∞	Ra	Nu	$\frac{N_u}{AR}$	$\frac{Ra}{AR^3}$
42.9	33.04	30.37	3599	15.101	5.03	133.2
88.3	35.43	30.5	6533.15	16.75	5.55	241.9
186.6	38.42	28.65	12821.6	17.67	5.89	474.8
352.16	46.67	28.78	22025.6	17.99	5.99	815.7
685.8	60.87	29.1	35049.0	19.34	6.44	1298.1
840.2	70.27	29.45	41846.0	18.21	6.07	1549.8
1172.9	79.9	29.6	48293.0	20.39	6.79	1788.6
1463.4	89.4	30.0	53013.0	21.285	7.09	1963.44

D = 3H, AR = 3.

Table 4.9 : Setup with Slit
(No Conduction to the supporting plate)

q	T_c	T_∞	Ra	Nu
45.36	33.81	30.37	3964.6	14.81
97.341	36.72	31.1	7333.9	16.28
130.85	37.57	30.5	9215.2	17.25
374.39	49.26	28.78	24801.0	16.67
705.03	67.21	29.25	39971.0	16.54
983.2	77.53	29.5	49940.0	17.96
1227.45	87.96	29.6	52948.0	18.25
1503.88	97.00	30.02	57070.0	19.23

D = 3H, AR = 3.

Table 4.10 : Single Chip Natural Convection
Heater with Reduced Aspect Ratio

q	T_{chip}	T_∞	Ra	Nu	ΔT	$\frac{Nu}{AR}$	Ra/AR^3
141.6	36.99	29.7	2106.21	10.75	7.29	5.37	263
329.49	43.29	28.9	3888.7	12.74	14.39	6.37	486
791.3	58.23	28.7	7006.6	14.59	30.93	7.29	875
1453.0	77.29	28.7	9776.3	15.890	48.59	7.942	1222
2135.4	98.75	29.4	11654.4	15.892	69.35	7.945	1456
3004.3	118.93	29.9	12729.7	16.96	89.03	8.48	1591
3859.6	133.8	29.0	13441.1	18.19	104.8	9.09	1680

D = 3H, AR = 2

Table 4.11: Natural Convection 3-D Heater Mounted on a Horizontal Plate. All sides exposed to ambient

q	T_c	T_∞	Ra	Nu	ΔT
2355	58.55	25.2	4898	32.2	33.5
2765	62.9	25.2	5363	33.2	37.7
3214	67.5	26.6	5574	35.32	40.94
3484	72.89	29.4	5585.9	35.65	43.49
5329	93.21	28.79	7208.0	35.87	64.42
5966	99.52	29.31	7495	36.5	70.21
6573	107.14	29.08	7926.5	35.84	78.06

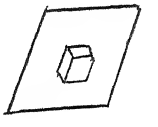

Table 4.12: Natural Convection 3-D Heater Mounted on a Vertical Plate. All side exposed to ambient

q	T_c	T_∞	Ra	Nu	ΔT
2195	54.09	26.2	4202	36.1	27.9
2812	59.50	25.8	4893	38.0	33.7
3426	66.89	26.8	5476	38.47	40.1
3957	76.25	26.9	6299	35.6	49.4
4101	78.24	27.5	6359	35.8	50.7
5291	84.61	28.4	6693	41.2	56.2
6069	91.66	26.0	7566	40.34	65.66

Table 7.13 : Natural Convection 3-D Heater Vertical Configuration Enclosure

Spacing D	q	T_c	T_∞	Ra	Nu	ΔT ^oC
5H	1058	45.6	33.3	1847	39.46	12.32
	1553	51.7	33.1	2703	40.59	18.56
	2280	59.9	33.6	3596	39.1	26.29
	2588	62.21	33.6	3844	40.65	28.5
	3539.7	67.5	33.1	4472	45.9	34.42
	6267	94.6	33.2	6720	42.4	61.4
4H	1364	49.2	32.7	2446	38.02	16.42
	1844	52.21	33.13	2769	44.0	19.08
	2770	61.83	35.08	3570	46.42	26.75
	3813	73.23	34.14	4843	43.2	39.09
	4540	79.55	34.19	5374	43.9	45.36
	6206	93.04	33.68	6429	45.04	59.36
	7619	107.66	34.84	7089	44.2	72.81
2H	1626	53.26	32.0	3088	34.8	21.266
	2174	58.16	30.69	3886	35.9	27.4
	2637	62.06	30.1	4414	37.2	31.96
	3130	66.19	29.08	5007	37.9	37.11
	3932	73.35	29.32	5640	39.2	44.03
	4342	78.94	30.98	5836	39.8	47.96
	5604	89.08	30.71	6630	41.75	58.37
	6372.5	96.70	31.19	7038	41.84	65.51

Table 4.14 : Multichip Natural Convection
Open Closure

q_2	T_1	T_2	T_3	T_∞	Nu_2	Ra_2	$\Delta T_1 = T_1 - T_\infty$	$\Delta T_2 = T_2 - T_\infty$	$\Delta T_3 = T_3 - T_\infty$
207.27	24.56	29.67	21.1	20.2	12.58	3106.33	4.36	9.47	0.9
500.00	27.46	40.08	23.93	20.3	14.31	5981.78	7.16	19.78	3.63
878.18	31.3	52.62	24.6	20.0	14.98	8991.36	11.3	32.62	4.6
1274.5	39.52	67.47	27.23	20.2	14.68	11657.3	19.32	47.27	7.03
1798.1	46.63	83.5	29.83	20.6	15.22	13787.0	26.03	62.9	9.23
2625.5	50.09	102.6	30.5	19.9	16.50	15933.0	30.19	82.7	10.6
3341.8	59.69	122.93	33.56	20.0	16.44	17266.3	39.69	102.93	13.56
3920	68.9	139.02	36.86	21.6	16.53	17532.4	47.3	117.42	15.26

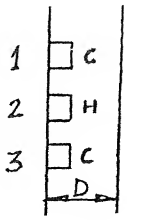

D = 3H, AR = 2.

Table 4.15 : Multichip Natural Convection (Closed Enclosure)

q_2	T_1	T_2	T_3	T_∞	Nu_2	Re_2	$\Delta T_1 = (T_1 - T_\infty)$	$\Delta T_2 = (T_2 - T_\infty)$	$\Delta T_3 = (T_3 - T_\infty)$
214	23.42	29.12	21.58	20.0	13.50	3009.1	3.42	9.12	1.58
507	26.82	39.46	21.81	19.0	14.07	6279.2	7.82	20.46	2.81
836.3	33.55	52.9	24.13	19.2	13.81	9325.33	14.35	33.7	4.93
1274.2	40.5	67.23	25.4	19.0	14.117	12019.9	21.5	48.23	6.4
1785.4	47.35	84.15	27.2	19.1	14.63	14339.4	28.25	65.05	8.1
2349.0	51.48	97.26	26.8	17.6	15.48	16181.8	33.88	79.66	9.2
3540.0	63.73	126.52	30.26	17.1	16.37	18270.7	46.63	109.42	13.16
4263.6	73.4	145.6	32.76	17.0	16.28	18956.8	56.4	128.6	15.76
4980.0	78.43	159.6	34.06	17.0	16.96	19217.0	61.43	142.6	17.06

D = 3H, AR = 2

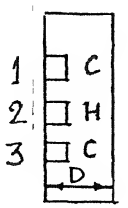

Table 4.16 : Multichip Natural Convection

q_2	T_2	q_3	T_3	T_∞	T_1	Nu_2	Nu_3	Ra_2	Ra_3	$\Delta T_1 = T_1 - T_\infty$	$\Delta T_2 = T_2 - T_\infty$	$\Delta T_3 = T_3 - T_\infty$
54.0	22.9	50.84	21.9	17.8	21.5	6.173	7.24	1782.6	1446.9	3.7	5.1	4.1
171.3	27.87	178.6	26.3	18.3	22.9	10.35	12.89	3130.0	2698.3	4.6	9.57	8.0
377.7	38.1	374.8	34.3	18.6	27.1	11.02	13.66	5876.11	4901.3	8.5	19.5	15.7
658.2	51.35	669.5	45.0	18.0	33.82	10.98	13.98	8970.5	7663.6	15.82	33.35	27.0
1141.2	73.47	1083	61.33	19.5	45.52	11.43	14.24	11809.5	10168.4	26.02	53.97	41.83
1680.3	94.3	1692.2	79.13	19.5	55.95	11.81	15.23	13748.7	12434.9	36.45	74.8	59.63
2228.8	113.77	2237.9	94.63	19.0	65.82	12.13	15.67	14794.2	13746.3	46.82	94.77	75.63
3180.8	141.37	3099.2	113.0	19.0	78.9	12.88	16.93	15598.9	14904.9	59.9	122.37	94.0

D = 3H, AR = 2.

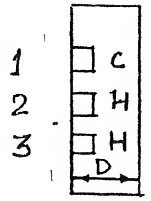

Table 4.17 : Multichip Natural Convection

q_2	T_2	q_3	T_3	T_{oo}	T_1	Nu_2	Nu_3	Ra_2	Ra_3
48.9	19.32	43.6	18.66	16.6	17.9	10.55	12.44	991.7	755
124.0	24.05	122.1	22.7	17.5	20.1	10.02	13.69	2268	1824
227.4	30.32	235.0	28.0	18.0	22.97	10.65	13.59	4001	3325
350.0	37.8	359.1	34.4	18.2	27.97	10.177	12.69	5937	5065
594.0	48.55	589.0	41.6	18.4	33.62	11.07	14.38	8256	6777.0
676.8	52.85	685.9	45.0	17.9	36.1	10.54	14.28	9534	7696.6
1025.0	69.3	980.0	56.36	18.3	44.75	10.95	14.31	11646	9724.8
1467.3	83.2	1437.4	69.85	18.3	50.15	12.19	15.71	13149	11718
1762.4	96.0	1768.2	80.1	17.8	56.47	11.85	15.24	14307	13009
2235.5	115.47	2237.9	96.0	18.2	67.95	11.77	15.11	15190	14203
2992.3	135.22	3008.3	112.6	18.8	77.22	12.77	16.48	15568	14936
3085.8	141.07	3068.8	116.6	18.8	81.52	12.52	16.03	15636	15091

D = 4H, AR = 2.

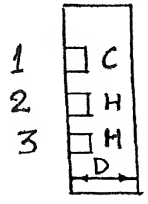

Table 4.18 : Multichip Natural Convection

Rise in temperature with heat flux

q_2	q_3	ΔT_1	ΔT_2	ΔT_3
48.9	43.6	1.3	2.72	2.06
124.0	122.1	2.6	6.55	5.2
227.4	235.0	4.97	12.32	10.0
350.0	359.1	9.77	19.6	16.2
594.0	589.0	15.22	30.15	23.2
676.8	685.9	18.2	34.95	27.1
1025.0	980.0	26.45	51.0	38.06
1467.3	1437.4	31.85	64.9	51.55
1762.4	1768.2	38.67	78.2	62.3
2235.5	2237.9	49.75	97.27	77.8
2992.3	3008.3	58.42	116.92	93.8
3085.8	3068.9	62.72	122.27	97.8

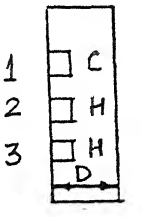

D = 4H, AR = 2.

Table 4.19: Multichip Natural Convection

q_1	T_1	q_2	T_2	q_3	T_3	T_∞	Ra_1	Ra_2	Ra_3	Nu_1	Nu_2	Nu_3
187.8	34.25	194.9	36.02	194.85	31.66	23.3	3323.8	3789.2	2500	9.75	8.69	13.28
459.1	48.45	468.72	48.6	464.6	40.16	21.2	7355.0	7385.5	5519	9.41	9.55	13.85
752.7	63.45	759.4	63.57	729.6	49.33	23.4	9336.1	9363.0	6854	10.25	10.30	15.65
1272.1	86.02	1298.6	85.8	1232.2	64.16	21.8	12479.9	12459.9	9913	10.50	10.75	15.88
1206.2	82.1	1287.1	83.05	1291.1	64.23	21.5	12188.33	12281.3	10011	10.61	11.13	15.58
1865.3	106.87	1873.2	107.8	1808.4	81.63	21.6	13999.5	14047.8	12155	11.28	11.19	16.06

D = 3H, AR = 2.

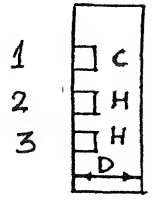

Table 4.20 : Multichip Natural Convection.

Rise in temperature with heat flux

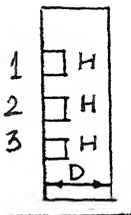

q_1	q_2	q_3	ΔT_1	ΔT_2	ΔT_3
42.8	50.1	53.81	2.4	2.53	2.0
187.8	194.9	194.85	10.95	12.72	8.36
459.1	468.72	464.6	27.25	27.4	18.96
752.7	759.4	729.6	40.05	40.17	25.93
1206.2	1287.1	1219.1	60.6	61.55	42.73
1272.1	1298.6	1232.2	64.22	64.0	42.36
1865.3	1873.2	1808.4	85.27	86.2	60.03

D = 3H, AR = 2.

Table 4.21: Single Chip Forced Convection

q	T_c	T_∞	Re	Ra	Nu	Ra/Re^2
39.36	20.2	18.0	0	3649.5	17.45	∞
40.29	19.9	18.0	250.7	3161.0	20.69	0.050
40.29	19.6	18.0	368.1	2669.7	24.58	0.019
43.50	19.25	18.0	452.2	2092.8	31.8	0.010
40.7	19.15	18.0	553.3	1927.2	34.4	$6.3x_{10}^{-3}$
40.5	19.0	18.0	637.3	1678.3	39.5	$4.1x10^{-3}$
40.5	18.83	18.0	721.5	1395.2	47.92	$2.68x10^{-3}$
40.7	18.77	18.0	805.8	1295.19	51.41	$1.99x10^{-3}$
40.29	18.76	18.0	889.9	1278.49	52.08	$1.61x10^{-3}$
40.29	18.70	18.0	973.9	1178.24	56.55	$1.24x10^{-3}$

AR = 3, Average q = 40.64 W/m^2

Table 4.22 : Single Chip Forced Convection

q	T_c	T_∞	Re	Ra	Nu	Ra/Re^2
67.12	25.2	21.5	0	5724.3	17.46	∞
71.64	24.65	22.0	260.7	4108.69	26.03	0.060
68.55	25.15	22.9	438.1	3452.7	29.28	0.017
64.31	25.04	23.4	517.9	2511.5	37.66	9.39×10^{-3}
69.27	24.8	23.0	698.3	2769.7	36.99	5.68×10^{-3}
71.82	25.05	23.3	778.2	2681.43	39.42	4.43×10^{-3}
69.37	25.2	23.6	858.9	2443.5	41.02	3.319×10^{-3}
71.82	25.35	24.6	939.4	2627.56	39.27	2.97×10^{-3}
71.64	25.6	25.0	1011.6	2390.9	42.8	2.33×10^{-3}

AR = 3 , Average q = 68.97 W/m^2

Table 4.2 : Single Chip Forced Convection

q	T_c	T_∞	Re	Ra	Nu	Ra/Re^2
104.2	27.0	21.5	0	8364.8	18.1	∞
107.1	26.35	22.1	243.13	6479.7	24.2	0.10
100.71	26.2	22.8	436.9	5168.9	28.2	0.027
98.9	25.15	23.1	614.47	4630.5	31.1	0.0122
101.8	26.3	23.5	774.9	4234.5	34.8	7.05×10^{-3}
99.62	25.05	23.6	856.0	3711.7	38.9	5.06×10^{-3}

AR = 3, Average q = 102.05 W/m^2

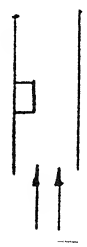

Table 4.24 : **Single Chip Forced Convection.**

q	T_c	T_∞	Re	Ra	Nu	Ra/Re^2
127.0	25.5	18.3	0.0	11329.4	17.06	∞
125.15	24.5	19.3	246.5	8209.85	23.27	0.135
126.12	24.1	19.3	443.8	7607.3	25.42	0.038
126.12	24.9	20.1	543.0	7512.1	25.36	0.025
129.78	24.15	20.1	622.0	6383.9	30.97	0.016
129.0	24.1	20.4	705.8	5824.1	33.68	0.0117
129.0	24.63	20.8	785.1	5983.5	32.49	9.70×10^{-3}
129.36	24.2	20.8	868.0	5333.6	35.88	7.07×10^{-3}
124.42	24.6	21.1	947.9	5459.4	34.28	6.08×10^{-3}
126.7	24.4	21.1	1030.2	5157.27	37.03	4.86×10^{-3}

AR = 3, Average q = 126.96 W/m^2

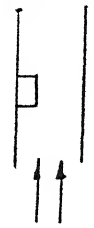

Table 4.25 : Single Chip Forced Convection

q	T_c	T_∞	Re	Ra	Nu	Ra/Re^2
520.0	44.95	18.6	0	34517.4	18.541	∞
534.0	42.0	19.6	248	29965.5	22.46	0.487
520.0	39.9	19.8	446	27379.8	24.44	0.137
529.0	38.9	20.3	545	25494.4	26.88	0.085
529.0	38.25	20.2	628	24751.6	27.89	0.0627
539.0	38.3	20.6	710	24351.5	28.80	0.048
534.0	37.95	21.0	792	23338.9	29.79	0.037
534.0	37.7	21.2	875	22744.4	30.61	0.0297
549.0	37.65	21.6	957	22081.1	32.33	0.0241
534.0	37.3	21.8	1040	21367.8	32.57	0.0197

AR = 3, Average q = 532.2 W/m^2

Table 4.26 : Single Chip Forced Convection

q	T_c	T_∞	Re	Ra	Nu	Ra/Re^2
1021.6	53.5	19.0	0	49381.3	20.92	∞
1014.7	58.25	19.1	248	45377.4	23.87	0.7377
1063.4	56.6	19.5	364	43532.8	26.45	0.328
1001.0	53.5	20.0	546	40290.2	27.67	0.1351
1001.0	53.4	20.7	628	39202.0	28.33	0.099
987.4	51.65	21.0	710	37258.0	29.87	0.0739
994.0	53.6	23.3	792	35713.2	30.24	0.0569
947.0	50.45	22.8	891	33617.3	31.73	0.0423
1038.5	52.25	24.1	981	33423.9	33.93	0.0347
1001.0	51.9	24.6	1040	32421.2	33.82	0.0299

AR = 3, Average q = 1006.66 W/m^2

Table 4.27 : Single Chip Forced Convection

q	T_c	T_∞	Re	Ra	Nu	Ra/Re^2
1535.4	86.5	22.3	0	57371.1	21.11	∞
1511.2	77.5	22.7	209.7	52686.6	24.61	1.206
1553.4	75.25	23.1	379.5	50988.8	26.65	0.354
1519.6	72.25	24.0	452.9	48151.0	28.26	0.235
1553.4	71.7	24.3	537.5	47445.0	29.42	0.164
1596.3	71.1	24.3	609.3	47085.2	30.64	0.126
1486.1	67.5	23.4	688.2	45995.5	30.46	0.097
1613.6	68.7	24.0	760.9	45985.2	32.55	0.079
1553.4	66.5	24.6	831.6	43779.2	33.5	0.0633
1579.1	66.9	24.7	873.4	43916.5	33.79	0.0576

AR = 3, Average q = 1550.25

Table 4.23 : Single Chip Forced Convection

q	T_c	T_∞	Re	Ra	Nu	Ra/Re^2
1879.3	99.2	22.8	0	61362.0	22.46	∞
1837.8	83.5	23.4	203.27	56875.2	24.80	1.38
1837.8	81.35	23.7	369.6	54884.6	26.62	0.40
1847.0	80.1	24.1	525.7	52264.8	29.28	0.189
1819.3	78.1	24.4	597.64	50882.9	30.14	0.142
1819.3	76.5	24.7	669.49	49666.3	31.30	0.110
1837.8	75.6	24.7	741.04	49176.2	32.22	0.089
1837.8	75.4	25.2	810.2	48446.4	32.66	0.073
1837.8	74.5	25.3	882.0	47817.4	33.36	0.061

AR = 3, Average q = 1852.48 W/m^2

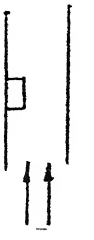

Table 4.4 : Single Chip Forced Convection with a Protrusion on the Opposite Wall

q	T_c	T_∞	Re	Ra	Nu	Ra/Re^2
100.43	23.5	22.5	0	8941	16.02	∞
108.5	27.4	23.1	338.31	6451	24.16	0.056
109.9	27.4	23.1	402.7	6451	24.47	0.039
109.3	27.35	23.1	499.49	6379	24.76	0.0256
104.7	25.6	21.8	569.10	5845	26.5	0.0180
103.02	26.07	22.5	631.9	5444	27.71	0.0136
102.5	25.3	21.8	683.5	5399	28.18	0.0115
100.8	25.3	21.9	732.1	5242	28.52	9.78×10^{-3}
99.97	25.27	22.0	780.7	5040	29.41	8.28×10^{-3}

AR = 3, Average q = 104.43 W/m^2

Table 4.30 : Single Chip Forced Convection with a Protrusion on the Opposite Wall

q	T_c	T_∞	Re	Ra	Nu	Ra/Re^2
227.9	34.7	22.5	0.00	17156.2	17.71	∞
220.7	36.25	27.0	325.8	12480.3	22.42	0.118
224.6	35.6	26.7	389.0	12102.0	23.75	0.079
219.16	35.9	27.8	480.3	10911.7	25.41	0.047
220.44	35.9	28.3	541.6	10207.7	27.22	0.034
219.8	35.9	28.4	603.2	10067.3	27.50	0.0276
226.93	35.3	28.2	651.2	9594.7	30.03	0.0226
219.8	35.85	29.0	695.0	9166.2	30.09	0.0189
232.18	36.5	29.9	738.0	8732.2	32.91	0.0160

AR = 3, Average q = 223.5 W/m^2

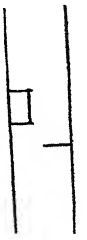

Table 4.31 : Single Chip Forced Convection with a Protrusion on the Opposite Wall

q	T_c	T_∞	Re	Ra	Nu	Ra/Re^2
768. 1	63.3	28.2	0.0	36939.7	19.77	∞
768.41	59.1	29.1	303.4	32578.53	23.24	0.354
780.47	57.9	29.8	361.87	30713.55	25.21	0.235
768.41	55.5	29.9	451.6	28559.42	27.34	0.140
768.41	55.0	30.4	509.8	27485.65	28.45	0.106
774.43	54.85	30.7	567.9	26971.98	29.20	0.083
780.47	54.6	30.9	611.67	26497.20	29.99	0.070
861.10	54.4	31.0	699.2	26192.8	33.52	0.0536

AR = 3, Average q = 783.77 W/m^2

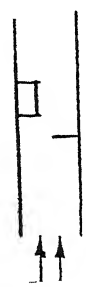

Table 4.32: Multichip Forced Convection

q_1	q_3	Re	Ra_1	Nu_1	Ra_3	Nu_3
188.4	174.2	00	2865	11.25	3083	9.59
184.5	170.3	142	2414	13.28	2555	11.52
187.0	167.3	243	1971	16.63	1855	13.88
182.4	163.9	348	1826	17.61	1942	14.81
178.2	159.5	448	1647	19.17	1794	15.66
190.5	168.4	524	1526	22.17	1466	20.44

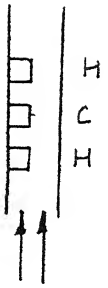

AR = 2

Average q_1 = 184.9 W/m^2

Average q_3 = 165.8 W/m^2

Table 4.33 : Multichip Forced Convection

q_1	q_3	Re	Ra_1	Nu_1	Ra_3	Nu_3
606.4	586.3	00	5818	14.83	6358	12.77
620.6	588.8	135	5597	16.16	5993	14.04
636.2	592.4	234	5000	19.04	5396	16.13
652.02	625.5	337	4925	19.97	5215	17.85
633.6	614.3	432	4795	20.09	4966	18.66
620.6	608.2	507	4710	20.15	4780	19.40

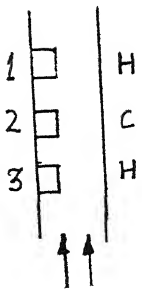

AR = 2

Average q_1 = 627.8 W/m^2

Average q_3 = 602.1 W/m^2

Table 4.34 : Multichip Forced Convection

q_1	q_3	Re	Ra_1	Nu_1	Ra_3	Nu_3
1329.3	1251.6	0	9430	15.74	9871	13.68
1338.7	1261.4	127	8760	17.87	9093	15.84
1435.4	1350.3	226	9038	19.58	9545	16.96
1545.6	1307.1	313	8902	20.05	8917	18.13
1525.2	1415.8	406	8520	21.23	8859	18.51
1425.6	1305.8	480	8349	20.48	8399	18.59

AR = 2

Average q_1 = 1432.8 W/m^2

Average q_3 = 1331.6 W/m^2

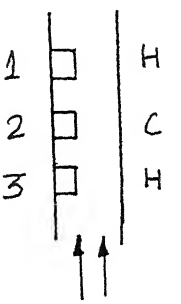

Table 4.35 : Multichip Forced Convection

q_1	q_3	Re	Ra_1	Nu_1	Ra_3	Nu_3
2380.0	2380.1	0	12605	16.40	12977	15.07
2304.7	2247.0	120	11416	19.26	11771	17.50
2392.7	2417.0	209	11662	19.05	11835	18.59
2279.8	2223.3	300	10973	19.73	11138	18.63
2418.1	2331.3	385	10860	21.05	11001	19.74
2469.5	2307.09	453	10765	22.04	10795	20.74

AR = 2

Average q_1 = 2373.0 W/m^2

Average q_3 = 2317.5 W/m^2

Table 4.36 : Multichip forced convection. Temperature variation with Reynolds number

q_1	q_3	Re	T_1	T_2	T_3	T_∞	ΔT_1	ΔT_2	ΔT_3
188.4	174.2	00	34.1	31.4	34.9	24.6	9.5	6.8	10.3
184.5	170.3	142	32.6	30.4	33.1	24.7	7.9	5.7	8.4
187.0	167.3	243	31.5	29.5	31.1	25.1	6.4	4.4	6.0
182.4	163.9	348	31.0	29.1	31.4	25.1	5.9	4.0	6.3
178.2	159.5	448	30.5	28.6	31.0	25.2	5.3	3.4	5.8
190.5	168.4	524	30.2	28.2	30.0	25.3	4.9	2.9	4.7

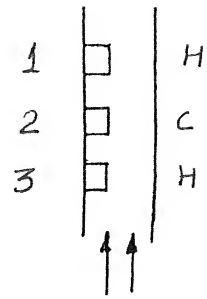

Table 4.37 : Multichip forced convection. Temperature variation with Reynolds number

q_1	q_3	Re	T_1	T_2	T_3	T_∞	ΔT_1	ΔT_2	ΔT_3
606.4	586.3	00	49.8	41.3	52.5	27.2	22.6	14.1	25.3
620.6	588.8	135	47.9	39.75	49.8	26.6	21.3	13.15	23.2
636.2	592.4	234	45.3	36.6	47.1	26.7	18.6	9.9	20.4
652.02	625.5	337	44.7	35.9	46.0	26.5	18.2	9.4	19.5
633.6	614.3	432	44.0	35.25	44.75	26.4	17.6	8.85	18.35
620.6	608.24	507	43.5	34.8	43.8	26.3	17.2	8.5	17.5

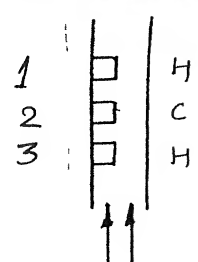

Table 4.38 : Multichip forced convection. Temperature variation with Reynolds number

q_1	q_3	Re	T_1	T_2	T_3	T_∞	ΔT_1	ΔT_2	ΔT_3
1329.3	1252.6	00	73.25	53.9	76.8	28.1	45.15	25.8	48.7
1338.7	1261.4	127	68.5	50.0	70.9	28.2	40.3	21.8	42.7
1435.4	1360.3	226	65.71	46.3	68.74	25.4	40.31	20.9	43.34
1545.2	1397.1	313	69.7	49.5	70.2	28.3	41.4	21.2	41.9
1525.2	1415.8	406	67.03	47.1	69.39	28.3	38.73	18.8	41.09
1425.6	1305.8	480	65.88	46.62	66.21	28.3	37.55	18.32	37.9

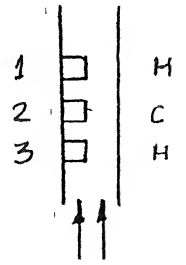

Table 4.39 : Multichip forced convection. Temperature variation with Reynolds number

q_1	q_3	Re	T_1	T_2	T_3	T_∞	ΔT_1	ΔT_2	ΔT_3
2380.0	2380.1	00	101.0	68.22	107.07	26.0	75.0	42.22	81.07
2304.7	2247.0	120	90.11	59.95	94.20	27.4	62.71	32.55	66.8
2392.7	2417.0	209	92.86	61.30	94.99	27.4	65.46	33.9	67.5
2279.8	2223.3	300	89.4	59.56	91.23	29.0	60.4	30.56	62.23
2418.1	2331.3	385	89.48	58.80	91.04	29.5	59.98	29.3	61.54
2469.5	2307.09	453	87.95	57.13	88.27	29.3	58.65	27.83	58.57

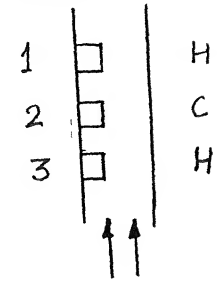

Table 4.40 : Multichip Forced Convection

q_1	Ra_1/Re^2	Nu_1	q_1	Ra_1/Re^2	Nu_1	q_1	Ra_1/Re^2	Nu_1	q_1	Ra_1/Re^2	Nu_1
184.9	∞	11.25	627.8	∞	14.83	1432.8	∞	15.74	2373	∞	15.40
	0.119	13.28		0.30	16.16		0.54	17.87		0.79	19.20
	0.033	16.63		0.09	19.04		0.176	19.58		0.26	19.05
	0.015	17.61		0.043	19.97		0.090	20.05		0.12	19.73
	0.0082	19.73		0.025	20.09		0.05	21.23		0.07	21.05
	0.005	22.17		0.018	20.15		0.037	20.48		0.052	22.04

q_3	Ra_3/Re^2	Nu_3	q_3	Ra_3/Re^2	Nu_3	q_3	Ra_3/Re^2	Nu_3	q_3	Ra_3/Re^2	Nu_3
166.8	∞	9.59	602.1	∞	12.77	1331.6	∞	13.68	2317.5	∞	15.07
	0.126	11.52		0.32	14.04		0.563	15.84		0.8174	17.50
	0.031	15.88		0.098	16.13		0.186	16.96		0.270	18.59
	0.016	14.81		0.0459	17.85		0.091	18.13		0.123	18.63
	0.00893	15.66		0.0266	18.66		0.053	18.51		0.074	19.74
	0.0053	20.44		0.0185	19.40		0.036	18.59		0.052	20.47

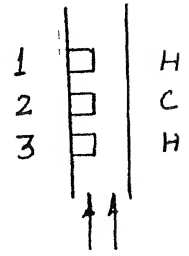

Table 4.41 : Multichip Forced Convection

q_2	T_1	T_2	T_3	T_∞	Re	Re_2	Nu_2	ΔT_1	ΔT_2	ΔT_3
181.53	31.45	36.95	31.17	26.6	0	3004.13	9.9	4.85	10.35	4.27
183.22	31.7	36.7	31.56	26.5	141	2969.12	10.13	5.2	10.2	5.06
178.49	31.0	35.46	31.0	26.3	240	2700.34	11.01	4.7	9.15	4.7
180.85	29.65	33.9	29.5	26.4	345	1972.32	13.55	3.25	7.5	3.1
186.99	28.6	32.94	28.23	26.4	445	1525.5	16.21	2.2	6.54	1.83
180.85	27.6	31.73	27.23	26.4	523	1625.6	15.27	1.2	5.33	0.83

AR = 2, Average q_2 = 181.3 W/m^2

q_2	T_1	T_2	T_3	T_∞	Re	Re_2	Nu_2	ΔT_1	ΔT_2	ΔT_3
625.5	34.3	50.1	31.2	26.6	0	6349.3	14.14	7.7	23.5	4.6
619.2	33.8	48.0	31.55	26.6	139	5618.2	16.05	7.2	21.4	4.95
629.3	33.15	46.67	30.66	26.7	238	5302.7	17.51	6.45	19.97	3.96
670.33	33.1	46.56	29.53	26.7	434	5278.7	18.76	6.4	19.86	2.83
670.33	30.95	44.9	28.35	27.5	513	4672.5	21.44	3.45	17.4	0.85

AR = 2, Average q_2 = 648.1 W/m^2

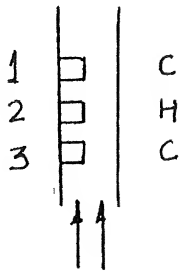

Table 4.42 : Multichip Forced Convection

q_2	T_1	T_2	T_3	T_∞	Re	R_{a_2}	m_2	m_1	m_2	ΔP_2
1274.0	43.55	71.06	36.03	26.5	0	9567.63	15.4	17.05	44.10	9.55
1283.0	40.3	67.46	35.16	28.3	135	8583.6	17.65	12.0	39.1	6.86
1319.0	40.6	67.0	34.6	274	231	8758.8	17.08	13.2	39.6	7.2
1283.0	40.0	64.4	33.7	27.3	332	8396.6	18.73	12.7	37.1	6.4
1283.0	39.05	63.23	33.6	27.2	426	8242.09	19.32	11.85	35.03	6.4
1274.0	38.35	62.26	33.0	27.5	500	8005.06	19.91	10.85	34.76	5.5

AR = 2, Average q_2 = 1286.1 W/m^2

2139.2	52.15	94.93	39.8	26.5	0	12046.3	16.27	25.65	68.43	13.3
2341.4	48.8	92.86	37.56	26.4	131	11904.7	18.9	22.4	66.46	11.1
2305.0	48.6	91.2	37.2	26.3	224	11790.3	18.6	22.3	64.9	10.9
2186.0	45.4	85.8	35.3	26.4	322	11275.1	19.4	19.0	59.4	8.9
2281.0	44.3	85.06	34.3	26.6	416	11152.6	20.6	17.7	58.46	7.7
2293.0	44.15	84.13	34.1	26.4	489	1110.9	21.0	17.75	57.73	7.7

AR = 2, Average q_2 = 2257.5 W/m^2

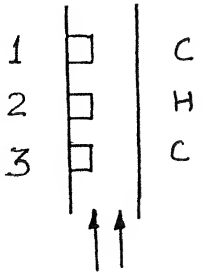

Table 4.44 : Multichip forced convection

q_1	q_2	q_3	Re	Ra_1	Nu_1	Ra_2	Nu_2	Ra_3	Nu_3
180.30	174.1	189.80	0	3017	9.44	3314	8.20	3116.05	9.59
198.10	195.8	219.16	139	2763	11.66	3117	10.06	3006.00	11.73
205.90	202.2	205.90	237	2464	13.58	2754	11.78	2446.00	13.70
108.66	180.5	210.50	339	1886	16.19	2147	13.47	2080.00	15.26
184.80	181.9	208.20	435	1863	16.10	2144	15.82	2035.00	16.76
200.30	192.7	235.30	509	1726	18.98	2049	18.55	1968.50	19.39

AR = 2

Average q_1 = 179.67 W/m^2

Average q_2 = 187.33 W/m^2

Average q_3 = 211.1 W/m^2

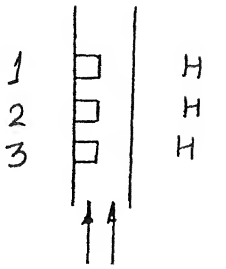

Table 4.45 : Multichip forced convection

q_1	q_2	q_3	Re	Ra_1	Nu_1	Ra_2	Nu_2	Ra_3	Nu_3
628.3	585.0	596.90	0	6992	11.93	7458	10.14	6722	11.97
671.3	636.0	652.27	132	6464	14.43	6995	12.3	6140	15.03
660.0	661.0	623.10	226	6119	15.18	6647	13.6	5601	16.07
671.0	661.0	620.10	330	5735	16.72	6132	15.0	5377	16.77
630.0	610.0	615.00	415	5283	17.40	5685	15.34	5088	17.80
650.0	630.0	623.20	479	4933	19.50	5369	17.0	5022	18.32

AR = 2

Average q_1 = 651.6 W/m^2

Average q_2 = 630.5 W/m^2

Average q_3 = 621.5 W/m^2

Table 4.46 : Multichip Forced Convection

q_1	q_2	q_3	Re	Ra_1	Nu_1	Ra_2	Nu_2	Ra_3	Nu_3
1330.1	1340.2	1335.1	0	9948	14.7	9937	14.84	9699	15.43
1324.9	1345.7	1330.1	130	9758	15.08	9758	15.26	9224	15.61
1335.3	1351.1	1336.1	220	9621	15.6	9647	15.7	8844	17.98
1335.8	1344.1	1345.9	321	9251	16.65	9399	16.31	8817	18.15
1339.8	1348.2	1344.7	410	8924	17.5	9063	17.16	8491	19.0
1320.1	1310.2	1324.6	470	6995	18.3	8806	17.62	8268	19.66

AR = 2
Average q_1 = 1331.0 W/m^2
Average q_2 = 1339.9 W/m^2
Average q_3 = 1336.0 W/m^2

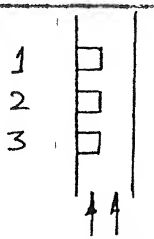

Table 4.47 : Multichip forced convection. Temperature variation with Reynolds number

q_1	q_2	q_3	Re	T_1	T_2	T_3	T_∞	ΔT_1	ΔT_2	ΔT_3
180.3	174.1	189.8	0	39.0	40.19	39.39	28.3	10.7	11.88	11.09
198.1	195.8	219.16	139	36.97	38.33	37.90	27.4	9.57	10.93	10.5
205.9	202.2	205.9	237	36.5	37.63	36.46	28.0	8.52	9.63	8.45
108.66	180.56	210.5	339	35.95	36.92	36.67	29.4	6.55	7.52	7.27
184.8	181.9	208.2	435	34.87	35.90	35.5	28.5	6.36	7.40	7.00
200.3	192.7	235.3	509	35.14	36.33	36.03	29.2	5.93	7.13	6.82

Table 4.48 : Multichip forced convection. Temperature variation with Reynolds number

q_1	q_2	q_3	Re	T_1	T_2	T_3	T_∞	ΔT_1	ΔT_2	ΔT_3
628.3	585	596.9	0	56.3	58.97	54.8	27.5	28.83	31.4	27.3
671.3	636	652.2	132	52.3	55.1	50.67	26.7	25.6	28.4	23.9
660.0	661	623.1	226	51.0	53.7	48.48	27.0	24.0	26.7	21.4
671.0	661	620.1	330	49.4	51.4	47.7	27.2	22.2	24.2	20.5
630.0	610	615.0	415	47.4	49.3	46.5	27.3	20.1	22.1	19.7
650.0	630	623.2	479	45.8	47.8	46.2	27.3	18.5	20.5	18.9

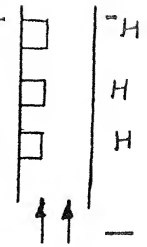

Table 4.49 : Multichip forced convection. Temperature variation with Reynolds number

q_1	q_2	q_3	Re	T_1	T_2	T_3	T_∞	ΔT_1	ΔT_2	ΔT_3
1330.1	1340.2	1335.1	0	75.5	75.4	73.5	27.2	48.3	48.2	45.2
1329.9	1345.7	1330.1	130	74.5	74.6	70.5	27.5	47.0	47.1	43.0
1335.3	1351.1	1336.1	220	73.1	73.3	68.4	27.3	45.8	46.0	41.1
1335.8	1344.1	1345.9	321	70.5	71.6	67.4	27.4	43.1	44.2	40.0
1339.8	1348.2	1344.7	410	69.1	70.1	66.0	27.9	41.2	42.2	38.1
1320.1	1310.2	1324.6	470	66.5	67.7	64.1	27.6	38.9	40.1	36.5

Table 4.50 :

q_1	Ra_1/Re^2	Nu_1	q_1	Ra_1/Re^1	Nu_1	q_1	Ra_1/Re^2	Nu_1
	∞	9.44		∞	11.93		∞	14.73
	0.143	11.56		0.370	14.43		0.577	15.08
179.67	0.0438	13.53	351.6	0.119	15.18	1331.0	0.19	15.6
	0.0154	15.19		0.052	16.72		0.089	16.65
	0.0098	15.10		0.030	17.4		0.053	17.5
	0.0065	18.08		0.0215	19.53		0.031	18.3
q_2	Ra_2/Re^2	Nu_2	q_2	Ra_2/Re^2	Nu_2	q_2	Ra_2/Re^2	Nu_2
	∞	8.2		∞	10.14		∞	14.84
	0.15	10.06		0.40	12.3		0.577	15.26
187.33	0.049	11.78	630.5	0.13	13.6	1339.9	0.199	15.7
	0.018	13.47		0.056	15.0		0.91	16.31
	0.0113	15.32		0.032	15.34		0.053	17.16
	0.0079	18.55		0.023	17.0		0.039	17.62
q_3	Ra_3/Re^2	Nu_3	q_3	Ra_3/Re^2	Nu_3	q_3	Ra_3/Re^2	Nu_3
	∞	9.59		∞	11.97		∞	15.43
	0.155	12.73		0.352	15.03		0.34	16.61
211.1	0.043	13.7	621.5	0.109	16.07	1336.0	0.18	17.98
	0.018	16.26		0.0493	16.77		0.085	18.15
	0.010	16.76		0.029	17.8		0.050	19.0
	0.0076	19.39		0.021	18.32		0.0374	19.66

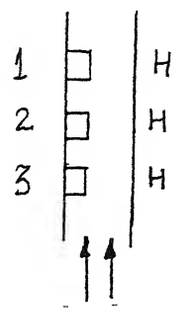

Table 4.51 : Multichip Forced Convection

q_1	q_2	T_1	T_2	T_3	T_∞	Re	Ra_1	Nu_1	Ra_2	Nu_2	ΔT_3	ΔT_1	ΔT_2
174.1	168.2	38.15	38.45	31.35	29.4	0	2470	11.15	2543	10.41	2.45	.75	9.05
147.0	140.01	35.46	35.7	30.51	28.9	139	1904	12.6	1969	11.58	1.6	5.35	6.8
175.15	169.6	34.5	34.9	29.63	28.3	239	1822	15.97	1932	14.49	1.33	6.2	6.5
174.12	172.0	34.07	34.67	29.34	28.3	344	1702	17.0	1869	15.23	1.04	5.7	6.3
176.87	174.1	33.81	34.38	29.13	28.3	440	1629	18.1	1798	16.16	0.83	5.51	6.08
175.49	174.10	33.69	34.21	29.0	28.4	516	1565	18.7	1711	16.91	0.6	5.29	5.81

Average q_1 = 170.47 W/m^2

Average q_2 = 166.16 W/m^2

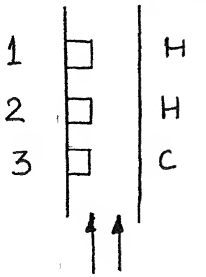

Table 4.52 : Multichip forced convection

q_1 = 170.4		q_2 = 166.16	
Ra_1/Re^2	Nu_1	Ra_2/Re^2	Nu_2
∞	11.15	∞	10.41
0.098	12.6	0.101	11.58
0.03189	15.97	0.0338	14.49
0.0143	17.0	0.0157	15.23
0.00841	18.1	0.00923	16.16
0.00877	18.7	0.00642	16.19

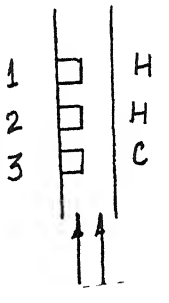

Table 4.53 : Numerical results for the heat transfer over a flush heater for flat and parabolic velocity profiles.
Time step marched = 800

R_e	Gr	Ra	Nu Flat	Nu Parabolic
100	00	00	9.63	8.967
	10^2	70	9.64	8.975
	10^3	$7x10^2$	9.68	9.050
	10^4	$7x10^3$	10.13	9.759
	$5x10^4$	$35x10^3$	11.75	11.669
	10^5	$7x10^4$	13.18	13.049
	10^6	$7x10^5$	19.15	19.166
500	00	00	15.06	13.296
	10^2	70	15.06	13.298
	10^3	$7x10^2$	15.07	13.316
	10^4	$7x10^3$	15.16	13.503
	$5x10^4$	$35x10^3$	15.55	14.260
	10^5	$7x10^4$	16.01	15.05
	10^6	$7x10^5$	20.52	19.941
1000	00	00	18.04	15.97
	10^2	70	18.042	16.120
	10^3	$7x10^2$	18.046	16.135
	10^4	$7x10^3$	18.085	16.22
	$5x10^4$	$35x10^3$	18.260	16.61
	10^5	$7x10^4$	18.47	17.02
	10^6	$7x10^4$	19.15	20.62

CONCLUSION

The present work concerns the study of free, mixed and forced convective heat transfer from the single discrete heater and an array of three heaters in the vertical configuration. Results obtained experimentally show the follow:

(1) Single Heater: Flow patterns in the vicinity of a single heater are complex and a universal self similar relationship between the average heat flux and the wall temperature is not possible. Nusselt numbers for a protruded heater generally exceed values quoted for flush heater. As the heater length reduces the average Nusselt number increases owing to the approach towards point source. Heat transfer is unaffected by the presence of a neighbouring wall and infact goes down when the flow path is baffled. Unlike the problem of a flush heater buoyancy effects do not enhance heat transfer monotonically over and above the forced convection value. Adverse stratification effects and the stabilizing effect of buoyancy on recirculation can lower the Nusselt number over portions of mixed convection regime.

(2) Array of Three Heaters: The heater placed at the lowest position shows the best thermal performance while the next to it shows the worst performance. Subsequent heaters do not show further deterioration mainly because acceleration of flow and

disturbances introduced by the heaters themselves. Considerable advantage is gained when an unpowered heater is placed between two powered components. As in the problem of a single heater the role of the neighbouring passive wall is minimum. In natural convection the plume is diverted towards the passive wall and this suggests the use of cooling strategies in engineering practice. Experiments for an array of heaters show that a definite heat transfer augmentation is possible in mixed convection. However the thickening of the thermal boundary-layer effectively reduces this augmentation as one moves vertically upwards.

REFERENCES

Afrid, M. and Zebib, A., 1989, "Natural Convection Air Cooling of Heated Components Mounted on a Vertical Wall. Numerical Heat Transfer, Part A, Vol. 15, pp. 243-259, 1989.

F.P. Incropera, 1988, "Convection Heat Transfer in Electronic Equipment Cooling", ASME HTD-Vol. 110, pp. 1097-1109.

Gebhart, B., Jaluria, Y., Mahajan, R.L., Sammakia, B., "Buoyancy Induced Flows and Transport", Hemisphere Publishing Co., New York.

Habchi, S. and Acharya, S., 1986b, "Laminar Mixed Convection in a Partially Blocked Vertical Channel", International Journal of Heat and Mass Transfer, Vol. 29, pp. 1711-1752.

Keyhani, M., Prasad, V. and Vox, R., 1988, "An Experimental Study of Natural Convection in a Vertical Cavity with Discrete Heat Sources", Transaction of ASME HTD Vol. 110, August 1988, pp. 616-624.

Muralidhar, K. and Kullacki, F.A., "Stability of Mixed Convection Flow", 1987, International Journal of Heat and Fluid Flow, pp. 228-234.

McEntire, A.B. and Webb, B.W., 1990, "Local Forced Convective Heat Transfer from Protruding and Flush-Mounted Two-Dimensional Discrete Heat Sources", International Journal of Heat and Mass Transfer, Vol. 33, No.7, pp. 1521-1533.

Moffat, R.J. and Anderson, A.M., 1990, "Applying Heat Transfer Coefficient Data to Electronic Cooling", Transactions of ASME, Vol. 112, November 1990, pp. 882-890.

Ortega, A. and Moffat, R.J., "Heat Transfer from an Array of Simulated Electronic Components. Experimental Results for Free Convection with and without a Shrouding Wall", Heat Transfer in Electronic Equipment-1985, ASME HTD, Vol. 48, May 1985.

Ravine, T.L. and Richards, D.E., 1988, "Natural Convection Heat Transfer from a Discrete Thermal Source on a Channel Wall", Transaction of ASME HTD Vol. 110, November 1988, pp. 1004-1009.

Sadik Kakac and Yaman Yener, "Convective Heat Transfer", Hemisphere Publishing Co., New York.

Shou-Shing Hsieh, Huei-Jan Shih and Ying-Jong Hong, 1990, "Laminar Forced Convection From Surface Mounted Ribs", International Journal of Heat and Mass Transfer, Vol. 33, No. 9, pp. 1987-1999.

Tsang-Yuan Lin and Shou-Shing Hsieh, 1990, "Natural Convection of Opposing/Assisting Flows in Vertical Channels with Asymmetrically Discrete to Heated Ribs", International Journal of Heat and Mass Transfer, Vol. 33, No.10, pp. 2295-2309.

Tewari, S.S. and Jaluria, Y., 1990, "Mixed Convection Heat Transfer from Thermal Sources Mounted on Horizontal and Vertical Surfaces", Transaction of ASME, HTD, November 1990, Vol. 112, pp. 975-987.

Wing Aung, "Cooling Technology for Electronic Equipment", Hemisphere Publishing Co., New York.

Goldstein, R.J., "Fluid Mechanics Measurement", Hemisphere Publishing Co., New York.

Anand, N.K., Kim, S. and Fletcher, "Natural Convection between a Series of Vertical Plates having Embedded Line Sources", Transaction of ASME HTD Vol/113 Feb 1991, pp. 108-115

APPENDIX-1

UNCERTAINTY ANALYSIS

Bias and random errors are the two types of errors associated with experimentation. Bias errors are related to the measuring probes and measurement system. With the most modern systems having a self calibrating capacity, these errors can be minimized. The random errors are difficult to control since they arise from a number of factors that simultaneously affect the experiment. These include room temperature changes supply voltage fluctuations, air currents, building vibrations and roughness of nominally smooth surfaces. These errors inherently exist in any experiment rendering the experimental data as fundamentally irreproducable. For a large number of experimental runs, provided the experiments are of good qualit results are distributed about a stable mean value. Such a distribution is called scatter and all efforts are needed to maintain a low scatter value. Overall improvement in the quality of measurement systems and test cell along with control of external factors influencing the experiments may result in a reduced scatter. The level of scatter is determi by a series of experiments dedicated to determination of scat only. These experiments involve performing runs in identical conditions on different days, runs with measurement systems having identical specifications and runs on different apparat that look alike.

Error Propagation

Due to scatter an uncertainty is always associated

with a measured variable. If a new quantity is defined on the basis of this variable then the uncertainty involved may also affect the value of the new quantity. If δ_i be the uncertainty involved with a variable x_i and y be the function of x_i then uncertainty in y, δ_y will be

$$\delta_y = \left[\sum_i^r \left(\frac{\partial f}{\partial x_i} \delta_i \right)^2 \right]^{1/2}$$

On the basis of error propagation formula and a series of experiments dedicated to the determination of scatter, we present the level of scatter for this work.

Natural Convection Experiments

We have,

$$Nu = \frac{hL}{k} = \frac{qL}{\Delta T k} = \frac{V^2 L}{ARk\Delta T}$$

V is the voltage applied, volts

L is the characteristic length of heater, m

A is the area, m^2

R is the resistance, Ohms

k is the fluid thermal conductivity, W/mK

ΔT is the temperature difference between heater surface and ambience, ^oC .

For this problem the resistance R of nichrome wire with length L and area A of the heater can be considered as constant. The uncertainty in the Nusselt number will depend upon the uncertainty in the measurements of voltage,

temperature and thermal conductivity of fluid. By error propagation formula we get the uncertainty δ Nu in Nusselt number as

$$\frac{\delta Nu}{Nu} = \left[4 \left(\frac{\delta V}{V}\right)^2 + \left(\frac{\delta \Delta T}{\Delta T}\right)^2 + \left(\frac{\delta k}{k}\right)^2 \right]^{1/2}$$

and uncertainty in Rayleigh number as

$$\frac{\delta Ra}{Ra} = \left[\left(\frac{\delta \beta}{\beta}\right)^2 + \left(\frac{\delta \Delta T}{\Delta T}\right)^2 + \left(\frac{\delta \nu}{\nu}\right)^2 + \left(\frac{\delta \alpha}{\alpha}\right)^2 \right]^{1/2}$$

The prefix δ indicates the maximum variation of any quantity from its mean value. The denominator quantities are the mean values of different variables. We have carried out the experiments with nearly same input heat flux on different days in identical external conditions. Table A 11 presents the data for these experiments. From table we calculate -

V_{mean} = 28.58 V

Q_{mean} = 11.84 Watts

$T_{m(mean)}$ = 62.03 ^{o}C

ΔT_{mean} = 61.92

k_{mean} = 28.83×10^{-3} W/mK

Maximum variation in -

Voltage from its mean value - 0.21 volts

ΔT from its mean value: -2.32 ^{o}C

k from its mean value: -0.3×10^{-3} W/mK The uncertainty in the Nusselt number can be calculated as,

Table A1.1: Values of different properties at different power input

V	Q	T_c	$T_m = \frac{T_c+T_\infty}{2}$	$\Delta T = T_c - T_\infty$	$k \times 10^3$	$\nu \times 10^6$	$\alpha \times 10^5$	$\beta = \frac{1}{(T_c+273)}$	Nu	Ra
Volts	Watts				W/mK	m^2/sec	m^2/sec	1/K		
28.65	11.878	95.12	64.25	61.91	29.05	19.11	2.73	2.71×10^{-3}	20.67	5280
28.5	11.837	91.14	64.46	61.89	28.75	18.88	2.85	2.74×10^{-3}	20.82	5618
28.69	11.92	94.62	63.01	63.52	28.95	19.07	2.87	2.71×10^{-3}	20.36	5516
28.37	11.64	92.41	61.05	62.71	28.9	18.88	2.72	2.73×10^{-3}	20.48	5515
28.7	11.96	90.32	61.4	59.6	28.53	18.8	2.68	2.75×10^{-3}	21.37	5576

$$\frac{\delta Nu}{Nu} = \left[4\left(\frac{0.21}{28.58}\right)^2 + \left(\frac{2.32}{61.92}\right)^2 + \left(\frac{0.3}{28.83}\right)^2 \right]^{1/2}$$

$$\frac{\delta Nu}{Nu} = 0.041$$

The uncertainty in the Nusselt number is $\pm$ 4.1%.

Uncertainty in Rayleigh Number

$$Ra = \frac{\beta \Delta T g L^3}{\nu \alpha}$$

Value of β depends on the heated surface temperature

$$= \frac{1}{(T_c + 273)} /K$$

The value of g and L can be considered as constant.

$$\alpha_{mean} = 2.77 \times 10^{-5} \ m^2/sec$$

$$\Delta T_{mean} = 61.92^{\circ}C$$

$$\beta_{mean} = 2.728 \times 10^{-3}/K$$

$$\nu_{mean} = 18.95 \times 10^{-6} \ m^2/sec$$

Maximum variation in

β from its mean value : $0.022 \times 10^{-3}/K$

α from its mean value : $0.1 \times 10^{-5} \ m^2/sec$

ν from its mean value : $0.16 \times 10^{-6} \ m^2/sec$

ΔT from its mean value: $-2.32^{\circ}C$

Now,

$$\frac{\delta Ra}{Ra} = \left| \left(\frac{0.022}{2.728}\right)^2 + \left(\frac{2.32}{61.92}\right)^2 + \left(\frac{0.16}{18.95}\right)^2 + \left(\frac{0.1}{2.77}\right)^2 \right|^{1/}$$

$$\frac{\delta Ra}{Ra} = 0.053$$

The uncertainty involved in Rayleigh number is 5.3%.

We have $Q = V^2/R$

$$= \delta Q/Q = \frac{2\delta V}{V}$$

Maximum variation in voltage is 0.7% and the corresponding variation in heat input is 1.4%.

It can be stated that for a variation in supply volt within $\pm$ 0.7%.

Power input varies within $\pm$ 1.4%

Nusselt number varies within $\pm$ 4.1%

and Rayleigh number varies within $\pm$ 5.3%.

We have also carried out experiments to determine scatter at different power input the results of which are stated below.

Power Input Q = 5.611 Watts

For a variation in supply voltage within $\pm$ 2.09%

Variation in power input Q is within $\pm$ 3.56%

Variation in the Nusselt number is within $\pm$ 5.69%

Variation in the Rayleigh number is within $\pm$ 8.3%

Power Input Q = 2.801 Watts

For a variation in supply voltage within $\pm$ 1.735%

Variation in power Q is within $\pm$ 3.49%

Variation in the Nusselt number is within $\pm$ 7.25%

Variation in the Rayleigh number is within $\pm$6.87%

We observe that the uncertainty in the Nusselt and the Rayleigh number increases with a lowering in input power. This is because of the fact that as the power input is lowered the natural convective flow gets weaker and weaker and are likely to be affected more by the external influences. For the present work the overall uncertainty in the Nusselt number can be taken as 5% and that in the Rayleigh number as 6%.

Forced Convection Experiments

A similar analysis has been done for the forced convection experiments. The uncertainty in the Nusselt number and the Rayleigh number is found to be 4%. The uncertainty in Reynolds number varies with velocity. At lower velocities ($U \sim 0.3$ m/s) the uncertainty involved is high and is about 6%. At higher velocities ($U \sim 0.65$ m/s) the uncertainty involved is low and is about 3%.

Appendix 2

WORKING PRINCIPLE OF INTERFEROMETER

The interferometer works on the principle of interference of light. Interference is the phenomena of redistribution of light energy which takes place when two light waves originating from the same monochromatic source get superimposed. Light is characterised as the visible spectrum of electromagnetic waves. For a monochromatic source only one wavelength is significant and the propagation of light originating from a monochromatic source can be expressed as

$$E = A \sin 2\pi(\nu t - \frac{x}{\lambda})$$

where E is the electric field. A is amplitude ν is frequency, λ is wavelength, t is time and x is distance.

The superimposition of two waves having a phase difference ϕ from the same monochromatic source can be expressed as

$$E_1 + E_2 = A\left[\sin 2\pi(\nu t - \frac{x}{\lambda}) + \sin(2\pi(t\nu - \frac{x}{\lambda}) + \phi\right]$$

The amplitude of both the waves is same because they are produced by the same source. The sum of the electric field vectors is,

$$E_1 + E_2 = 2A \cos\frac{\phi}{2} \sin(2\pi(\nu t - \frac{x}{\lambda}) - \frac{\phi}{2})$$

The intensity of a light wave is proportional to square of amplitude. The intensity of combined beam is $4A^2 \cos^2 \frac{\phi}{2}$. This can be plotted as

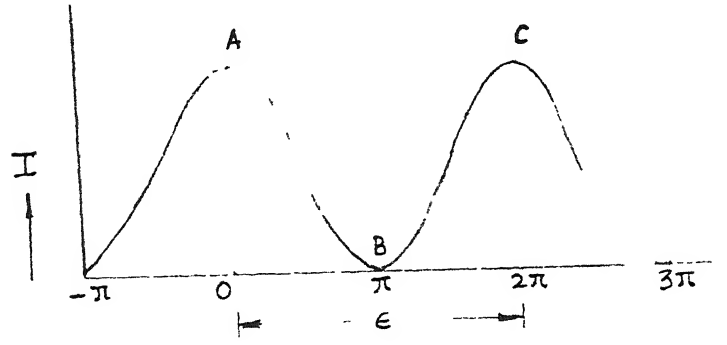

Fig. A.2.1

It is clear from the plot that at some points there is an addition of intensities which will form the bright spots and at some points the intensity is zero which will form the dark spots. This redistribution of energy leads to an interference pattern in the form of dark and bright regions A and B respectively . The spacing between two consecutive points of maximum or minimum intensity is termed as fringe spacing or fringe width.

An interference pattern is stable only if the conditions of spatial and temporal coherence are satisfied. For spatial coherence, each wave should have traversed the same length x and for temporal coherence the phase at a point and the phase difference between two points should be

constant with time.

No light source is perfectly coherent in all respects. The degree of coherence is judged by its coherence length which is the distance over which the waves emitted by the light source satisfy the conditions of coherence. Laser is a source which gives the coherence length of the order of few kilometers.

In the present study we have used a He-Ne laser as a light source . It has a continuous wave output of 35 mW and a wavelength of 632.8 nm. Figure A 2 2 shows schematic diagram of interferometer.

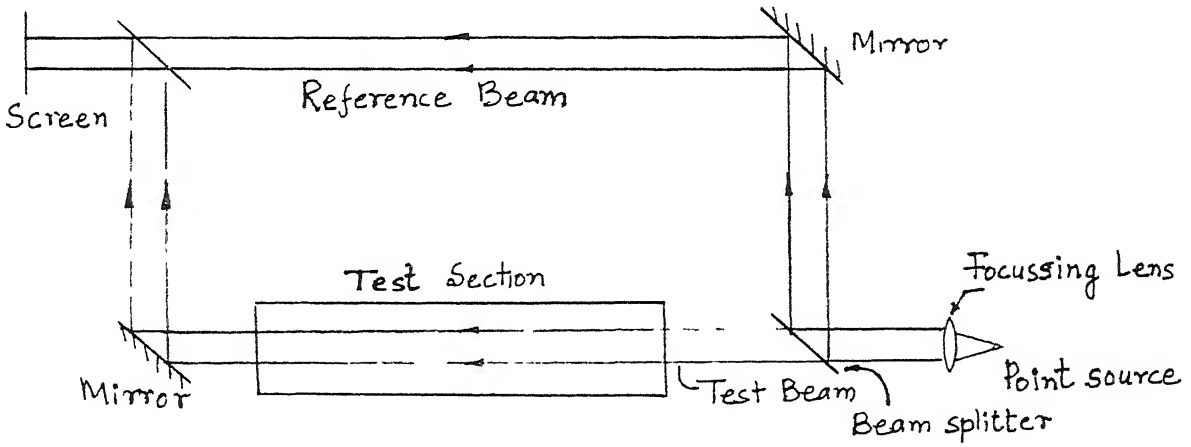

Schematic diagra of Mach-Zhender Interferometer

In the Mach-Zhender interferometer, the interference pattern is formed due to a phase difference between the test and reference beam.

The index of refraction of a homogeneous medium is a function of the thermodynamic state, often only density. According to Lorenz-Lorenz relation, the index of refraction

of a homogeneous medium can be obtained from

$$\frac{1}{\rho}\,\frac{n^2-1}{n^2+2} = \text{constant}$$

When $n \simeq 1$, this reduces to

$$\frac{n-1}{\rho} = c \quad \Rightarrow \quad \frac{dn}{d\rho} = \text{constant}$$

For small changes in temperature (upto 20°C in air) density and temperature are linearly related.

$\frac{dn}{d\rho}$ = constant can then be written as $\frac{dn}{dT}$ = constant and any change in T will have a simultaneous effect on n. If a beam of light passes through a medium of varying temperature then the optical path length traversed by beam will be more than the geometrical path length.

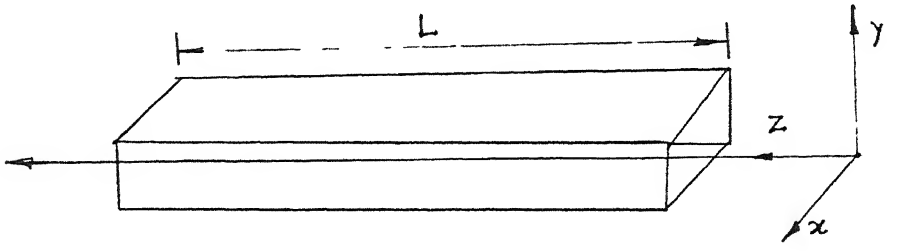

Fig.A.2.3

$$\text{Path length PL} = \int_0^L n\,dz > L \quad \text{since } n > 1.$$

Let the test beam moves through a region of variable n and reference beam moves through a region of constant n then

$$PL = PL_1 - PL_2 = \int_0^L (n_1 - n_2)dz$$

$$= \frac{dn}{d\rho} \int_0^L (\rho_1 - \rho_2)\, dz$$

$$= \frac{dn}{dT} \int_0^L (T_1 - T_2)\, dz$$

If T_1 is a two dimensional temperature field then the integral simplifies to

$$PL = (T_1 - T_2) \frac{dn}{dT} \cdot L$$

A path length difference of λ generates one fringe shift, the ΔT for one fringe shift can be evaluated as

$$\Delta T = \lambda / \left(L \frac{dn}{dT}\right)$$

For air $\left(\frac{dn}{dT}\right) = 0.927 \times 10^{-6}/^{\circ}C$.

For He-Ne laser $\lambda = 632.8$ nm. Hence ΔT per fringe shift for a He-Ne laser is 0.682 $m^{\circ}C$ in air. The temperature change per fringe shift depends upon the length L of test section. More the length, more sensitive the interferometer will be. But large values of L lead to high refraction errors. Each fringe is a line of constant phase, refractive index, density and temperature and is an isotherm.

Consider a ray travelling in a medium of varying refractive index and temperature.

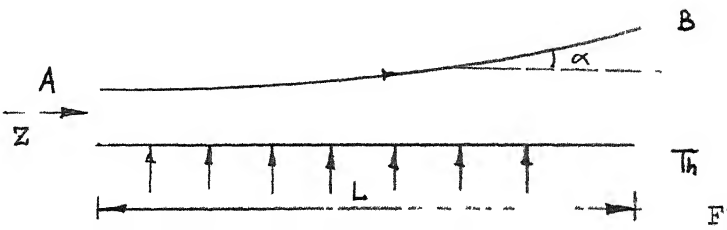

Fig.A.2.4

The effect of refraction is to displace the beam towards regions of higher refractive index n, hence higher density and lower temperatures. This increases the optical path traversed by the beam.

Interference patterns now formed are due to the combined effect of difference between the average refractive indexes for the test and reference beam and an additional path difference introduced by gradients n in test cell.

The fringe shift ε can be considered to be:

$$\varepsilon_{total} = \varepsilon_{true} + \varepsilon_{refraction}$$

ε_{true} is the fringe shift caused due to the difference in average refractive index.

ε_{ref} is fringe shift introduced by the refraction of test beam when it passes through test section.

Temperature is related to the difference in average refractive index for the two beams alone hence any fringe shift introduced by the refraction is a source of error.

The $\varepsilon_{refraction}$ can be calculated by the formula

$$\varepsilon_{ref} = \frac{1}{6n} \left(\frac{dn}{dT}\right)^2 L^3 \left(\frac{\partial T}{\partial Y}\right)^2$$

As the length L increases this term increases as L^3. In practical values of L > 1m the refraction errors are substantial.

In the present study the maximum length of test section is 0.2m. Hence the magnitude of refraction error is small. To find out the local wall heat flux the fringe spacings closest to the wall is measured and heat flux is given by

$$q(x) = k(\text{fluid}) \cdot \frac{\Delta T/\text{fring shift}}{\varepsilon(x)}$$

and

$$Nu = \frac{\Delta T/\text{fringe shift}}{\varepsilon(x)} \cdot L\,(T_w - T_\infty)$$

When the heat flux is large the wedge fringe mode is preferred as the initial setting of interferometer. In this mode the fringes are initially made perpendicular to the surface to be heated.

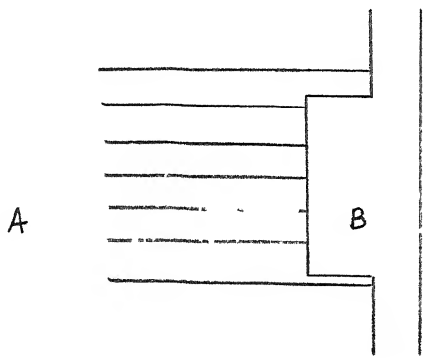

Fig.A.2.5: Initial wedge fringe setting

As the temperature of the surface rises the fringes get shifted close to wall.

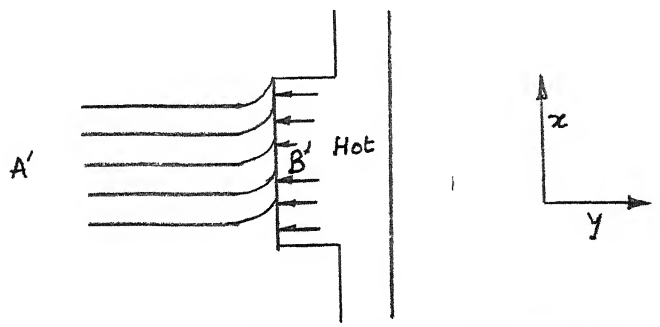

Fig.A.2.6 : Wedge fringes at heated state

This fringe shift is due to an increase in the temperature and is a measure of temperature change in that region. The curve A'B' represents the temperature profile at an x location A' and the slope of this curve at wall is proportional to the wall heat flux.

This slope can be calculated from a photographic film and the heat flux calculated as

$$q = -k \left.\frac{\partial T}{\partial y}\right|_{y=0} .$$

A curve can also be fitted through some points away from from the heated surface and approximate temperature profile can be obtained. This method has been elaborated in Chapter 3.

Appendix 3

CALCULATION OF RADIATIVE HEAT LOSS FROM A SINGLE CHIP HEATER

Here we estimate the radiation heat loss in a black enclosure. The size and geometry of the enclosure are given in Figures below. Radiation losses are significant only in natural convection problems; they are negligible when forced flow is present.

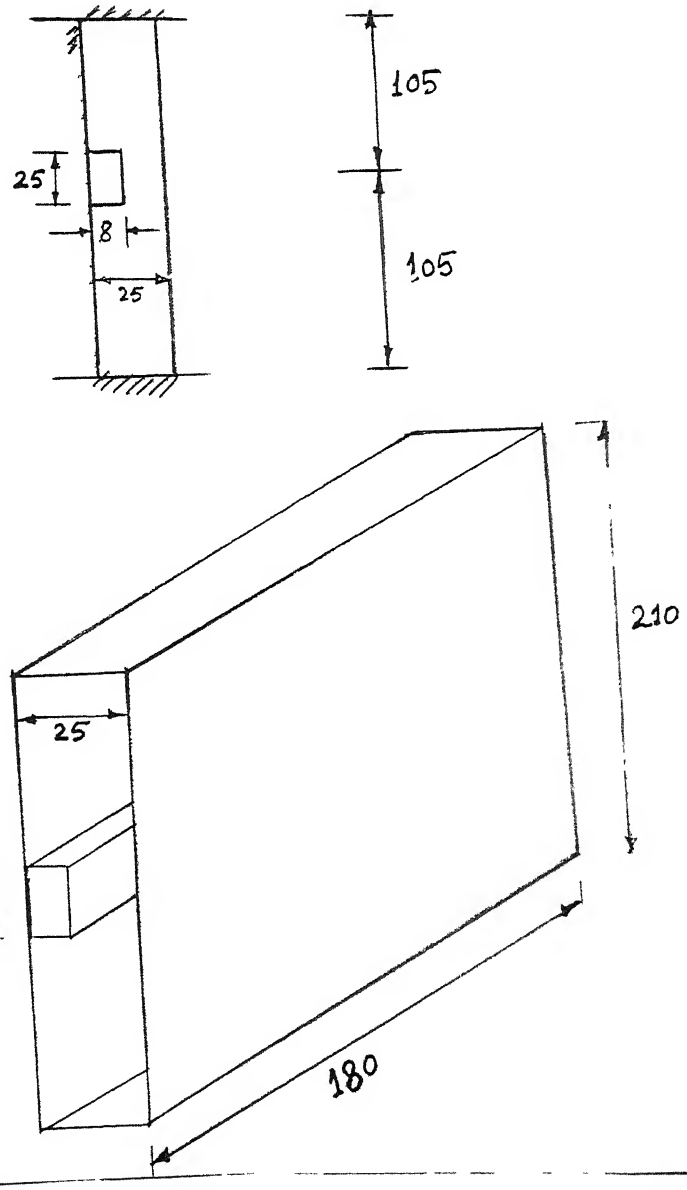

Fig.A.3.1

Heat exchange between the aluminium strip and walls of the enclosure can be found out using the formula,

$$Q_{c-e} = \frac{A_c \sigma (T_c^4 - T_e^4)}{\frac{1-\epsilon_c}{\epsilon_c} + \frac{1}{f_{c-e}} + \frac{1-\epsilon_e}{\epsilon_e}\frac{A_c}{A_e}}$$

where subscript c refers to the heated strip and e refers to enclosure.

ϵ is emissivity and A is area f_{c-e} is the shape factor between the chip and the enclosure. This formula assumes that the temperature of surfaces is uniform. In the present case the temperature inside the enclosure varies with position. To circumvent this problem the enclosure is divided into many parts each of which is assumed to be isothermal. The heat exchange between the strip and each isothermal part is determined separately. The shape factors for all the geometries are determined using standard tables. The enclosure is divided as shownbelow. The associated shape factors are given along with the figures.

(1)

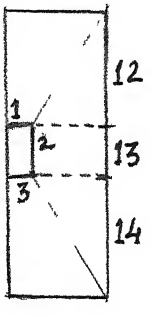

$f_{2-12} = f_{2-14} = 0.196$

$f_{2-13} = 0.5$

(2)

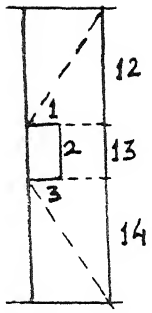

$f_{1-12} = f_{3-14} = 0.29$

(By symmetry)

(3)

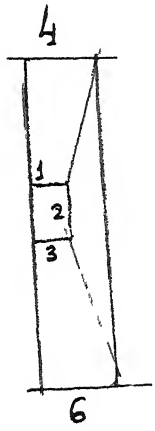

$f_{1-4} = f_{3-6} = 0.1354$

(By symmetry)

(4)

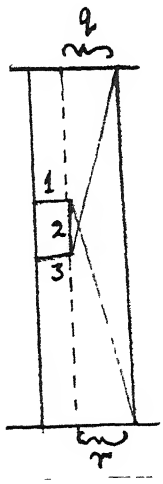

$f_{2-q} = f_{2r} = 0.012$

(By symmetry)

(5)

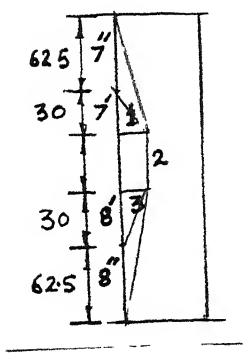

$f_{1-7'} = f_{3.8'} = 0.375$

$f_{1-7''} = f_{3-8''} = 0.075$

(By symmetry)

(6)

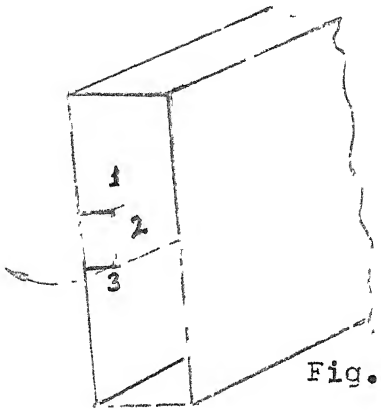

$f_{2\text{-ambient}} = 0.0494$

Fig. A.3.2

Heat exchange in enclosure = Heat exchange in the configurations (1+2+3+3+5+6).

for the polished aluminium e' strip can be taken as 0.2 (from the standard books).

for the black enclosure is assumed as 1 because it gives the maximum radiation loss.

In the present work,

$$\varepsilon_1 = \varepsilon_2 = \varepsilon_3 = 0.2$$

Table A3.1 gives the temperatures at various positions in the enclosure and the amount of heat lost from the strip purely by radiation.

Sample Calculation

The heat lost from surface 2 to surface 12 can be calculated as shown below:

$$Q_{2\text{-}12} = \frac{A_2 \sigma (T_2^4 - T_{12}^4)}{\frac{1-\varepsilon_2}{\varepsilon_2} + \frac{1}{f_{2\text{-}12}} + \frac{1-\varepsilon_{12}}{\varepsilon_{12}} \cdot \frac{A_2}{A_{12}}}$$

$\varepsilon_2 = 0.2 \qquad A_2 = 2.5 \times 18 \times 10^{-4}\ m^2$

$\varepsilon_{12} = 1 \qquad f_{2-12} = 0.196$

$= \text{Planck's constant} = 5.66 \times 10^{-8} \ \frac{\text{Watt}}{m^2 K^4}$

$T_2 = 95.2^{\circ}C = 368.2A, \ T_{12} = 52^{\circ}C = 325A$

$$Q_{2-12} = \frac{2.5 \times 18 \times 10^{-4} \times 5.66 \times 10^{-8} \left(368.2^4 - 325^4\right)}{\frac{1-0.2}{0.2} + \frac{1}{0.196}}$$

$Q_{2-12} = 0.202$ watts.

Similarly heat exchanges for other pairs of surfaces can be calculated.

Experiments have also been performed in a white enclosure to determine the role played by radiation in chip cooling. This is discussed in Chapter 4. Results presented in this work have been obtained in a white enclosure.

Table A3.1

Radiation Loss Calculation

No.	Heat Exchange between	Temp. of hot surface - °C	Temp. of cold surface - °C	Emissivity of heated surface	Emissivity of cold surface	Shape factor	Heat loss watts	Heat Input = 12.05 watts
1	Q_{2-12}	95.2	T_{12} = 52	0.2	1	0.196	0.202	
2	Q_{2-14}	95.2	T_{14} = 40.3	0.2	1	0.196	0.243	% loss
3	Q_{2-13}	95.2	T_{13} = 46.5	0.2	1	0.5	0.338	= $\frac{1.533}{12.05}$
4	Q_{2-q}	95.2	T_q = 49	0.2	1	0.012	0.022	
5	Q_{2-r}	95.2	T_r = 36	0.2	1	0.012	0.027	= 12.7%
6	Q_{3-6}	95.2	T_6 = 36	0.2	1	0.1345	0.0663	
7	Q_{1-4}	95.2	T_4 = 49	0.2	1	0.1345	0.054	
8	Q_{1-12}	95.2	T_{12} = 52	0.2	1	0.29	0.079	
9	Q_{3-14}	95.2	T_{14} = 40.3	0.2	1	0.29	0.101	
10	$Q_{1-7'}$	95.2	T'_7 = 60.5	0.2	1	0.375	0.073	
111	$Q_{3-8'}$	95.2	T'_8 = 54.4	0.2	1	0.375	0.0841	
12	$Q_{1-7''}$	95.2	T''_7 = 53.3	0.2	1	0.075	0.0043	
13	$Q_{3-8''}$	95.2	T''_8 = 40.2	0.2	1	0.075	0.0411	
14	$Q_{2-amb.}$	95.2	T_{amb} = 33.3	0.2	1	0.049	0.0995x2 =0.199	Strip is exposed t ambient on both th sides of enclosure hence a multiplyir factor of 2
							1.533	

Radiation heat loss for a three dimensional heater.

Emissivity of copper block can be assumed to

$$\epsilon = 0.15$$

Shape factor = 1

$$\sigma = 5.66 \times 10^{-8} \quad W/m^2 k^4$$

$$T_c = 53.2^{\circ}C = 53.2 + 273 = 326.2 \text{ A}$$

$$T_{oo} = 32^{\circ}C = 305 \text{ A}$$

$$q_{rad} = \sigma\epsilon (T_c^4 - T_{oo}^4)$$

$$= 0.15 \times 5.67 \times 10^{-8} (326.2^4 - 305^4)$$

$$q_{rad} = 22.78 \ W/m^2$$

$$q_{in} = 1626 \ W/m^2$$

$$q_{rad} = 1.4\% \text{ of } q_{in}.$$

It is seen that amount of radiation loss is very small in case of three dimensional heater when when compared with a two dimensional heater. This is due to the smaller surface area of three-dimensional heater and lower maximum temperature reached for same heat input because of higher heat transfer coefficients.

Appendix 4

NUMERICAL CALCULATION OF HEAT TRANSFER FROM A FLUSH HEATER INSIDE A CHANNEL

Here we present mathematical modelling of a flush heater mounted on one wall of a channel. The other wall is assumed to be insulated and the top portion is modelled as an isothermal reservoir. The configuration is shown below.

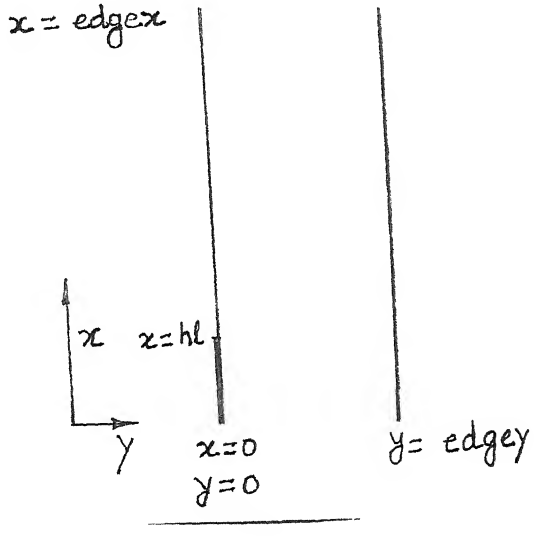

Fig. A.4.1 : Configuration of flow and heat transfer over a flush heater

The channel is assumed to have infinite dimension in the third direction. Therefore the flow is two dimensional. A flat velocity profile has been taken but the scheme can easily be modified for a parabolic velocity profile.

Formulation

The stream function ψ, vorticity ω and temperature T form the governing differential equation for a 2-D flow.

The equations are given as

$$\psi_{xx} + \psi_{yy} = -\omega \qquad \text{(A.4.1)}$$

$$\omega_t + u.\omega_x + v.\omega_y = \omega_{xx} + \omega_{yy} + \frac{Ra}{Pr}\frac{1}{Re^2} T_x \qquad \text{(A.4.2)}$$

$$T_t + u\,T_x + v\,T_y = \frac{1}{Pr}(T_{xx} + T_{yy}) \qquad \text{(A.4.3)}$$

where

$$u = \psi_y \quad \text{and} \quad v = -\psi_x .$$

Boundary conditions

$y = 0$ $\quad 0 < x < hl, \quad T = 1$

$\quad\quad\quad n > hl, \quad T_y = 0$

$y = edgey$, $T_y = 0$ and $\psi = 1$

$x = 0$, $\psi = y$ $\omega = 0$ and $T = 0$

$x = edgex, \psi_x = 0$, $\omega_x = 0$ and $T_x = 0$

In the present study edgex = 5, edgey = 1 and hl = 1.

The method of false transient is used to calculate steady state flow and temperature patterns and average Nusselt number. In the method of false transient equations (A.4.1) to (A.4.3) are cast in the following form

$$C^{\phi}\frac{\partial \phi}{\partial t} = a^{\phi}(\phi_{xx} + \phi_{yy}) - b^{\phi}((u\phi)_x + (v\phi)_y) + S^{\phi} \qquad \text{(A.4.4)}$$

For incompressible flow since $u_x + v_y = 0$ we have

$$(u\phi)_x + (v\phi)_y = u\phi_x + v\phi_y$$

In equation (A.4.4) ϕ stands for any of the dependent variables and a,b,c depend on the choice of ϕ. This correspondence is given in Table A.1 below:

ϕ	a	b	c	S
ψ	1	0	1	ω
ω	1	1	1	$\frac{Ra}{Pr\ Re^2}$
T	1/Pr	1	1	0

Above differential equation is solved using numerical technique.

Finite Difference Approximation

The finite difference approximation for differential equation is given below.

Present scheme uses

a. Full differencing for the transient term for ϕ_t

$$\phi_t = \frac{\phi^{n+1} - \phi^n}{\Delta t}$$

b. Central differencing for diffusion term

$$\nabla^2\phi = \frac{[\phi_{i+1} + \phi_{i-1} - 2\phi_i]_j}{\Delta x^2} + \frac{(\phi_{j+1} - \phi_{j-1} - 2\phi_j)_i}{\Delta y^2}$$

c. Upwinding for the advective term:

$$\nabla \cdot \underset{\sim}{u}\phi = \frac{\phi_r u_r - \phi_l u_l}{\Delta x} + \frac{\phi_u v_u - \phi_b v_b}{\Delta y}$$

[illegible] the current time level at which the solution must [illegible]. We assume constant step sizes, Δt, Δx and Δy. Equation (A.4.4) is now written in the finite difference form as follows:

$$\Gamma^{\phi} \frac{\phi^{n+1} - \phi^{n}}{\Delta t} = a^{\phi}[\nabla^2\phi]^{n+1} - b^{\phi}[\underset{\sim}{\nabla} \cdot \underset{\sim}{u}\phi]^{n+1} + S^{\phi}(\phi^{n+1}) \qquad \text{(A.4.5)}$$

In the [illegible] terms, r,l,u and v refer to right, left, [illegible] below reference point (i,j) respectively with respect to the local flow direction. This is shown in Fig. A.4.2

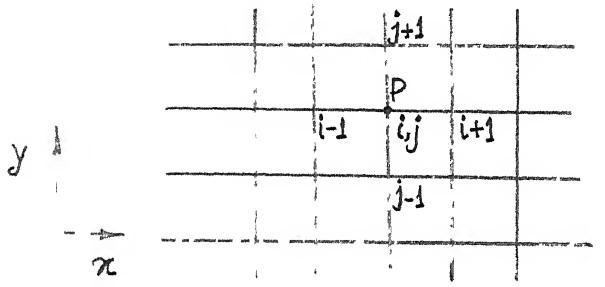

We describe a second order upwinding method for the advective terms ($\underset{\sim}{\nabla} \cdot \underset{\sim}{u}\phi$) below. The upwinding involves backward differencing with respect to local flow direction. Define,

$$u_r = \frac{1}{2}(u_i + u_{i+1})_j ,$$

$$u_l = \frac{1}{2}(u_i + u_{i-1})_j ,$$

$$v_u = \frac{1}{2}(v_j + v_{j+1})_i \quad \text{and}$$

$$v_b = \frac{1}{2}(v_j + v_{j-1})_i \quad \text{then}$$

$$\phi_r = \phi_i \text{ if } u_r \geq 0, \quad = \phi_{i+1} \text{ if } u_r < 0$$

$$\phi_l = \phi_{i-1} \text{ if } u \geq 0, \quad = \phi_i \text{ if } u_l < 0,$$

$$\phi_u = \phi_j \text{ if } v_u \geq 0, \quad = \phi_{j+1} \text{ if } v_u < 0 \quad \text{and}$$

$$\text{Denm} = c^{\phi} + \frac{2\ \Delta t\ a^{\phi}}{(\Delta x)^2} + \frac{2\ \Delta t\ a^{\phi}}{(\Delta y)^2} +$$

$$\frac{\Delta t\ b^{\phi}}{\Delta x}\,(a_1\ u_r - a_2\ u_\ell)^{n+1} + \frac{\Delta t\ b^{\phi}}{\Delta y}\,(b_1\ v_u - b_2\ v_b)^{n+1}$$

If equation (A.4.6) is cast as a matrix equation the identical form of this equation for each dependent variable ($\phi = \omega, \psi$ and T) provides for some simplification in computer programming effort. In the method of false transient $c^{\phi} = 1$ for the stream function and $C^{\phi} = 0$ when the real transient solution must be obtained. Except when changes in the flow quantities is rapid the approach to steady state can be accelerated by choosing $c^{\phi} > 1$. The precise value of this quantity must be decided based on numerical experimentation. The choice of $c^{\phi} > 1$ is equivalent to the successive over-relaxation (SOR) method that is used with the Gauss-Seidel scheme for matrix inversion.

The equation (A.4.6) is repeatedly applied for each node and for each time step. Further, within a time step iterations are required for matrix inversion (in the Gauss-Seidel sense) as well as for the non-linearity of the governing equations (Equation A.4.2). Typically 5-10 iterations are required per time step when the solution at the nth time level is used as the initial guess for the (n+1)th time level. A convergence criterion of 0.1 - 0.01 percent change per iteration in any of the flow variables at any node is generally used.

The grid used for a particular problem is chosen on the basis of several factors. Since a highly refined grid can lead to a high cost of computation the grid must be coarse but, a. must be fine enough to resolve boundary-layers, and b. must give a small excess energy balance at steady state.

In dimensionless form, heat transfer rate is given by the Nusselt number, Nu. Nu is conventionally defined as hL/k(fluid), where L is a length scale and h is the heat transfer coefficient. For this problem Nu reduces to $(-\frac{\partial T}{\partial y}\big|_{y=0})$ and the average value of Nu is, $Nu = \int_0^{hL} Nu\, dx$. The Nusselt number is specified as $= Nu\ (Ra, Pr)$.

Grid Refinement

In wall-driven flows it is necessary to discretize the wall region with a sufficiently large number of nodes to resolve the boundary-layers. If a uniform grid is used a large number of nodes would be present in regions where velocity as well as temperature vary gradually in space. This is computationally uneconomical. Hence it is desirable to refine the grid locally near the wall while the central core has only a few nodes in it. This is schematically shown in Figure.

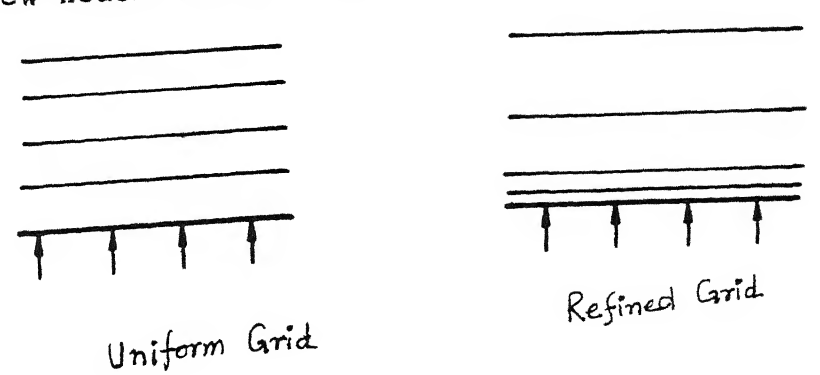

grid refinement referred here keeps the total number of nodes unchanged while it is selectively redistributed over the flow domain. On a grid where the spacing Δy is a variable conventional formulae for derivatives given earlier do not hold. A grid transformation approach is described to circumvent this problem.

For the channel considered here the boundaries y = 0 to x = hl and y = edgeyfor all x are respectively heated and cooled. Hence we consider grid refinement in the y-direction in which the grid spacing is non-uniform. Let η be a transformed plane in which the grid appears uniform. Conventional finite difference formulae are applicable in this domain. Without proof we state that the following equation accomplishes grid refinement in the y-plane for uniform grid in the η-plane.

$$\frac{d^2y}{d\eta^2} + Q \left(\frac{dy}{d\eta}\right)^3 = 0 \qquad \text{(A.4.7a)}$$

where $Q(\eta) = - \sum_{i=1}^{2} A \operatorname{sign}(\eta - \eta_i) \exp(-c\,|\eta - \eta_i|)$

i = 1 is the lower wall, i = 2 is the top wall, $\eta_1 = 0$, $\eta_2 = 1$ and A and C are constants. Typical values of these constants are, C = 0.2 and $0 < A < 25$. Equation (A.4.7a) must be solved subject to the boundary conditions,

$$y(\eta = 0) = 0, \quad y(\eta = 1) = 1 \qquad \text{(A.4.7b)}$$

This solution can be accomplished using finite differences and is not described here.

Equation (A.4.7a) is equivalent to,

$\frac{d^2\eta}{dy^2} = Q$ when y is used as an independent variable. In two dimensions grid is generated using equations of the form $\nabla^2\eta = \eta_{xx} + \eta_{yy} = 0$. This is called as elliptic grid generation and is a separate field of study. Use of differential equations of the form given above guarantees that the movement of the grid lines within the physical plane is gradual as well as confined within the true physical domain.

The effect of grid refinement is shown in Table A.4.2 below.

Table A.4.2 Grid Refinement. C = 0.2

	$\Delta\eta = 0.1$	$\Delta\eta = 0.01$
A = 0	$\Delta y(min) = 0.1$	$\Delta y(min) = 0.01$
10	0.082	0.00799
25	0.065	0.00617

Viewed through the coordinate η the governing equation (A.4.2) gets transformed to,

$$c^{\phi}\frac{\partial \phi}{\partial t} = a^{\phi}[\phi_{\xi\xi} + Q(\eta)\phi_{\eta} + \nu\phi_{\eta\eta}] - b^{\phi}[(u\phi_{\xi}) + (v\phi_{\eta})/y_{\eta}] + s^{\phi} \qquad (A.4.8)$$

Here $\xi = x$ and we use the transformation rules $\phi_y = \phi\eta/y_\eta$ and $\phi_{yy} = \nu\phi_{\eta\eta} + Q(\eta)\phi_\eta$ where $\nu = (1/y_\eta)^2$. The wall temperature gradient is evaluated as $\partial T/\partial y\big|_{y=0} = T_\eta/y_\eta\big|_{\eta=0}$. The discretized version of Equation (A.4.8) is similar to Equation (A.4.6) and given below.

$$\phi_{ij}^{n+1} = \Big[c^{\phi}\ \phi_{ij}^{n} + \frac{\Delta t\ a^{\phi}}{(\Delta x)^2}\ (\phi_{i+1} + \phi_{i-1})_j^{n+1} +$$

$$Q_j\ \frac{\Delta t\ a^{\phi}}{2\Delta y}\ (\phi_{j+1} - \phi_{j-1})_i^{n+1} + \frac{\Delta t\ a^{\phi}}{(\Delta y)^2}$$

$$(\phi_{j+1} + \phi_{j-1})_i^{n+1} - \frac{\Delta t\ b^{\phi}}{\Delta x}\ (a_3\ \phi_r\ u_r - a_4 \phi_\ell\ u_\ell)^{n+1}$$

$$- \frac{1}{(y_\eta)_j}\ \frac{\Delta t\ b^{\phi}}{\Delta y}\ (b_3\ \phi_u\ v_u - b_4\ \phi_b\ v_b)^{n+1} \Big] /\ \text{Denm}$$

(A.4.9)

$$\text{Denm} = c^{\phi} + \frac{2\ \Delta t\ a^{\phi}}{(\Delta x)^2} + \frac{2\ \Delta t\ a^{\phi}}{(\Delta y)^2} \gamma_j +$$

$$\frac{\Delta t\ b^{\phi}}{\Delta x}\ (a_1\ u_r - a_2\ u_\ell)^{n+1} +$$

$$\frac{1}{(y_\eta)_j}\ \frac{\Delta t\ b^{\phi}}{\Delta y}\ (b_1\ v_u - b_2\ v_b)^{n+1}$$

In Eq. (A.4.9), Δx is the grid spacing in ξ (= x) direction, Δy is the uniform grid spacing in η direction and j is an index in the η direction.

It is noted that the grid generated from Equations (A.4.7) using a finite difference method will itself be affected by discretization and round-off errors. The flow solution obtained from such a grid can be in considerable error since the metric derivatives such as $dy/d\eta$ are involved in the flow calculation. Hence one must solve for $y(\eta)$ as accurately as possible. Usually y is determined on a grid with twice as many points as what is required for flow calculations.

Three programs are to be run separately in a fixed order to arrive at the solution

1 For generating grid.

2 For initializing the flow and stemperature field.

3 For solving the flow and temperature equations using the method of false transient ($c^{\emptyset} = 1$).

The results are obtained by varying the values of Ra and Re in the program each time. The solution at a lower value of Ra can act as the initial condition for the new problem. For the present case the runs have been made with a grid size of 41x11, with c = 0.2 and A = 50. Convergence criterion of 0.1% is used, Δt is 0.01 and time step marched for each case is 800.

ME-1992-M-SHR-EXP